

UCLA

UCLA Electronic Theses and Dissertations

Title

Polymeric Protein Nanocapsules for Catalytic, Imaging and Therapeutic Applications

Permalink

<https://escholarship.org/uc/item/5q92x0tg>

Author

Du, Juanjuan

Publication Date

2012

Peer reviewed|Thesis/dissertation

UNIVERSITY OF CALIFORNIA

Los Angeles

Polymeric Protein Nanocapsules for Catalytic, Imaging and Therapeutic Applications

A dissertation submitted in partial satisfaction of the
requirements for the degree Doctor of Philosophy
in Chemical Engineering

by

Juanjuan Du

2013

ABSTRACT OF THE DISSERTATION

Polymeric Protein Nanocapsules for Catalytic, Imaging and Therapeutic Applications

by

Juanjuan Du

Doctor of Philosophy in Chemical Engineering

University of California, Los Angeles, 2013

Professor Yunfeng Lu, Chair

Enzymes are catalysts bearing excellent properties (high activity, selectivity and specificity) that modulate the most complex chemical processes under the most benign conditions. They participate in every biological process and mediate various functions in living organisms. However, the poor stability largely limits the application of enzymes. As our knowledge on the structure and function of enzymes accumulated, more and more applications require additional properties beyond what nature has gifted.

In this dissertation, a novel strategy was successfully developed to address the stability issues while simultaneously introduce new functionality to enzymes. This is achieved by an aqueous *in-situ* polymerization around a single enzyme molecule, yielding a novel class of enzyme nanocapsules containing a single enzyme core and a thin layer of network polymer shell.

Nanocapsules of over twenty enzymes were successfully synthesized for various therapeutic, analytic and bio-catalytic applications briefly outlined below:

1. With the presented technique, we obtain enzyme nanocapsules with highly-retained activity and significantly enhanced stability against various inactivating factors. These properties

provide the pre-conditions for prolonged storage and facile handling of enzymes, enabling the application of enzymes in non-physiological environment, such as field decontamination and sensor fabrication.

2. Our research demonstrated a general, effective, low-toxic intracellular protein delivery based on cationic single-protein nanocapsules. Additionally, the nanocapsules delivered intracellularly can exert their biological functions in cells, harboring great potentials for cellular imaging, cancer therapies, anti-aging, cosmetics, and many other applications.
3. By conjugating PEG and PEG-lipid on the nanocapsule surface, we obtained nanocapsules with high intracellular delivery efficiency and decreased cytotoxicity. The delivered protein is uniformly distributed in cytosol after cellular uptake. Moreover, similar levels of cellular uptake were achieved even in the presence of endocytosis inhibitors.
4. By conjugating quantum dot on bioluminescent nanocapsules, we obtain QD-nanocapsule conjugates with continuously tuned red-shifted emission, suitable for in-vivo bioluminescence imaging.

Overall, my research establishes a novel strategy to stabilize enzymes and create new surface functions of enzyme. With this technology, we can envision a promising prospect in industrial, environmental, therapeutic and analytical applications of the great gift from nature – the enzymes.

The dissertation of Juanjuan Du is approved.

Tatiana Segura

Yu Huang

Harold Monbouquette

Yunfeng Lu, Committee-Chair

University of California, Los Angeles

2013

TABLE OF CONTENTS

Chapter 1. Application Scope of Proteins and Existing Challenges	1
1.1. Protein Immobilization	2
1.2. Protein Engineering	4
Chapter 2. Intracellular Protein Delivery	6
2.1. CPP mediated Intracellular Protein Delivery.....	7
2.2. Liposome mediated Intracellular Protein Delivery.....	9
2.3. Polymer Mediated Intracellular Protein Delivery.....	12
Chapter 3. Fabrication of Single Protein Nanocapsules	19
3.1. Introduction	19
3.2. Experimental.....	20
3.3. Synthetic Approach and Structural Characterization.....	22
3.4. Engineerable Surface	32
3.5. Summary.....	33
Chapter 4. Bioactivity of Nanocapsules.....	34
4.1. Introduction	34
4.2. Experimental.....	35
4.3. Retained activity of nanocapsules.....	37
4.4. Nanocapsules define microenvironment around enzyme surface.....	39
4.5. Summary.....	41
Chapter 5. Enhanced Stability of Nanocapsules	41
5.1. Introduction	41

5.2. Experimental.....	42
5.3. Enhanced protein stability after encapsulation	43
5.4. Summary.....	51
Chapter 6. Cationic Nanocapsules for Intracellular Delivery	52
6.1. Introduction	52
6.2. Experimental.....	54
6.3. Intracellular delivery of the non-degradable nanocapsules	59
6.4. Intracellular delivery of the degradable nanocapsules.....	71
6.5. Polymer composition and intracellular delivery.....	74
6.6. Summary.....	78
Chapter 7. Nanocapsule as a Platform for Further Functionalization.....	78
7.1. Introduction	78
7.2. Experimental.....	80
7.3. Results	82
7.4. Summary.....	86
Chapter 8. Non-endocytotic Delivery of Nanoparticles	87
8.1. Introduction	87
8.2. Experimental.....	88
8.3. Results	92
8.4. Summary.....	102
Chapter 9. Conclusions	102

LIST OF FIGURES

Figure 1 Illustration of liposome-mediated intracellular protein delivery and endosomal escape	11
Figure 2 Schematic illustration of the noncovalent polymer delivery system.....	14
Figure 3 Schematic illustration of a protein nanocapsule.....	20
Figure 4 Schematic illustration of the synthetic approach of protein nanocapsules.....	23
Figure 5 Synthetic methods to conjugate acryl groups onto enzymes.....	23
Figure 6 MALDI-TOF mass spectra of proteins before and after modification with N-acryloxysuccinimide (NAS): (a) native EGFP and modified EGFP, (b) native HRP and modified HRP, (c) native SOD and modified SOD, (d) native Caspase-3 and modified Caspase-3	24
Figure 7 a) MALDI measurement to determine modification degree of enzymes; b) AKR1C4 activity monitored by measuring absorption change at 340 nm by UV spectrometer.....	26
Figure 8 IR spectra of native OPH, modified OPH, nOPH(AAm) and nOPH(APm).....	28
Figure 9 size and zeta potential distribution of (a) native BSA, (b) nBSA-AAm and (c) nBSA-DMAEMA	30
Figure 10 Agarose gel electrophoresis image of (1) native BSA, (2) nBSA-AAm, and (3) nBSA-DMAEMA. These samples were pre-labeled with fluorescein isothiocyanate.	31
Figure 11 representative TEM and AFM images of the HRP nanocapsules and TEM image of nanocapsules containing a single 1.4 nm gold-quantum-dot-labeled HRP core	32
Figure 12 (a) zeta potential distribution of BSA nanocapsules with different composition: from top to bottom DMAEMA:AAm = 0:1, 1:3, 1:1; (b) zeta potential distributions of anionic BSA nanocapsules with different compositions: from top to bottom AA:AAm = 0, 1, 4....	33
Figure 13 (a) Relative enzyme activity of native OPH and nOPH under various pHs, activities were normalized using their activities at pH 10.5 as 100% standards; (b) Fluorescence	

intensity of free fluorescein, OPH-FITC, and nOPH-FITC containing the same amount of fluorescein (n = 3, ** p < 0.01); (c) Fluorescence intensity of FITC-OPH and FITC-nOPH as a function of pH values..... 40

Figure 14 nOPH with Enhanced Enzyme Stability. a) Relative activities of native OPH and nOPH incubated at 65 °C. b) After incubation at 65 °C, relative activities of native OPH (a) and nOPH prepared from OPH treated with increasing NAS/OPH molar ratio of (b) 10:1, (c) 20:1, (d) 30:1, (e) 40:1 and (f) 50:1. Relative activities of native OPH and n(OPH) exposed to 50mM HEPES buffer (pH=8.5) solution containing different diffractions of c) DMSO or d) methanol, e) subject to 5 freeze-thaw cycles, and f) stored at 4 °C in solution. 45

Figure 15 Rate constants of the forward and the reverse reaction of nOPH thermal inactivation 47

Figure 16 reactivity decrease of GOx and nGOx at 60 °C. red line: native GOx; blue line: GOx nanocapsules 49

Figure 17 Dissociation of FAD from GOx (a) Schematic illustration of the dissociation of coenzyme FAD, (b) fluorescent emission of GOx solution after incubation for different time, (c) fluorescent emission of GOx nanocapsule solution after incubation for different time.. 50

Figure 18 Relative activity of native SOD and SOD nanocapsule after incubation at 37 °C with pepsin for different time..... 51

Figure 19 Schematic showing the synthesis and cellular uptake of cationic single-protein nanocapsules with degradable and non-degradable polymeric shells prepared by in situ copolymerization of acrylamide (1), 2-dimethylaminoethyl methacrylate (2) and non-degradable crosslinker methylenebisacrylamide (3) or acid-degradable glycerol dimethacrylate (4): I) formation of polymerizable proteins by conjugating polymerizable

acryl groups to the protein surface; II) formation of non-degradable nanocapsules from (1), (2) and (3); III) formation of degradable nanocapsules from (1), (2) and (4); IV) cellular uptake of the degradable or non-degradable nanocapsules via endocytosis; V) Shells of degradable nanocapsules break down after internalization to release the protein cargoes, allowing them to interact with large molecular substrates..... 54

Figure 20 Fluorescent images show uptake of nEGFP but not native EGFP after 3 hr incubation. Cells were counter-stained with DAPI for nuclei. 60

Figure 21 Fluorescence-assisted cell sorting of HeLa cells incubated with different concentrations of nEGFP (11.7nm, zeta potential 10.9 mV), TAT-EGFP fusion proteins, Antp-EGFP fusion protein or native EGFP. 60

Figure 22 (a) Cellular fluorescence distribution of HeLa cells after incubation with nEGFP; (b) HeLa cell fluorescence intensity after incubation with 400 nM nEGFP for different time; (c) Uptake of nEGFP by HeLa cells increased with zeta potential after 3hr; (d) Cellular fluorescent intensity distribution of HeLa cells after incubation with nEGFP with different sizes (red: 7.53 nm, green: 10.6 nm, purple: 15.7 nm) 61

Figure 23 Average cellular fluorescence intensity of HeLa cells at different temperatures and in the presence of endocytosis inhibitors. Fluorescence intensity normalized to cells incubated with nEGFP at 37 °C..... 62

Figure 24 (Up) Trafficking of Rhodamine B-labeled nBSA through endocytosis. Early and late endosomes were stained by EEA1 antibody (Up-left) and Rab7 antibody (Up-right), respectively. HeLa cells were incubated with 400 nM nBSA at 37 °C for various time points of 5, 30, 60 and 120 min. (Bottom) Quantification of nEGFP co-localized with EEA1 (black) or Rab7 (red) endosomes at different incubation times. 63

Figure 25 MTT assay showing nEGFP has similar cytotoxicity to native EGFP after 3 hr.....	63
Figure 26 Stability of nanocapsules. (a) Fluorescence intensity of native EGFP and nEGFP after exposure to trypsin and chymotrypsin. Fluorescence intensities normalized to native EGFP before exposure to protease (b) Cellular fluorescence intensity of cells after treatment with nEGFP or TAT-EGFP fusion proteins at different times.	64
Figure 27 Overlay of the optical image and fluorescence image of mouse subcutaneously injected with nEGFP (left) and native EGFP (right) at different times post injections.....	65
Figure 28 Fluorescence signal of injection site at different times post injection.....	66
Figure 29 Overlay of the optical image and fluorescence image of mouse subcutaneously injected with nEGFP at different times post injections	67
Figure 30 Fluorescence signal of injection site at different times post injection.....	67
Figure 31 Fluorescence microscope images of mouse epidermis/dermis tissue sections, the slides were counter-stained with DAPI.....	68
Figure 32 Confocal microscope images of mouse skin tissue	69
Figure 33 (a) HeLa cells after incubation with HRP or nHRP at different concentrations, followed by PBS washes and incubation with TMB and H ₂ O ₂ . (b) MTT assay showing HeLa cell viability after transduction with native HRP or nHRP and incubation with IAA. Cell proliferation rates normalized to untreated cells.	70
Figure 34 Intracellular lactamase activity CCR5 cells pre-incubated with VSVG-lac, nLac, nLac-lipid. 150 nM Bafilomycin is used to inhibit the acidification of endocytosis.	71
Figure 35 Degradable nanocapsules. a, Sizes of degradable Caspase-3 nanocapsule (de-nCAS) and non-degradable Caspase-3 nanocapsule (nCAS) at pH 7.4 (a) and pH 5.5 (b). c, Fluorescence intensity of native EGFP, non-degradable EGFP (nEGFP) and degradable	

EGFP nanocapsules (*de*-nEGFP) after exposure to trypsin and chymotrypsin. Fluorescence intensities normalized to native EGFP before addition of proteases. d, Fluorescence intensity of HeLa cells at different times after incubation with nEGFP or *de*-nEGFP for 3 hr followed by incubation in fresh media. Fluorescence intensities were normalized to the respective cells that received no further incubation with fresh media. e, MTT assay showing cell proliferation profile after incubation with various concentrations of *de*-nCAS, nCAS, caspase-3, *de*-nBSA or nBSA for 48 hrs. Data normalized to untreated cells. f, APO-BrdUTM TUNEL assay showing of HeLa cells transduced *de*-nCAS, nCAS or caspase-3. PI-stained nuclei (red) and Alexa Fluor 488-stained nick end label (green) in cells incubated with *de*-nCAS show apoptotic DNA fragmentation. 73

Figure 36 Image of agarose gel electrophoresis of fluorescence-labeled nHRP nanocapsules and zeta potential of nHRP nanocapsules..... 75

Figure 37 HeLa cell viability after incubation with HRP and nHRPs for 48 hours. The cells treated with PBS with equal volume is used as a control whose viability is set to 100%. 76

Figure 38 The fluorescence microscope images of HeLa cells after incubation with HRP nanocapsules with different polymer composition for 3 hours (left) or 12 hours (right). Cells were counter-stained with DAPI..... 77

Figure 39 Scheme of forming robust, cell-permeable bioluminescent nanocapsules..... 79

Figure 40 (a) Fluorescence spectra of CdTe QDs (excitation wavelength: 400 nm); (b) Luminescence emission of HRP-catalyzed oxidation of luminol (blue) and UV-Visible absorption of CdTe QDs. 83

Figure 41 TEM images of (A) QD-544 and (B) BN-544; (C) photographs of HRP and BNs in the presence of H ₂ O ₂ , luminol and <i>p</i> -iodophenol showing tunable-wavelength bioluminescence	84
Figure 42 (a) Number distribution of particle size of bioluminescent HRP nanocapsules determined by DLS; (b) Zeta potential distribution of bioluminescent HRP nanocapsules.	84
Figure 43 (A) luminescent spectra of (A) native HRP, BN-517, BN-544, BN-579, BN-724 and BN-754, (B) HRP-polymer conjugates (nHRP), mixture of nHRP and QD-544, and BN-544 with various QD/HRP ratios	85
Figure 44 (A) Luminescence spectra of HRP and BN-544 after incubation at 37 °C for 0 hr, 24 hr and 48 hr. HRP and BN-544 were exposed to same amounts of H ₂ O ₂ , luminol and <i>p</i> -iodophenol during acquisition of spectra. (B) Relative luminescence unit (RLU) of HeLa cells pretreated with BN-696 with different concentrations. Inset: Fluorescent microscope images of HeLa cells pretreated with BN-696, showing cellular uptake of BNs	86
Figure 45 Schematic illustration of the synthetic approach for PEG-lipid conjugated nanocapsules	88
Figure 46 Size and zeta potential distribution of BSA nanocapsules and nBSA-lipid	94
Figure 47 Cytotoxicity of BSA annocapsules and nBSA-lipid in HeLa Cells	95
Figure 48 Cellular Uptake of FITC-BSA, nBSA and nBSA-lipid	96
Figure 49 Fluorescence image and cellular fluorescence distribution of HeLa cells after incubation with nBSA-lipid with and without subsequent quenching with trypan blue	97
Figure 50 cellular fluorescence distribution of HeLa cells after incubation with FITC-BSA, nBSA and nBSA-lipid	97

Figure 51 Cellular uptake of nBSA and nBSA-lipid under conditions when endocytosis is inhibited	98
Figure 52 Transduction of FITC labeled nBSA and nBSA-lipid in CEM Cells	99
Figure 53 Transduction of FITC labeled nBSA and nBSA-lipid in HEK-293T-CCR5 Cells.....	99
Figure 54 Fluorescence intensity change of GeneBLAzer® FRET Assay after native lactamase, nLac and nLac-lipid-PEG were added to the assay buffer (ex: 405 nm, em: 535 nm).....	100
Figure 55 Intracellular lactamase activity CCR5 cells pre-incubated with VSVG-lac, nLac, nLac-lipid. 150 nM Bafilomycin is used to inhibit the acidification of endocytosis.	101

LIST OF TABLES

Table 1 fluorescent proteins derived from green fluorescent protein and their corresponding mutations.....	5
Table 2 Representative cell penetrating peptide and their sequences (adapted from ref. {Heitz:2009hm})	7
Table 3 Lipids used for composing liposomes for protein delivery	9
Table 4 Molecular weight of proteins before and after modification with N-acryloxysuccinimide (measured with MALDI-TOF mass spectrometer).....	25
Table 5 The molar ratio of NAS added to enzyme and the corresponding number of acryl groups attached to each enzyme	25
Table 6 monomers that are used to form the nanocapsule shells.....	26
Table 7 relative residual activities of nanocapsules with different enzyme cores	38
Table 8 Rate constants of the forward and the reverse reaction of nOPH thermal inactivation...	46
Table 9 Mole ratio of monomers, crosslinker and initiators to protein in the synthesis of nHRP nanocapsules	75
Table 10 recipes for encapsulation of BSA	89
Table 11 Recipe for synthesis of nLac.....	92
Table 12 Amounts of reagents added to conjugate nLac to PEG-lipid and PEG-NHS	92
Table 13 Average size and zeta potential	94
Table 14 Number of amine groups on nBSA, nBSA-lipid and nBSA-lipid-PEG	94

ACKNOWLEDGEMENTS

I would like to express the deepest appreciation to my committee chair, Professor Yunfeng Lu, who has the attitude and the substance of a genius: he continually and convincingly conveyed a spirit of adventure in regard to research and scholarship, and an excitement in regard to teaching. Without his guidance and persistent help, this dissertation would not have been possible.

I would like to thank my committee members, Professor Tatiana Segura, Professor Yu Huang and Professor Harold Monbouquette for their help with my research work and dissertation. I would also like to thank Professor Yi Tang, a former member of my committee and an intelligent collaborator for all his help with my research. In addition, a thank you to Professor Cheng Ji in University of Southern California, Prof. Michael Kolodney in Harbor-UCLA medical center, Dr. Neychelle Fernandes, Dr. Serge Lichtsteiner, with whom we had pleasant and fruitful collaborations.

I would like to express my appreciation to Dr. Ming Yan. At the beginning of my Ph.D. studies, he led me into the enzymology and bioconjugation field. His philosophy and method of research have been influencing me throughout my entire research life. I would like to thank Dr. Daocheng Pan, Dr. Qiangfeng Xiao, Dr. Chih-ning Pao, Dr. Ding Weng, Dr. Zheng Chen, Dr. Jing Wen, Dr. Jing Jin, Yang Liu, Xiaolei Wang, Jie Li, Qi Zhu, Wei Wei and Shuoran Li. Their diligent work attitude and insightful suggestions inspire me in my road of scientific exploration. I would also like to thank all the other Lu lab members and my friends in Department of Chemical Engineering at UCLA. You made me enjoy so much the research and life in UCLA. The five years spent with you will become a memorable gemstone in my life.

At last, I would like to thank my family for their support during my Ph.D. study, particularly my husband, Jingwei Bai. His encouragement, understanding and love are the strongest support for me throughout the joyful and the hard times in my studies.

VITA

Education:

September 2003-July 2007

Peking University

Degree: Bachelor of Science

College of Chemistry and Molecular Engineering,

Awards:

2011-2012 Dissertation Year Fellowship University of California at Los Angeles

2006-2007 University Graduate Fellowship University of California at Los Angeles

Publications:

1. **J. Du**; W. Wei; J. Li; M. Yan; Q. Zhu; J. Jin; X. Zhu; Y. Tang; Z. Hu; Y. Lu. *Advanced Materials*, in revision
2. **J. Du**, J. Jin, W. Wei, Y. Liu, J. Li, Z. Lu, X. Yuan, Y. Lu, *Angew. Chem. Int. Ed.*, in revision
3. **J. Du**; Y. Liu; M. Yan; E. Kao; M. Y. Lau; L. Shi; C. Ji; Y. Lu. *Nature Nanotechnology*, accepted
4. Y. Liu; H. Wang; M. Yan; **J. Du**; K.-J. Chen; M. A. Garcia; K. Liu; Z. Jiang; K. Kamei; G. S. Lipshutz; L. Wu; C. K.-F. Shen; L. Shi; H.-R. Tseng; Y. Lu. *Nature Nanotechnology*, in revision
5. **J. Du**; J. Jin; M. Yan; Y. Lu. *Current Drug Metabolism*, 2012, 13, 82-92.
6. J. Wen; S. M. Anderson; **J. Du**; M. Yan; J. Wang; M. Shen; Y. Lu; T. Segura. *Advance Materials* 2011, 23, 4549-53.
7. J. Zhang; Y. Lei; A. Dhaliwal; Q. K. Ng; **J. Du**; M. Yan; Y. Lu; T. Segura. *Biomacromolecules* 2011, 12, 1006-14.
8. J. Zhang; **J. Du**; M. Yan; A. Dhaliwal; J. Wen; T. Segura; Y. Lu. *Nano Res.* 2011, 4, 425-33.

9. **J. Du**; C. Yu; J. Li; W. Chen; M. Yan; T. Segura; Y. Tang and Y. Lu. *J. Am. Chem. Soc.* 2010, *132*, 12780-12781.
10. **J. Du**; M. Yan; Z. Gu; M. Liang; Y. Hu; W. Zhang; S. Priceman; L. Wu; H. Zhou; Z. Liu; T. Segura; Y. Tang; Y. Lu. *Nature Nanotechnology*, 2010, *5*, 48-53.
11. Y. Peng; D. Jiang; L. Su; L. Zhang; M. Yan; **J. Du**; Y. Lu; Y. Liu; F. Zhou. *Anal. Chem.* 2009, *81*, 9985-92.

Presentations:

1. “Non-endocytotic Intracellular Delivery of Therapeutic Nanoparticles”, 2011 Material Research Society Fall Conference
2. “Quantum-Dot-Decorated Enzyme Nanocapsules for Cancer Imaging and Therapeutics.” 2011 Material Research Society Fall Conference
3. “Targeted delivery of therapeutic proteins to mitochondrial, an approach based on Single protein Nanocapsules.” 2010 Material Research Society Spring Conference
4. “Biosensors based on single enzyme nanocapsules: toward organophosphate sensing.” 2009 Chemical and Biological Defense Science and Technology Conference

Patents:

1. (PCT/US2010/026678) Single Protein Nanocapsules for Protein Delivery with Long-term Effect (Licensed by Kythera Biotech, Inc)
2. (US 61/510,996) Organophosphate Hydrolase Nanocapsules for Organophosphate decontamination and detoxification
3. (US 61/510,997) AKR1C4 Nanocapsules for Treatment of Androgenetic Alopecia
4. (US 61/599,794) Therapeutic Hyperbranched Polyglycerol Encapsulated Biomolecules

Chapter 1. Application Scope of Proteins and Existing Challenges

Since the first time human beings learned how to use fire, how to build a house, how to hunt with tools, we never stop exploiting and changing the nature. Advances of modern science and technology offer us more and more knowledge and techniques to utilize and improve what nature presents us. Enzymes, as great gifts from nature, are catalysts bearing excellent properties (high activity, selectivity and specificity) that modulate the most complex chemical processes under the most benign conditions (room temperature, aqueous solution). They participate in every biological process, mediating various functions of living organisms, ranging from metabolism to neurotransmission, from photosynthesis to DNA synthesis.

As our knowledge on the structure and function of enzymes accumulates, enzymes have been found useful beyond their intrinsic biological roles. The very initial application of enzymes may dated back to thousands of years ago, when man used naturally occurring microorganisms and the enzyme they produce to make food, such as bread, cheese, beer and wine. Today, besides their applications in food processing, enzymes are used in an increasing range of applications. In chemical industry, especially fine chemical syntheses, enzymatic catalysis is considered as a promising field due to benign reaction conditions, high chemo- and stereo- selectivity, and tolerance to substrate functional groups. In therapeutic applications, therapeutic enzymes have been used to treat various diseases, especially the ones caused by enzyme deficiency. In addition, enzymes also play significant roles in biosensing, bioremediation, and so on.

In a technical perspective, recent advancement in biotechnology have paved the way for the applications of enzymes. Recombinant DNA techniques, in particular, make possible the production of most enzymes at a commercially acceptable cost^{1,2}. However, wide applications of enzymes are still facing other challenges.

Poor stability of proteins, especially in non-physiological environment, is one of the most critical obstacles for their wide applications^{3,4}. Due to the fast denaturation and inactivation, enzymes commonly associate with low-temperature storage, short shelf life, sensitivity to heat and spectator chemicals, and vulnerability to protease digestion. Enzyme's poor stability, therefore, largely limits the use of enzymes in almost every field of applications, including industrial catalysis, biopharmaceutical industry, protein therapeutics, environmental decontamination, and biosensor fabrication.

In addition, native proteins may appear inadequate in front of the designed task they are not empowered to do by nature. For example, therapeutic use of protein has been largely limited by its low pharmacokinetic accessibility to intracellular drug target⁵. Various other properties might need to be introduced or improved to meet the demand of specific applications, such as increased hydrodynamic radius for long circulation time in vivo^{6,7}, heterogeneous form to be recycled and reused in industrial catalysis⁸⁻¹⁰, altered substrate specificity for biosensor fabrication^{11,12}. Great endeavors have been made by biologists, chemists, and material scientists to fit enzymes into a wide spectrum of applications. However, in addition to enhancing protein stability, these task-oriented properties are too diverse to be introduced in a universal approach.

1.1. Protein Immobilization

In industry, the poor stability of enzymes is addressed by enzyme immobilization. Basically, enzyme immobilization can be divided into three main categories: immobilization to a support, entrapment and cross-linking⁸. Immobilization to a support involves binding of enzymes to a preformed matrix support via non-covalent interactions, such as hydrophobic interaction, electrostatic interaction, or covalent bonding¹³⁻¹⁵. The second approach is enzyme entrapment, in which enzymes are included into a gel matrix during the formation of the matrix^{10,16,17}. Although

enzymes can be physically entrapped, additional chemical conjugation is usually required to prevent any enzyme leakage. As a more recent approach, cross-linking of enzyme aggregates or crystals without support matrix has been demonstrated to exhibit various extraordinary characteristics, such as effective enzyme stabilization, concentrated bioactivity in the catalyst, and low production costs¹⁸⁻²⁰.

These immobilization strategies can improve the enzyme stability with various extents of successes. Some protocols in multipoint immobilization could result in impressive stabilizing effect, in many cases with stabilization factor as high as 1000–10,000-fold⁹. The high stabilization factors can be attributed to rigidification of enzyme 3D structures, thus reducing any conformational change involved in enzyme inactivation²¹⁻²³.

In addition to enhanced stability, enzyme immobilization offers other advantages: (1) Immobilization technique makes possible the fabrication of heterogeneous enzyme catalysts^{10,18,24}, enabling the separation and recycling of enzymes and therefore eliminating protein contamination of the product and reducing manufacture costs. (2) In the enzyme catalysis in organic solvents, immobilization technique significantly increases the solvent accessible surface of catalyst compared with traditional lyophilized powders^{18,25}. (3) Immobilization technique provides a platform to incorporate multienzyme or chemoenzymatic cascade catalysts to overcome inactivation issues associated with their mutual interactions in free solution²⁶⁻²⁹.

However, as enzyme immobilization technique is developed to meet the qualification of industrial biocatalysis, transferring this technology to other applications appears to be challenging. For example, most of the immobilized enzymes could not be applied into therapeutic applications due to the biocompatibility issues.

1.2. Protein Engineering

In contrast to the enzyme immobilization technique chemists and material scientists developed, biologists take the route nature evolution takes to endow polyaminoacids with designed functions suitable for specific applications^{30,31}. Via technologies such as site-directed mutagenesis^{32,33} and DNA-shuffling^{34,35}, protein engineers could mimic and accelerate natural evolution to provide mutant enzymes tailored for applications in research. In addition, the ever-increasing use of computational simulation greatly aids the understanding and design of protein structures and properties³⁶⁻³⁹.

As a consequence, protein can be engineered to acquire a variety of improved properties, such as greater specificity^{40,41}, higher stereoselectivity⁴²⁻⁴⁵, and altered pH optimum⁴⁶⁻⁴⁸. In addition, mutagenesis can also be used to remove undesired properties of native protein, such as ubiquitous binding and immune response⁴⁹⁻⁵¹. Inhibition site on enzyme can also be eliminated from native enzyme to create inhibitor-resistant mutant^{52,53}.

Advances in protein engineering have also allowed the exploration of the relationship between protein structure and stability, and thus guide the rationally design of the protein with improved stability in addition to screening for stable mutants. It was found that, improving packing in hydrophobic core⁵⁴, building intramolecular salt bridge^{4,55} or disulfide bond^{56,57}, and adding new metal binding sites⁵⁸ may cause beneficial effect in protein stability.

As a special case for protein engineering, fusion protein technique creates chimeric proteins via the combination of multiple genes, which originally code for separate proteins or peptides^{59,60}. This technique opens an avenue for combining two or more desired functionalities into one single protein. With this technique, a protein with function of interest can be labeled with an affinity tag for convenient separation; targeting modules can be installed on a therapeutic protein;

two enzymes in a tandem reaction can be closely associated to deliver enhanced catalytic efficiency²⁸.

Furthermore, active-site redesign is shown able to create new enzyme functions, which do not originally exist in the native form or even in nature. The creation of a complete spectrum of fluorescent proteins is a convincing example. Mutation introduced in different sites in wild-type green fluorescent protein (wtGFP) creates not only more stable variant (EGFP), but also fluorescent protein with altered excitation and emission wavelength (Table 1)⁶¹. More amazingly, substitution of the active site amino acid may completely change the bioactivity of an enzyme. A single amino acid mutation may convert a cyclophilin into a protease⁶², or a 3 α -hydroxysteroid dehydrogenase to a Δ^4 -3-ketosteroid-5 β -reductase (5 β - reductase)⁶³.

Table 1 fluorescent proteins derived from green fluorescent protein and their corresponding mutations (adapted from ref 61)

GFP variant	Mutations relative to wtGFP
EGFP ^{x,*}	F64L, S65T
Emerald ^x	F64L, S65T, S72A, N149K, M153T, I167T
EYFP ^{x,*}	S65G, V68L, S72A, T203Y
mYFP ^{x,*}	S65G, V68L, Q69K, S72A, T203Y, A206K
Citrine ^{x,*}	S65G, V68L, Q69M, S72A, T203Y
mCitrine ^{x,*}	S65G, V68L, Q69M, S72A, T203Y, A206K
Venus [*]	F46L, F64L, S65G, V68L, S72A, M153T, V163A, S175G, T203Y
YPet	F46L, I47L, F64L, S65G, S72A, M153T, V163A, S175G, T203Y, S208F, V224L, H231E, D234N
ECFP ^{x,*}	F64L, S65T, Y66W, N149I, M153T, V163A
mCFP ^{x,*}	F64L, S65T, Y66W, N149I, M153T, V163A, A206K
Cerulean ^{x,*}	F64L, S65T, Y66W, S72A, Y145A, H148D, N149I, M153T, V163A
CyPet	T9G, V11I, D19E, F64L, S65T, Y66W, A87V, N149I, M153T, V163A, I167A, E172T, L194I
EBFP [*]	F64L, S65T, Y66H, Y145F
T-Sapphire	Q69M, C70V, S72A, Y145F, V163A, S175G, T203I

However, the expensive and labor-intensive process to produce and purify mutant proteins still places a barrier for the application of mutant proteins. Secondly, the try-and-error methodology involved in most protein engineering work is case-specific, which fails to improve desired functions of some specific proteins. Third, combining two functionalities with protein fusion are usually entangled with unfavorable folding, causing decreased activity and/or stability⁶⁴. Fourth, the feasibility of protein mutation is largely confined by the expression functions of the host organism. Last but not the least, to maintain activity, protein engineers endeavor to revise the protein properties with minor change of its intrinsic structure, posing limited freedom to alter major properties, such as size, hydrophobicity, and surface charges.

In Summary, despite the recent efforts on improving enzyme performances, novel methods that could endow enzyme more versatile functions are still in demand, especially when considering the increasing call for combination of enzymatic activity and other properties, such as enhanced stability and defined surface properties.

Chapter 2. Intracellular Protein Delivery

The average eukaryotic cell contains thousands of proteins participating in its normal cellular functions. Intracellular protein delivery⁵ is considered to be the most direct, fastest and safest approach for curing gene-deficiency diseases⁶⁵⁻⁶⁸, enhancing vaccination⁶⁹⁻⁷¹, triggering cell transdifferentiation process^{72,73}, inducing the formation of pluripotent stem cells^{74,75}, and other applications. In contrast to gene delivery, intracellular protein delivery avoids permanently altering the genomic information of host cells, circumventing the concerns of potential mutagenesis associated with the delivered genes⁷⁶⁻⁷⁸. Complex proteins, such as multi-component protein assemblies and post-translationally modified proteins may also be delivered,

particularly when the expression of such complex proteins in host cells is limited due to the lack of required cellular machinery. Clinical use of intracellular protein delivery is, nevertheless, still very limited, mainly due to proteins' low cell-membrane permeability, poor stability, and other constraints.

To date, various vectors have been explored to facilitate intracellular delivery of proteins, such as cell-penetrating peptides, liposomes, polymers, antibodies and other biomolecules.

2.1. CPP mediated Intracellular Protein Delivery

Cell-penetrating peptides (CPPs) or protein transduction domains (PTDs) are generally peptides with less than 30 amino acids, which possess the ability to shuttle into the cellular interior. Ever since the discovery of CPP more than 20 years ago⁷⁹, hundreds of CPPs with a diversity of peptide sequences and 3D structures have been identified and applied to deliver cargo into cells, ranging from small molecules, biomacromolecules (such as proteins and DNAs) to much larger microparticles⁸⁰.

Table 2 Representative cell penetrating peptide and their sequences (adapted from ref. 81)

<i>Peptides</i>	<i>Origin</i>	<i>Sequences</i>
Peptides deriving from protein transduction domains		
Tat	HIV-Tat protein	PGRKKRRQRRPPQ
Penetratin	Homeodomain	RQIKIWFQNRRMKWKK
Transportan	Galanin-mastoparan	GWTLNSAGYLLGKINLKALAALAKKIL
VP-22	HSV-1 structural protein	DAATATRGRSAASRPTERPRAPAR-SASRPRRPVD
Amphipathic peptides		
MPG	HIV Gp41-SV40 NLS	GALFLGFLGAAGSTMGAWSQPKKKRKV
Pep-1	Trp-rich motif-SV40 NLS	KETWWETWWTEWSQPKKKRKV
MAP	Chimeric	KALAKALAKALA
SAP	Proline-rich motif	VRLPPPVRLLPPPVRLLPPP
PPTG1	Chimeric	GLFRALLRLLRSLWRLLLRA
Other cell-penetrating peptides: cationic peptides		
Oligoarginine	Chimeric	Agr8 or Arg9
hCT (9–32)	Human calcitonin	LGTYTQDFNKTFFPQTAIGVGGAP
SynB	Protegrin	RGGRLSYSRRRFSTSTGR
Pvec	Murine VE-cadherin	LLIILRRRIRKQAHASK

CPP-mediated protein delivery was initiated to circumvent the safety and technical issues associated with gene delivery. The CPP is typically installed on the cargo protein with fusion protein technique. It may also be covalently conjugated to the cargo protein or assembly with it via electrostatic interactions. Additionally, other vectors (such as liposomes, polymers, or virus) with CPPs as surface ligands can also be used for the delivery of proteins. Since 1990s, the intracellular delivery of intact protein has been demonstrated both *in vitro* and *in vivo*⁸²⁻⁸⁴. It was demonstrated that after intra-peritoneal injection, CPP fusion proteins can be observed in almost all tissues in mice, including the brain⁸⁴. After that, a vast amount of researches on CPP-based delivery has emerged with the endeavors to treat various diseases including cancer, neurodegeneration, asthma, ischaemia, autoimmunity and diabetes⁸⁵⁻⁸⁷. The *in vivo* administration route has also been extensively explored, with success achieved in intratumoural, intravenous and intratracheal injections, as well as transduction into oocytes, nasal sprays or transdermal delivery^{87,88}.

The cellular uptake mechanism of CPP-protein delivery agent has been extensively studied. It is now generally accepted that CPP-mediated protein delivery relies on the binding with heparin sulfate proteoglycans displayed on cell surface⁸⁹, which is consistent with other cationic delivery vehicles⁹⁰. Upon binding with the anionic proteoglycans, endocytosis is triggered to import CPP-protein delivery agent into cells. The specific pathway of the endocytosis, however, appears to be case specific, depending on cell and cargo type, as well as CPP sequence. Caveolae-mediated endocytosis was found to be related to GFP-TAT fusion proteins⁹¹, in accordance with the TAT-mediated cellular uptake route of virus particles⁹². Wadia and coworkers' suggestion on the endocytosis pathway of TAT-fusion proteins, however, partially conflicts with the findings with TAT-EGFP. With fluorescence labeled TAT-Cre recombinase

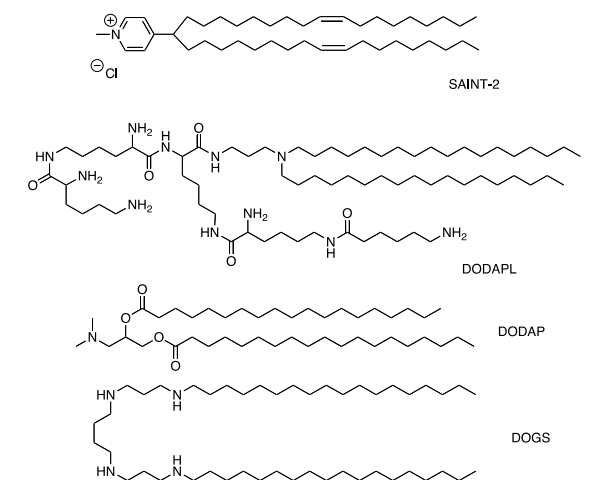
fusion protein, they found that TAT-fusion protein is internalized by cells via lipid raft-dependent macropinocytosis⁹³. Besides the cargo-specificity, cell type also affects the uptake pathway. In T cells, uptake of the Tat protein was proved to be mainly via clathrin-mediated endocytosis⁹⁴, disagreeing the other observations.

2.2. Liposome mediated Intracellular Protein Delivery

Liposomes, a class of lipid-based vesicles ranging from tens to thousands of nanometers in diameter, have been broadly used for drug delivery since the first observance several decades ago^{95,96}. In a typical liposomal delivery system, proteins are incorporated within vesicles where the lipid bilayers facilitate translocation of the protein cargo into cytoplasm or lysosomes. Table 3 lists some commonly used lipid molecules, including neutral lipids, pH-responsive lipids, and cationic lipids. The pH-sensitive lipids, in particular, contain carboxyl moieties that may be protonated or deprotonated in response to the pH of the local environment, and therefore facilitate release of their protein cargo.

Table 3 Lipids used for composing liposomes for protein delivery

Neutral lipid	
	DOPE
	DOPC
pH-responsive lipid	
	CHEMS
	DOSG
Cationic lipid	



Cell uptake of liposomes is generally believed to be mediated by the adsorption of liposomes onto cell surfaces followed by an endocytotic process. Using liposomes composed of neutral lipids, it was demonstrated that prolidase could be delivered into fibroblasts with retained activity and undetectable toxicity⁹⁷. The protein cargo, however, may be easily trapped within lysosomes due to poor endosomal escape ability⁹⁸. Therefore, therapeutic applications of neutral liposomes are limited to lysosome-related diseases, such as lysosome storage diseases.

To improve their endosomal escape capability, pH-responsive liposomes were formed from mixtures of pH-responsive lipids and neutral lipids. As shown in Figure 1, upon endocytosis, proton-induced liposome fusion⁹⁹ occurs between liposomes and cell endosomes. At the same time, in response to the acidic endosomal environment upon endocytosis, protonation of carboxyl moieties reduces the hydration capability of the lipid molecules, which helps to destabilize the liposomes and release their protein cargo into cytoplasm¹⁰⁰⁻¹⁰². To date, pH-responsive liposomes have been used to deliver various proteins, such as antigens⁹⁸ and superoxide dismutase¹⁰³. It is worth mentioning that pH-responsive liposomes were also used to deliver protein-polymer assemblies with enhanced delivery efficiency¹⁰⁴.

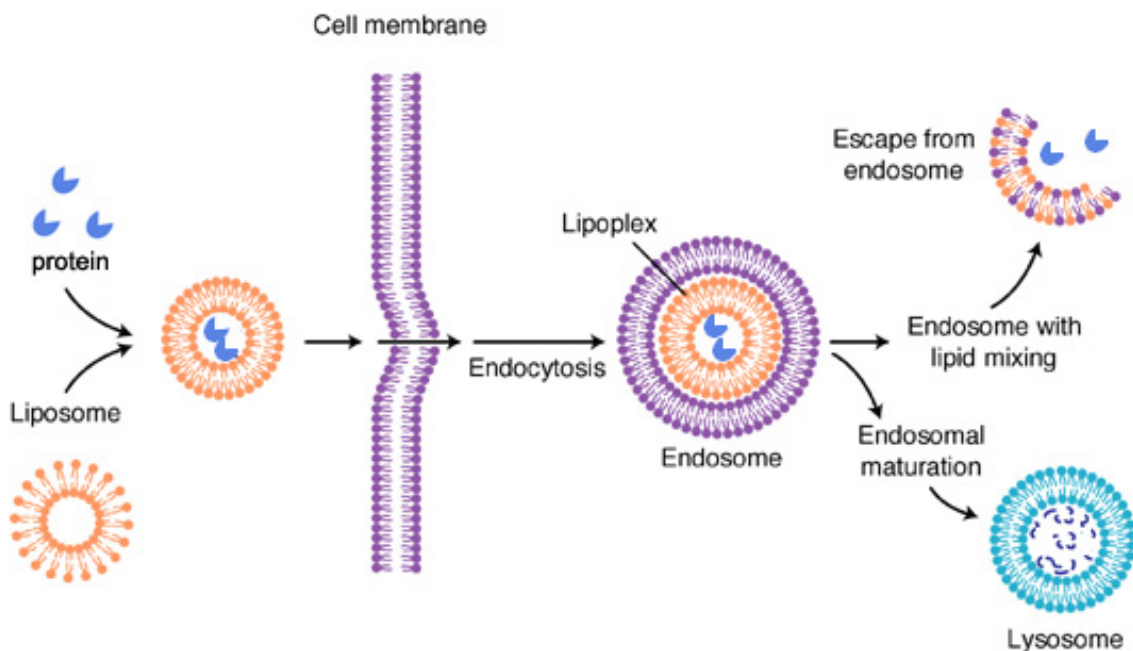


Figure 1 Illustration of liposome-mediated intracellular protein delivery and endosomal escape

To achieve effective protein delivery, enhancing cell-uptake efficiency of liposomes is essential. Toward this goal, cationic liposomes formed from mixtures of cationic and neutral lipids were developed to facilitate their binding to cell membranes and endocytosis¹⁰⁵. Most of the cationic lipids are capable of triggering protein release after endocytosis, owing to the increased protonation of cationic lipids in acidic environment. For example, cationic liposomes constructed from TFA-DODAPL and DOPE (see Table 1) were used to deliver β -galactosidase and caspases intracellularly with retained activities¹⁰⁶. The majority of the internalized proteins were distributed within the cytosol, indicating successful release of the proteins during endocytosis. Cationic liposomes containing lipospermine (DOGS, Table 1) were also used to deliver anionic proteins into the cytoplasm¹⁰⁷. Such protein-loaded liposomes were shown to enter cells via interaction with ubiquitously expressed syndecans followed by endocytosis. Although some cationic liposomes are commercially available for laboratory use¹⁰⁶, their clinical

use is still premature due to their incompatibility with serum proteins and poor in-vivo stability. Recently, the cationic amphiphilic lipid, SAINT-2 (N-methyl-4(dioleoyl)methyl- pyridinium-chloride, Table 1), was shown to form liposomes for protein delivery in the presence of serum¹⁰⁸. In this case, the cell uptake efficiency was not influenced by the size or charge of the liposomal protein complex. Despite the high delivery efficiency, cationic liposomes show certain degree of cytotoxicity¹⁰⁹, which might be related to apoptosis induced by their cationic moiety.

To further enhance liposomes' cell uptake efficiency, cell-penetrating peptides (CPPs) were conjugated to liposomes. The first example of CPP-conjugated liposomes was reported by Torchilin *et al.*¹¹⁰, where TAT (a cell penetrating peptide derived from HIV virus with sequence of GRKKRRQRRRPPQ) was conjugated to liposomes with a short poly(ethyleneglycol) (PEG) as a spacer. Proteins such as BSA, β -galactosidase and IgG were delivered with high efficiency using other CPP-modified liposomes, such as oligoarginine-modified liposomes¹¹¹. Note that, in this case, proteins were absorbed on the surface of the liposomes rather than entrapped within the liposomes; delivery efficiencies were found to be related to the length of the oligoarginines. In addition to CPPs, antibodies¹¹²⁻¹¹⁴, folic acid¹¹⁵ and transferrin^{114,116} were also conjugated to liposomes to facilitate their internalization and tissue-specific targeting. Moreover, to realize targeted delivery, TAT and antibodies were conjugated to liposomes with short and long PEG spacers, respectively. TAT was therefore embedded within and shielded by the long PEG chains containing acid-labile linkers. Mediated by antibody, the liposomes could be delivered to tumor cell surfaces. The long PEG chains were then cleaved off to expose the TAT moieties and facilitate their endocytosis¹¹⁷, realizing specific targeting and enhanced transduction at the same time.

2.3. Polymer Mediated Intracellular Protein Delivery

Synthetic polymers with designed composition and function are attractive vectors for protein delivery^{118,119}. In fact, PEG has been conjugated to proteins to extend the circulation time of protein drugs since the 1970s¹²⁰, and hydrogels¹²¹ have been used to control the release of protein drugs. Polymeric protein delivery systems generally rely on the formation of micrometer- or nanometer- size polymer particles containing protein cargo. Based on their synthetic process and structure, such system can be classified into noncovalent and covalent delivery systems.

In noncovalent delivery systems, delivery particles are synthesized by assembling polymer and protein cargo through noncovalent interactions, such as hydrophobic interactions, hydrogen bonding, and electrostatic interactions. Polymers with a variety of structures and morphologies, such as block copolymers containing a PEG block and a polycationic block, lipidic dendrimers, amphiphilic polycarbonhydrates containing cholesterol moieties, hyperbranched polyhydroxyl (HBPH) polymers, poly(butylcyanoacrylate) (PBCA) nanoparticles, and linear polyethyleneimine (PEI) with infinity tags, have been used to form protein-polymer complexes (Figure 1)¹²²⁻¹³⁰. Based on their assembly processes, noncovalent delivery system can be divided into two categories.

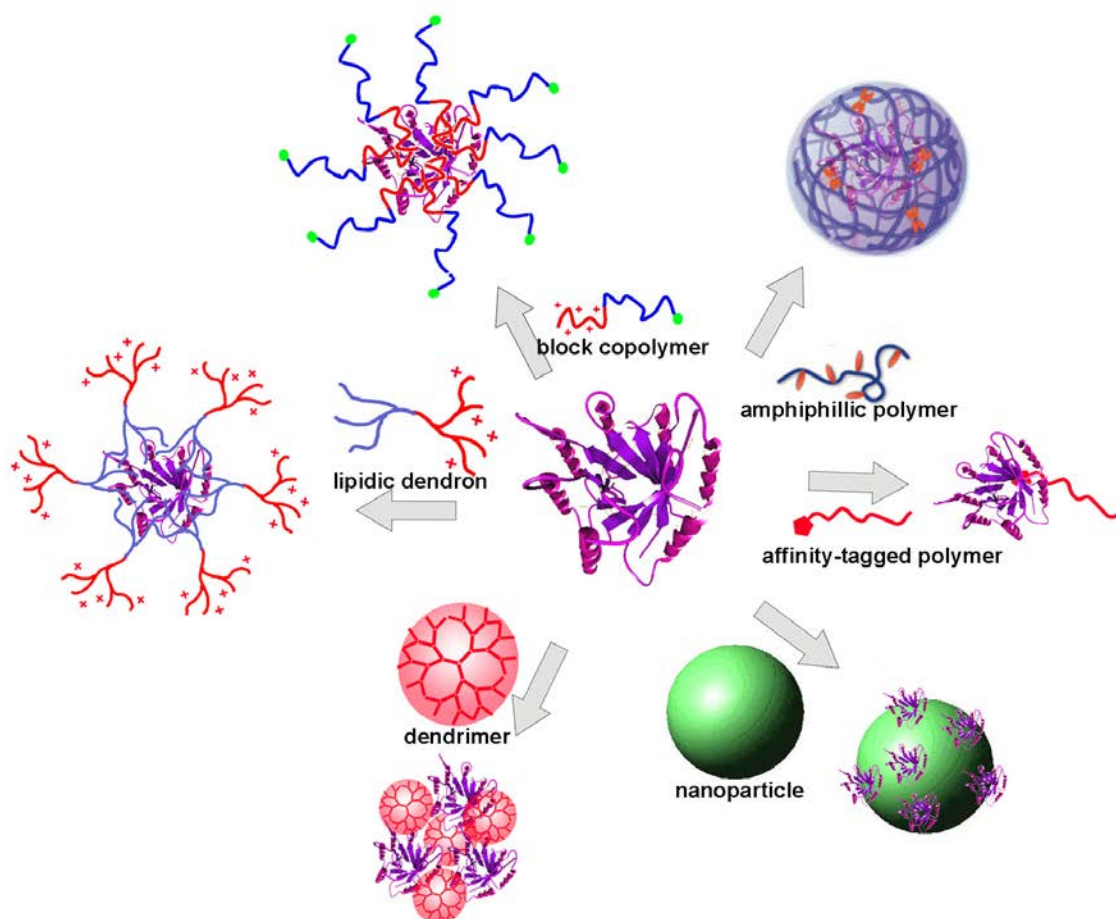


Figure 2 Schematic illustration of the noncovalent polymer delivery system

In the first category, proteins are adsorbed onto polymer particles or dendrimers. For example, PBCA nanoparticles have been used to deliver proteins across the blood brain barrier¹²². In that study, proteins were adsorbed onto nanoparticles and entered neuronal cells via lipoprotein receptor-mediated endocytosis. Similarly, mixing glutathione S-transferase (GST) with cationic dendrimers led to formation of polydisperse complexes with diameters centered at 36 nm. The positive charge on the dendrimers greatly facilitated their cellular uptake. This delivery approach was also extended to the delivery of luciferase and antibodies¹²³. It has also been claimed that HBPH could encapsulate proteins inside its amphiphilic nanocavities¹²⁴. By assembling cytochrome C with folate-conjugating HBPH, monodisperse nanoparticles with a

mean diameter of 63 nm were obtained. Since the size of HBPH dendrimer (Mwt = 36400 Da) is around 5 nm, the complex formed should be an assembly of multiple HBPH dendrimers and multiple proteins.

In the second category, polymers with heterogeneous molecular structure were used. During their assembly process with protein molecules, a section of the polymer chain complexes with the protein through electrostatic interactions, hydrophobic interactions or other noncovalent interactions. The other section of the polymer helps to stabilize the complexed structure, resulting in stable protein-polymer complexes in solution. Among many cases, formation of protein-polymer complexes from block copolymers containing a cationic block and a PEG block is particularly common. The cationic block effectively binds with anionic proteins via electrostatic interaction, while the PEG block forms an exterior hydration layer that stabilizes the complex structure. Moieties that facilitate cell uptake or targeting capability can also be linked to the end of the PEG block (Figure 2). This design provides an effective approach for protein delivery. For example, Kim et al. synthesized polylysine-co-poly(ethylene glycol) (PLL-PEG) block copolymer with folic acid linked to the end of the PEG chains. Complexing such copolymer with anionic proteins resulted in delivery vessels with enhanced cellular uptake¹²⁵. However, such a technique may be limited to anionic proteins and the stability of the micellar complex is heavily dependent on the surface charge of proteins. To overcome this limit, lysine groups on proteins were modified with citraconic acid or cis-aconitic acid, forming acid-labile amide bonds, which can be degraded in acidic endosomal environment upon endocytosis^{126,127}. Such molecular modification provides enough negative charge to enable the formation of protein-polymer complexes. Additionally, it also enables responsive release of cargo proteins intracellularly.

Similarly, proteins can be readily complexed to the hydrophobic moieties of amphiphilic polymers through hydrophobic interactions. For example, cholesterol-bearing pullulan (CHP) or its derivative CHPNH₂ were assembled with proteins, resulting in the formation of cationic nanocapsules with diameters less than 50 nm¹²⁸. In this case, hydrophobic domains formed by the cholesterol moieties on the polymer chains served as complexing sites for the proteins. Enhanced cellular uptake, as well as retained intracellular enzymatic activity, was reported. Effective endosomal release of the proteins was also observed 18 hours after transduction.

In addition to non-specific assemblies mediated by electrostatic force or hydrophobic/hydrophilic interactions, more specific affinity bindings were also utilized to form protein-polymer complexes. For example, PEI-glutathione conjugates could bind with glutathione S-transferase-fused proteins and induce cellular uptake in mammalian cells¹²⁹. The affinity binding approach has the advantage of minimized protein denaturation and well-controlled complex structure. However, its application is still limited to proteins that are able to fuse with their binding ligands.

Overall, noncovalent polymeric delivery systems provide a facile strategy for intracellular protein delivery. Stability of the assembled complexes, as well as protein denaturation during complexing, is still problematic. In fact, the complexes may rapidly dissociate upon dilution in vivo¹³⁰. Competitive binding of serum proteins with polymer vectors may also lead to rapid complex dissociation. Moreover, strong interactions between polymers and proteins may alter the protein structures. For example, the Tajmir-Riahi group performed detailed studies on the complexes of dendrimer and BSA¹³¹ and found that BSA conformation was altered, with a major reduction of α -helix and an increase in random coil and turn structures observed upon complexing.

A two-sided dilemma confronts the noncovalent approach: weak noncovalent interactions make the complexes vulnerable to dissociation while strong noncovalent interactions may cause denaturation. Applying an additional crosslinking process after complex formation may stabilize the complexes. Recently, the Murthy group reported disulfide-crosslinked poly(ethylene glycol)-block-poly(L-Lysine) (PEG-PLL) protein assemblies as a protein delivery system. In this work, after complexing poly(ethylene glycol)-block-poly(L-lysine-dithiopyridine) (PEG-PLDTP) with proteins, 3,6- dioxo-1,8-octanedithiol was added to crosslink the complex. The disulfide crosslinking provided stability to the assembled complexes and protected them from serum degradation. In addition, the disulfide bonds are designed to be cleaved by intracellular reducing agents for more effective protein delivery¹³².

In a covalent polymeric delivery system, polymer and protein are connected through covalent bonds, providing significantly enhanced stability. In 2005, Futami et al. first reported conjugates of cationic PEI with protein for intracellular protein delivery¹³³. Enhanced green fluorescent protein (EGFP) conjugated with PEI shows orders of magnitude higher cell uptake than TAT-EGFP fusion proteins. When similar conjugation was performed on ribonuclease (RNase), the cytotoxicity of RNase increased dramatically. Additionally, the cytotoxicity of PEI-RNase was found to relate to the length of PEI chains on the RNase surface, validating the authors' claim about PEI's role in cellular uptake of PEI-protein conjugates.

Such a strategy was also extended to deliver antibodies with the capability to bind antigens. For example, biotin and antibodies were conjugated to PEI, respectively; after binding with streptavidin- or protein G-conjugated proteins, the PEI conjugates were delivered into cells with high efficiency¹³⁴. β -catenins were also delivered via conjugation with PEI with high efficiency; as delivered proteins could activate the Wnt canonical signaling pathway (a pathway

that contributes to the self-renewal of mouse hematopoietic stem cells)¹³⁵. In addition to the permanent conjugation of the polymer and protein, cleavable disulfide bonds were also used to form cleavable conjugates. For example, conjugates of PEI and denatured p53 were delivered into cells. Upon endocytosis, the PEI chains were cleaved off and the unfolded proteins could refold to their native form¹³⁶.

As a conclusion, protein therapy, endowed with a more defined action mechanism than small molecule drugs and safer administration than gene therapy, harbors great promises for the treatment of many diseases. In recent years, the market penetration of the pharmaceutical protein industry has already started to gain momentum. Up to now, over 140 FDA-approved protein drugs have been placed on the market, and more are coming. Despite its fast growth in the recent years, protein therapy, especially that with intracellular therapeutic targets, is still in its adolescence, mainly owing to the incapability to deliver functional proteins inside cells.

Various intracellular delivery carriers for protein drugs have been developed during decades. Pros and cons exist simultaneously in each of the delivery systems, though. CPP-fusion proteins, although have been extensively studied, are associated with limitations such as vulnerability to protease, limited transduction efficiency, and toxicity. Liposomes, despite its relatively long history of investigation, are commonly associated with unresolved issues such as low delivery efficiency and low in-vivo stability, rendering them a less competitive strategy. Polymeric delivery systems, despite certain disadvantages such as toxicity for some polymers, hold great potentials, since it is relatively easy to synthesize biocompatible nanocarriers with designed functionality and structure.

An ideal protein delivery system should satisfy many criteria not limited to efficient cellular uptake, minimized toxicity, high stability in serum and ability to target subcellular compartments. When these requirements are met, we are likely to see more protein pharmaceuticals on the market in the foreseeable future. Effective integration of knowledge from chemistry, material science, biology, medical science and other fields may provide effective design tools and concepts for the successful protein delivery.

Chapter 3. Fabrication of Single Protein Nanocapsules

3.1. Introduction

In my research, we developed a strategy to simultaneously solve the stability issue and to install novel functions on the protein. Our design concept resembles the natural theme in virus capsid and cell membrane. Viruses and cells enclose their main biological functionalities inside their interior with a shell composed of protein or lipid membrane to protect the internal structure. At the same time, the surface is functionalized with signaling and targeting moieties, responsible for the interaction with exterior environments. In our design, similar with the theme in viruses and cells, we designed a protein-polymer core-shell structure to give protein a “nanocapsule” (Figure 3).

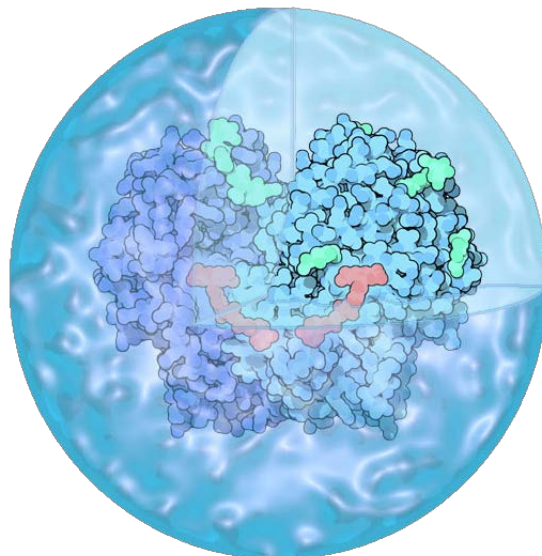


Figure 3 Schematic illustration of a protein nanocapsule

The synthesis of such structure is achieved by aqueous *in-situ* polymerization on protein surface.

Enzyme nanocapsules offer a series of unique characteristics: 1) Multi-covalently attached polymer layer stabilizes the protein 3D structure; 2) Hydrophilic polymer layer offers an environment resembling physiological environment, providing proteins the resistance against denaturation; 3) Net-like polymer allows the free diffusion of substrates and products of enzymes; 4) The nano-scale size is suitable for a wider range of applications compared with bulk immobilized proteins; 5) The polymer layer offers a platform to engineer the surface properties of enzyme without interfering enzyme's intrinsic activity.

3.2. Experimental

Modification: one milligrams of protein in 0.2 mL of pH 8.0 20 mM borate buffer was reacted with a defined amount of 10% N-acryloxysuccinimide (NAS) in DMSO for 2 h at 4 °C. The ratio of NAS to protein typically varies from 5 to 100. After that, the reaction solution is thoroughly dialyzed against pH 7.0 20 mM phosphate buffer with a CE dialysis membrane with MWCO of 10 kDa. To modify the carboxylic groups, 1 mg of protein in 1 mL 20 mM pH 6.0

MES buffer added in a glass vial with stir bar. To this solution, *N*-(3-Aminopropyl) methacrylamide hydrochloride (100x mole ratio), *N*-hydroxysuccinimide (10x mole ratio), and *N*-(3-Dimethylaminopropyl)-*N'*-ethylcarbodiimide hydrochloride (100x mole ratio) is added subsequently. The reaction is stirred gently at 4 °C for 2 hours and dialyzed against 20 mM pH 7.0 phosphate buffer with a CE dialysis membrane with MWCO of 10 kDa to remove the unreacted reagents.

Polymerization: To a 1 mL acryloylated protein solution at 1 mg/mL, appropriate amounts of backbone monomer (eg. Acrylamide, AAm), crosslinker (eg. Bisacrylamide, BIS), and co-monomer (eg. 2-dimethylaminoethyl methacrylate, DMAEMA) are added during gentle stirring. Then specific amounts of ammonium persulfate (APS) and *N,N,N',N'*-tetramethylethylenediamine (TEMED) are added to initiate the reaction. The reaction is allowed to proceed for 2 hours at room temperature. Finally, dialysis against 20 mM pH 7.0 phosphate buffer is used to remove monomers and initiators with a CE dialysis membrane with MWCO of 10 kDa.

MALDI-TOF Spectroscopy: The degree of modification is measured using matrix assisted laser desorption/ionization–time of flight (MALDI). Briefly, 1 µL of 1 mg/mL MSA in 10mM phosphate buffer pH 7.0 should be mixed with 9 µL of 10% w/v sinapinic acid (in 30% v/v acetonitrile/water solution with 0.1% v/v trifluoroacetic acid). A droplet of 2 µL of the resulting solution is on a KFF Gold plate. After the droplet is dry, load the into an Applied Biosystem Voyager-DE-STR MALDI-TOF mass spectrometer. The spectrum is measured under a linear mode with 25000 acceleration voltage, 90% grid and 400 ns delay time.

Infrared spectra acquisition: Fourier Transformed Infrared Spectroscopy (FT-IR) for native OPH, acrylated OPH, nOPH(AAm) and nOPH(APm-AAm) were acquired with KBr disks on a JASCO FT/IR-420 spectrometer.

TEM: TEM samples were prepared by drop-coating of 2 μ L nanocapsules solution onto carbon-coated copper grids. Droplets of samples were contacted with the grids for 45 s; then excess amount of samples was removed. The grid was then rinsed, and stained with 1% sodium phosphotungstate at pH 7.0 for 2 min. For better imaging, silver enhancement of AuNPs was performed prior to observation with TEM. Briefly, AuNP-labeled nHRP solution was first contacted with a TEM grid for 45s. After rinsing with deionized water, the grid was floated on a drop of freshly prepared silver enhancement reagent (Nanoprobe, NY) for 1 min. The grid was then rinsed again, followed by staining with 1% sodium phosphotungstate at pH 7.0.

Size and zeta potential measurements: DLS Measurements of nanocapsules were taken with a protein concentration of 1 mg/mL in 10 mM phosphate buffer with a Malvern Zetasizer Nano.

Agarose gel electrophoresis: 0.7 % (w/v) agarose gel is prepared in pH 7.2 1 \times TAE buffer. Protein nanocapsule sample with concentration of 0.2-1 mg/mL is mixed with 20% glycerol with a volume ratio of 9:1 and loaded in the gel. Electrophoresis is conducted with an Edvoket M12 electrophoresis cell under constant voltage of 110 V for 15 min.

3.3. Synthetic Approach and Structural Characterization

In general the synthetic approach of protein nanocapsules follows a two-step protocol. As illustrated in Figure 4, the first step involves modification of the enzymes with polymerizable moieties and the second step is the formation of polymer shells around each of the modified protein to the construct a single-protein nanocapsules (termed nProtein hereafter).

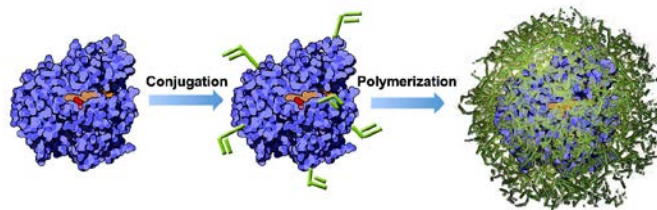


Figure 4 Schematic illustration of the synthetic approach of protein nanocapsules

Synthesis Step I: Enzyme generally contains surface amino acids, among which lysine, cystine, glutamic acid or aspartic acid are commonly present and can be used for conjugation to various molecules. In our research, we can use either lysine group or glutamic acid/aspartic acid for the conjugation of polymerizable acryl groups (Figure 5). However, modifying amino acid residues on proteins may cause decreased activity, especially when the active site of the enzyme contains reactive amino acids. Therefore, having multiple options for modification gives us better chances to preserve the active site. For example, superoxide dismutase (SOD) harbors lysine residual in its active site. Modifying lysine groups causes total loss of SOD activity. Modifying carboxylic groups, instead, preserves 90% of the original SOD activity.

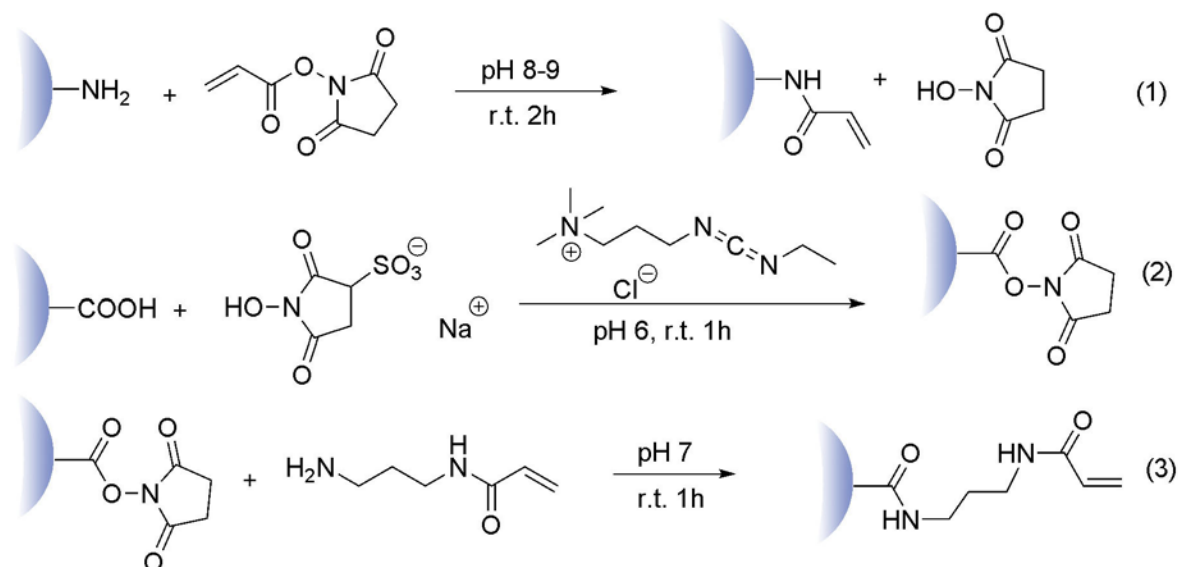


Figure 5 Synthetic methods to conjugate acryl groups onto enzymes

In a typical modification step, N-acryloxysuccinimide (NAS) is used to modify the amine groups on protein. The ratio of NAS to protein typically varies from 5 to 100. To modify the carboxylic groups, *N*-(3-Aminopropyl) methacrylamide hydrochloride (100x mole ratio) is conjugated to the protein via EDC/NHS chemistry. After the reaction is complete, the conjugated protein is purified via dialysis.

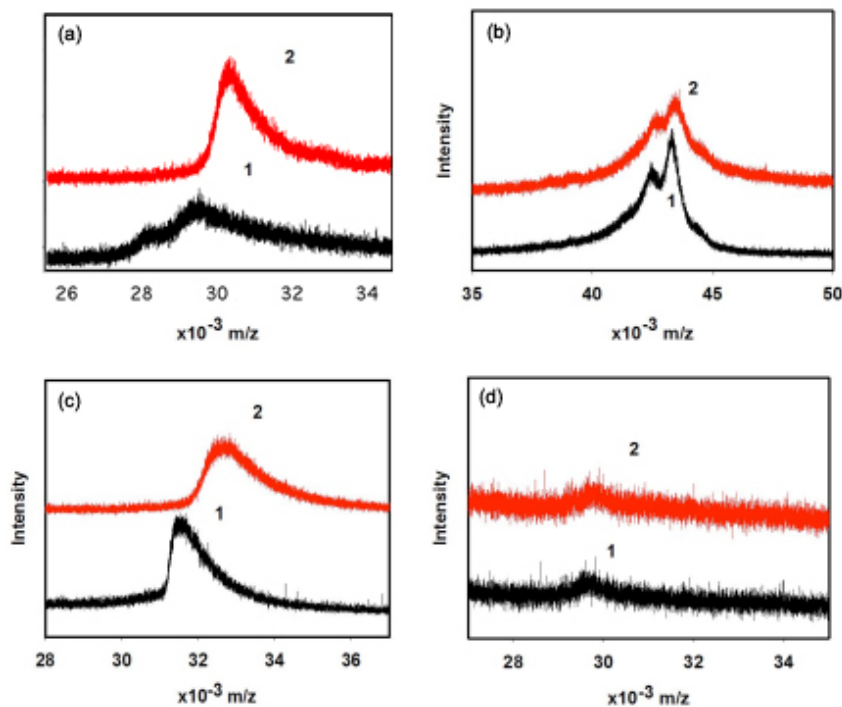


Figure 6 MALDI-TOF mass spectra of proteins before and after modification with N-acryloxysuccinimide (NAS): (a) native EGFP and modified EGFP, (b) native HRP and modified HRP, (c) native SOD and modified SOD, (d) native Caspase-3 and modified Caspase-3

The degrees of modification can be measured using MALDI-TOF mass spectroscopy. Figure 6 is the MALDI-TOF mass spectra of native and modified proteins. In these cases, EGFP, HRP and caspase 3 were reacted with NAS to modify amine groups, whereas SOD is carboxylic-modified. In each of the unmodified/modified pairs, a clear molecular weight increase can be visualized. A quantitative calculation presents the average number of modification on each protein (Table 4).

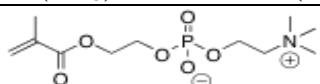
The residual activities after modification are also presented in this form, indicating minimized loss of activity due to the modification.

Table 4 Molecular weight of proteins before and after modification with N-acryloxysuccinimide (measured with MALDI-TOF mass spectrometer)

Name	Molecular Weight (MALDI-TOF MS)	Molecular weight increase	Number of vinyl groups	Residual activity (%)
Native EGFP	29422	-	-	-
EGFP modified with N-acryloxysuccinimide	30352	930	17.2	-
Native HRP	43248	-	-	100
HRP modified with N-acryloxysuccinimide	43512	264	4.9	98
SOD	31469	-	-	100
SOD modified with N-acryloxysuccinimide	32543	1073	8.6	90
Native caspase 3	59128	-	-	100
Caspase 3 modified with N-acryloxysuccinimide	59650	522	9.8	91

Additionally, the number of acryl groups per protein can be finely tuned by adjusting the amount of reagents added into the modification step. With this strategy, the modification degree can be controlled to avoid significant inactivation of protein. Take AKR1C4 (aldo-keto reductase family 1 member C4) as an example. Although AKR1C4 does not contain lysine residue in active site, it is sensitive to the modification of lysine residuals, possibly due to destabilization of its 3D structure caused by lysine modification. To preserve the bioactivity of AKR1C4, the correlation between number of modified lysine and the activity of AKR1C4 was explored. We demonstrated that we could form acrylated AKR1C4 by increased molecular weight determined by MALDI-TOF mass spectroscopy (Table 5 ,Figure 7). Additionally, controlling the number of modified amine groups under 5 leads to minimized loss of AKR1C4 activity (Figure 7).

Table 5 The molar ratio of NAS added to enzyme and the corresponding number of acryl groups attached to each enzyme

Positively charged	<i>N</i> -(3-Aminopropyl) methacrylamide Dimethylamino ethyl methacrylate	$\text{CH}_2=\text{C}(\text{CH}_3)\text{CONH}(\text{CH}_2)_3\text{NH}_2$ $\text{CH}_2=\text{C}(\text{CH}_3)\text{COCH}_2\text{CH}_2\text{N}(\text{CH}_3)_2$
Zwitterionic	2-methacryloyloxyethyl phosphorylcholine	

A detailed synthetic protocol can be depicted as follows. To a 1 mL acryloylated protein solution at 1 mg/mL, appropriate amounts of backbone monomer (eg. Acrylamide, AAm), crosslinker (eg. Bisacrylamide, BIS), and co-monomer (eg. 2-dimethylaminoethyl methacrylate, DMAEMA) are added during gentle stirring. Then specific amounts of ammonium persulfate (APS) and *N,N,N',N'*-tetramethylethylenediamine (TEMED) are added to initiate the reaction. The reaction is allowed to proceed for 2 hours at room temperature. Finally, dialysis against 20 mM pH 7.0 phosphate buffer is used to remove monomers and initiators.

Several criteria apply when determine the amounts of reagents we chose, which are listed as follows:

- The mole ratio of monomer mixture (including backbone monomer and co-monomer) to protein is between 2000 and 8000. Too little monomer results in failure to form polymer shell. Too much monomer, however, leads to gelation.
- The mole ratio of backbone monomer to co-monomer can be adjusted in order to adjust the amount of surface functional group or to tune microenvironment provided by the polymer shell.
- The mole ratio of monomer mixture to crosslinker typically varies from 10 to 20.
- The mole ratio of monomer mixture to APS typically varies from 10 to 20.
- The mole ratio of TEMED to APS typically varies from 2 to 10.

The successful formation of polymeric shell can be validated by a variety of characterizations. Figure 8 shows the infrared spectra of native organophosphorous hydrolase (OPH), modified

OPH, OPH nanocapsules with acrylamide (AAm) as monomer, and OPH nanocapsules with acrylamide/ *N*-(3-Aminopropyl) methacrylamide (AAm/APm) as monomers. Characteristic IR absorption (arrows in Figure 8) at 3350 cm^{-1} , 1600 cm^{-1} , 1450 cm^{-1} (for pAAm) and 1100 cm^{-1} (for pAPm) confirms the formation of polymeric shell around protein surface.

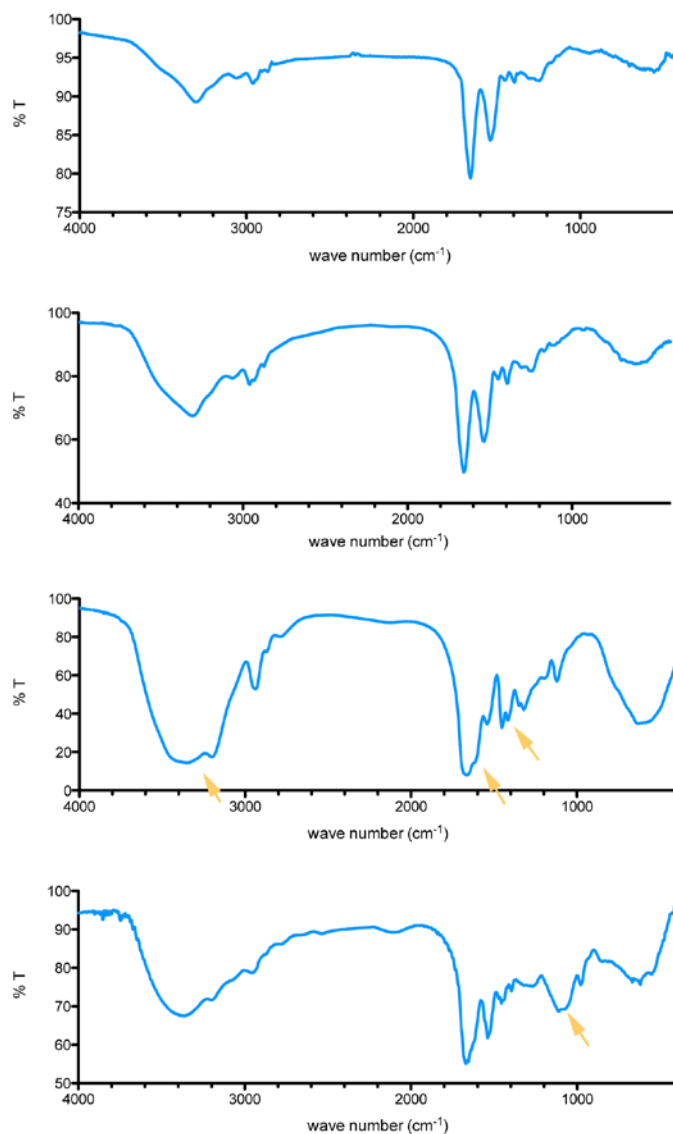


Figure 8 IR spectra of native OPH, modified OPH, nOPH(AAm) and nOPH(APm)

Besides the compositional characterization to confirm the existence of polymer chains on the protein surface, other characterization can be also used to demonstrate the formation of the

polymer shell. Dynamic light scattering, a technique to detect the hydrodynamic radius of particles in suspension is used to determine the size increase after encapsulation. In addition, the surface charge can be probed by measuring the zeta potential. Figure 9 shows the size and zeta potential distribution of native bovine serum albumin (BSA), anionic BSA nanocapsules (nBSA-AAm), and cationic BSA nanocapsules (nBSA-DMAEMA). Compared with native BSA, both cationic and anionic nBSA shows increased size. Additionally, the surface charge also alters after the encapsulation. While the native BSA exhibits a zeta potential of -10.8 ± 4.5 mV, anionic and cationic nBSA display zeta potential of -13.9 ± 5.3 mV and $+15.1 \pm 3.4$ mV, respectively. The significantly altered size and zeta potential clearly demonstrate the successful formation of the polymeric shell around the protein.

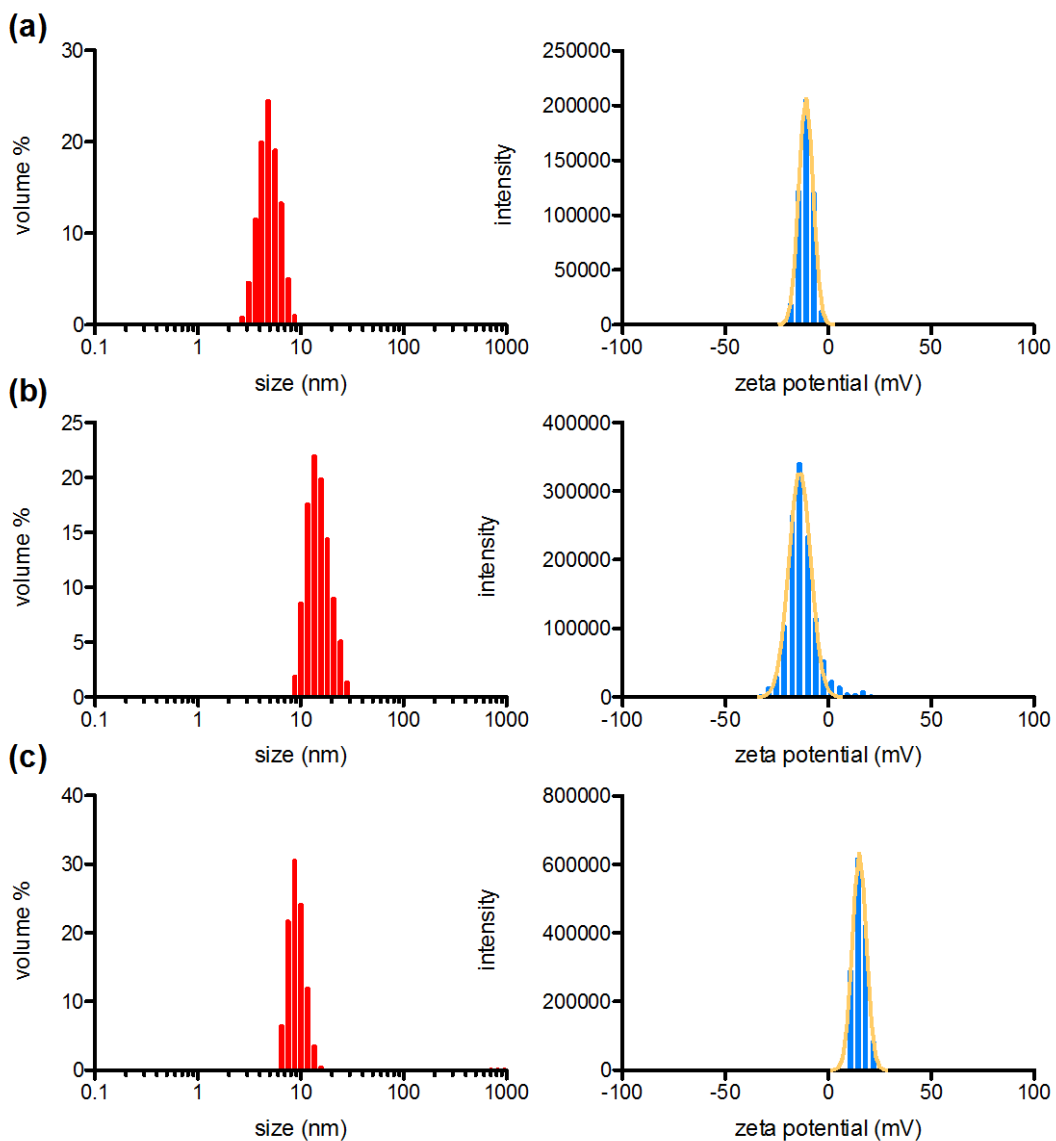


Figure 9 size and zeta potential distribution of (a) native BSA, (b) nBSA-AAm and (c) nBSA-DMAEMA

Agarose gel electrophoresis is also used to verify the formation of the nanocapsule and the change in size and surface charge after encapsulation. Electrophoresis is an analytical technique typically used to separate DNA or RNA fragments. It can also be applied to separate nanoparticles by charge and size. Figure 10 shows the image of an agarose gel after electrophoresis. Similar with the native BSA, nBSA-AAm migrates to the anode, indicating a

negative surface charge. However, the rate of migration toward the anode is much slower than native BSA, possibly due to the increased size. nBSA-DMAEMA, on the other hand, exhibits different electrophoresis behavior. It migrates toward the cathode, with similar migration rate with nBSA-AAm. These observations suggest that nBSA-DMAEMA is positively charged with a radius similar with nBSA-AAm.

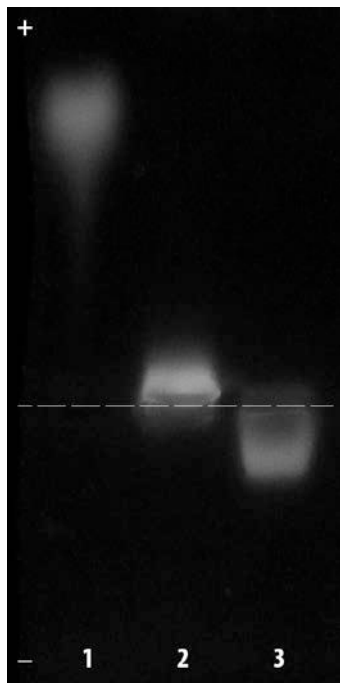


Figure 10 Agarose gel electrophoresis image of (1) native BSA, (2) nBSA-AAm, and (3) nBSA-DMAEMA. These samples were pre-labeled with fluorescein isothiocyanate.

More direct evidence of the formation of nanocapsules can be visualized under TEM or AFM. Exemplified using the synthesis of nHRP, TEM and AFM images of nHRP indicate these nanocapsules are spherical with uniform diameter around 15 nm (Figure 11), which is consistent with DSL measurement. Since the radius of a HRP molecule is around 5 nm, the average shell thickness is approximately 5 nm. By labeling each HRP molecule with a single 1.4 nm gold nanoparticle, most nanocapsules observed contain only one single gold nanoparticle, further confirming a single-protein core-shell structure (Figure 11).

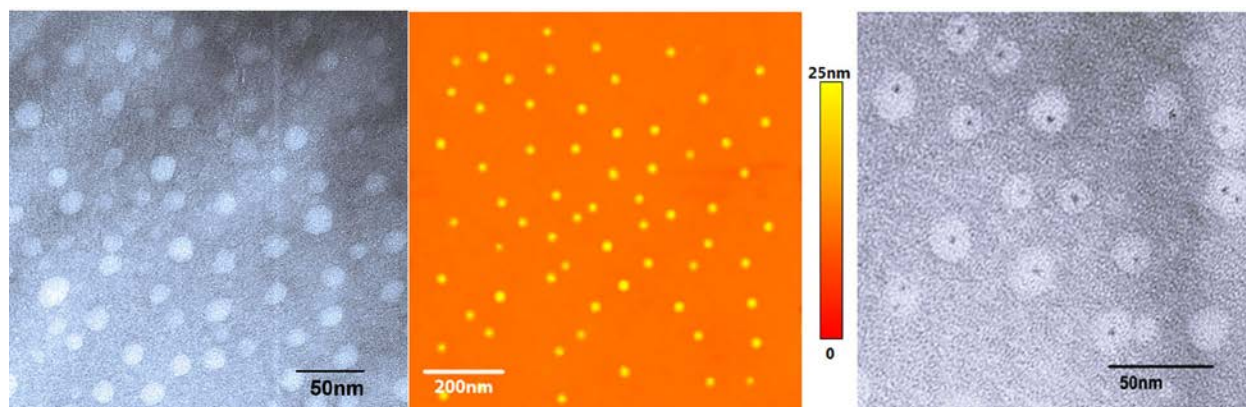


Figure 11 representative TEM and AFM images of the HRP nanocapsules and TEM image of nanocapsules containing a single 1.4 nm gold-quantum-dot-labeled HRP core

3.4. Engineerable Surface

The surface charge could also be engineered. Both anionic and cationic monomers can be incorporated onto polymer shells around enzymes, either forming a monopolymer or forming copolymers with other comonomers. Furthermore, by varying the ratio of ionic monomer versus neutral monomer, we could tune the surface charge. As shown in Figure 12a, the polyacrylamide nanocapsules are anionic, due to the sulfate groups introduced by initiator ammonium persulfate. But, with the weight ratio of DMAEMA: AAm increasing from 0:1, 1:3 to 1:1, the average zeta potential of the nanocapsules increased from -12.8 mV, 8.64 mV to 15.2 mV (Figure 12). In the case of anionic copolymer, similarly, the surface charge could be easily controlled. Figure 12b shows the correlations between surface charge and weight ratio of acrylic acid to acrylamide (AA: AAm). The zeta potential shifted to lower value as the amount of anionic monomer increased. The adjustable surface charge offers us more chance engineering our enzymes to fit certain application purposes.

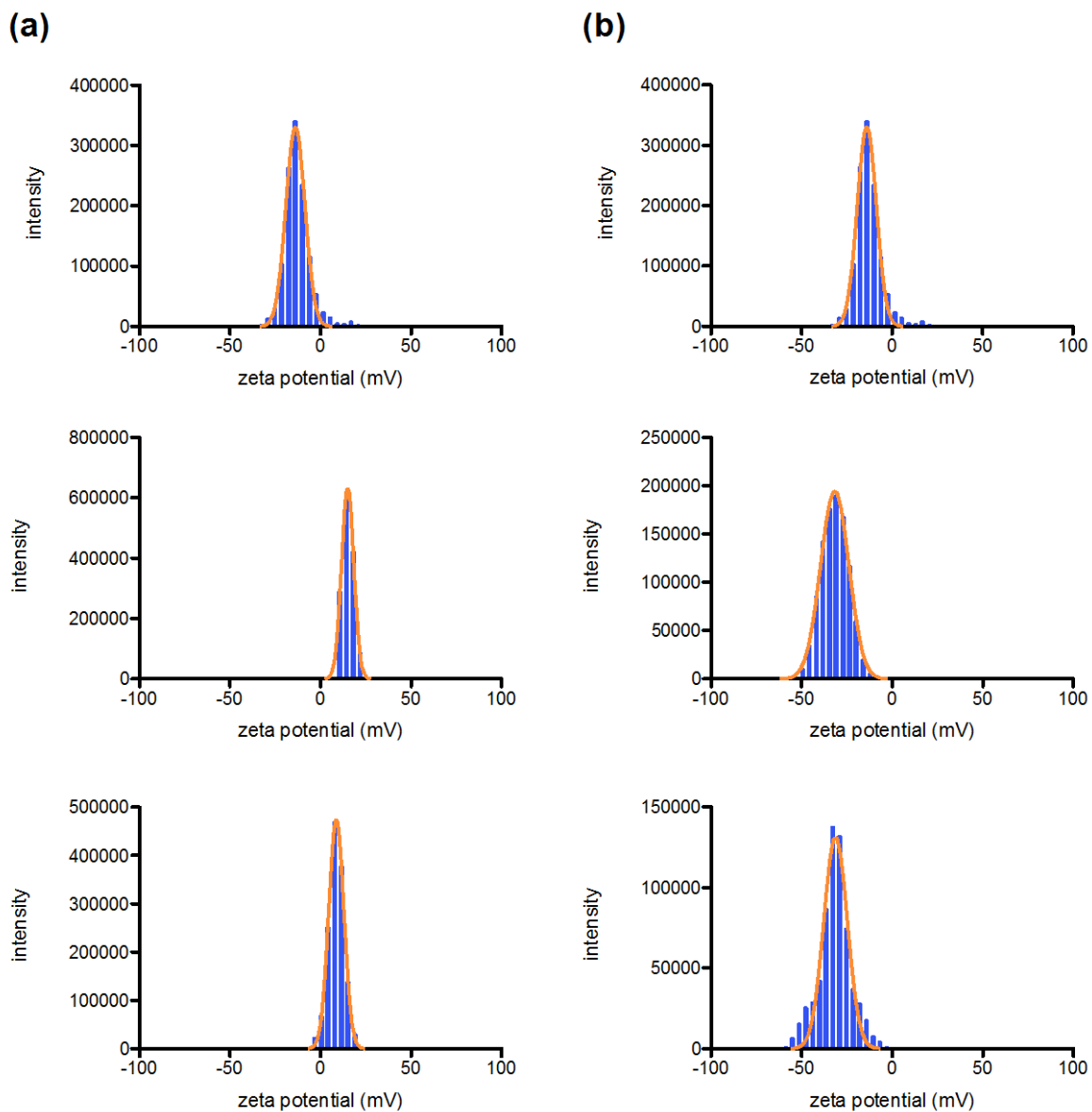


Figure 12 (a) zeta potential distribution of BSA nanocapsules with different composition: from top to bottom DMAEMA:AAm = 0:1, 1:3, 1:1; (b) zeta potential distributions of anionic BSA nanocapsules with different compositions: from top to bottom AA:AAm = 0, 1, 4

3.5. Summary

In this chapter, I present the design and synthetic route of protein nanocapsules. This strategy is based on a two-step *in-situ* polymerization on protein surface, conducted in aqueous environment at room temperature. The first step involves the conjugation of polymerizable groups on protein surface. The increased molecular weight can be detected by MALDI-TOF spectroscopy. By varying the amount of conjugation reagents, protein conjugate with different conjugation degree can be obtained. The second step is an aqueous free radical polymerization, in which a thin layer of polymer network is formed on protein surface. The successful formation of the polymer layer is confirmed with IR spectroscopy, dynamic light scattering, agarose gel electrophoresis, and transmission electron microscopy. The composition of the polymer layer can be readily adjusted by changing the monomer added in the polymerization. In addition, the surface function can be finely tuned by incorporating copolymerization and varying the ratio between co-monomers.

Chapter 4. Bioactivity of Nanocapsules

4.1. Introduction

Proteins perform various biological functions in every organism, ranging from catalysis to signaling. The demand to study protein structure and functions and, more recently, to use them as for new therapeutics and materials has created an increasing need for chemical conjugation and protein immobilization. A significant reduction in apparent enzyme activity, however, is often observed in enzyme modification, immobilization or encapsulation. The loss of activity is mainly attributed to the following causes¹³⁸. First, functionalization of the critical amino acid causes inactivation of the active site or destabilization of the 3D conformation. Second, the rigid matrix used for immobilization hinders the substrate accessibility to the enzyme. Third, the rigid matrix also restricts the enzyme conformation change required in the reaction. In comparison, the

encapsulation in the nanocapsule we developed has only posed a minor effect on the apparent activity of the enzyme, owing to the mild reaction condition we used for the synthesis and the excellent permeability and elasticity of the thin polymer network formed on the protein surface. Beyond the well-retained activity, the nanocapsule technique harbors a unique property that can be hardly realized with other protein-conjugation technique. We discovered that the polymer largely contributes to the microenvironment of the core protein, in spite of the environment in the bulk solution.

4.2. Experimental

Horseradish peroxidase activity assay: During a run, 0.9 ml of pH 5.5, 100mM phosphate citrate containing 1.1mM H₂O₂, 0.05 ml of 0.02 M H₂O₂, and 10uL of 0.2μg/mL HRP was added into a test tube. The reaction was initiated by adding 0.05 ml of DMSO containing 0.02 M 3,3',5,5'-tetramethylbenzidine (TMB) and monitored at 655 nm. The oxidation rate of TMB is interpreted from slope of the initial linear parts of the adsorption curve at 655nm using a molar absorption coefficient (39,000 M⁻¹cm⁻¹) for the oxidation product of TMB.

Glucose oxidase activity: Glucose oxidase assay is conducted in 50 mM pH 5.1 sodium acetate buffer containing 0.17 mM o-Dianisidine and 1.72% glucose (w/v). Fresh-prepared HRP solution is added to the mixture to reach a final concentration of 0.01 mg/mL. Then GOx (0.4-0.8 U/mL) is added to the mixture and the absorbance at 500 nm is monitored with a UV-Visible spectrometer.

Activity of Enhanced green fluorescence protein and mCherry: The activities of eGFP and mCherry is determined with fluorescence. The protein or nanocapsule is diluted with 20 mM pH 7.0 phosphate buffer to a final concentration of 0.01 – 0.1 mg protein/mL. The fluorescence with

$\lambda_{\text{ex}} = 485 \text{ nm}$, $\lambda_{\text{em}} = 535 \text{ nm}$ or $\lambda_{\text{ex}} = 585 \text{ nm}$, $\lambda_{\text{em}} = 610 \text{ nm}$ was measured to represent the activity of EGFP or mCherry, respectively.

Alkaline phosphatase activity: To measure the activity of alkaline phosphatase, add 0.5 mL 100 mM Glycine Buffer w/ 1 mM MgCl_2 pH 10.4 into 0.5 mL 15.2 mM *p*-nitrophenyl phosphate, mix well. 0.1 mL alkaline phosphatase (0.1-0.2 U/mL) was then added to the mixture. Absorbance at 405 nm was monitored and the slope was used to quantify the activity of alkaline phosphatase.

AKR1C4 activity: Oxidation of the steroid substrate androsterone by AKR1C4 in the presence of the co factor NAD^+ was monitored spectrophotometrically @ 340nm. Each reaction well contained a total of 50 μl of reaction mixture containing 100mM potassium phosphate (pH 7.2), substrate: 80 μM androsterone and enzyme AKR1C4. All components of the reaction mixture were at room temperature and mixed well before initiation with 2.3 mM NAD^+ .

Tyrosinase activity: To a 1 ml 20 mM pH 6.5 phosphate buffer containing 0.3 mM L^- tyrosine, 50 - 100 units tyrosinase was added. The absorbance at 280 nm is immediately monitored. And the slope of the absorbance increase is used to evaluate the tyrosinase activity.

Superoxide dismutase activity: Briefly, the assay mixture contained 2.4 mL of 50 mM Tris HCl buffer containing 1 mM EDTA (pH 8.0), 300 μL of 0.2 mM pyrogallol and 300 μL enzyme source. The increase in absorbance was measured immediately at 420 nm against a blank containing all the components except the enzyme and pyrogallol at 10 s intervals for 3 min. The amount of SOD needed for 50% inhibition of pyrogallol auto-oxidation is used to evaluate the activity of SOD.

Catalase activity: 30% H_2O_2 was added to a 50 mM phosphate buffer to a final concentration of 0.036% (w/w). Determine the absorbance at 240 nm to make sure the $A_{240\text{nm}}$ is between 0.55 and

0.52. Dilute the catalase sample to approximately 100 units/mL in 50 mM phosphate buffer. After that, add 100 μ L catalase solution to 2.9 mL 0.036 % H_2O_2 and mix well. Start timing the reaction when $A_{240\text{nm}}$ reaches 0.45 absorbance units and record the time required for the $A_{240\text{nm}}$ to decrease from 0.45 to 0.40 absorbance units. The slope during this period of time is used to stand for the activity of catalase.

Firefly luciferase activity: Firefly luciferase is assayed with the Pierce Firefly Luciferase Glow Assay kit according to the manufacture's manual.

OPH activity assay: The organophosphate hydrolysis mediated by native OPH and OPH nanocapsules were determined by monitoring absorbance change at 405 nm in 50mM HEPES buffer (pH 8.5) with Paraoxon-ethyl as the substrate.

Probing local pH environment with fluorescein: To 100 μ L native OPH or nOPH solution with the same protein concentration (1 mg/mL in 10 mM pH 8.5 borate buffer), 100 μ L 9 μ M 5-Carboxy-fluorescein diacetate N-succinimidyl ester aqueous solution (prepared fresh) was added. The mixtures were stirred at room temperature in dark for 4 hours to allow complete reaction. After that, the solutions were diluted with 100 mM pH 7.0 phosphate buffer to a final concentration of 0.025 mg OPH/mL. The fluorescence intensity of each sample was measured with a plate reader ($\lambda_{\text{ex}} = 485 \text{ nm}$, $\lambda_{\text{em}} = 535 \text{ nm}$). Each data point was done in triplicate. And free fluorescein with the same concentration was used as a control.

4.3. Retained activity of nanocapsules

Encapsulation in the nanocapsule we present has posed a minor effect on the apparent activity of the enzyme. In my research, the nanoencapsulation technique has been applied to a collection of enzymes. As shown in Table 7, over 80% of original activity can be preserved after encapsulation in nanocapsules composed of polyacrylamide as the polymer shell, in spite of the

diversity in the enzyme structure. The 14 enzyme systems I used include monomeric proteins (eg. HRP), dimeric proteins (eg. GOx), tetrameric proteins (eg. Cat), metal enzymes (eg. SOD), non-metal enzymes (eg. PLAP), enzymes with cofactor (eg. GOx), fluorescence protein (eg. EGFP), proteins with β -sheet as the structure theme (eg. EGFP) and proteins with α -helix as structure theme (eg. HRP). These results suggest that our nanoencapsulation technique offers a generally applicable platform for encapsulation of enzymes with highly retained bioactivity.

Table 7 relative residual activities of nanocapsules with different enzyme cores

Name	Abbre.	Molecular weight	Relative Residual Activity	Additive
Horseradish peroxidase	HRP	43 kDa	98.5 \pm 3.5 %	DMAAP [†]
Glucose oxidase	GOx	16 kDa	95.4 \pm 4.2 %	-
Enhanced green fluorescence protein	EGFP	29 kDa	99.5 \pm 1.6 %	-
mCherry	mCherry	28.8 kDa	96.3 \pm 3.7 %	-
Placenta Alkaline Phosphatase	PLAP	58.0 kDa	90.1 \pm 6.4 %	-
Alkaline phosphatase from calf small intestine	CIAP	69.0 kDa	92.3 \pm 8.5 %	-
AKR1C4	AKR1C4	37.3 kDa	85.4 \pm 7.4 %	DMAAP
Mushroom Tyrosinase	TYR	63.9 kDa	89.3 \pm 6.3 %	DMAAP
Human Tyrosinase	TYR	42.9 kDa	86.7 \pm 5.6 %	DMAAP
Superoxide dismutase	SOD	32.5 kDa	90.4 \pm 3.9 %	-
Catalase	CAT	250 kDa	83.7 \pm 6.9 %	DMAAP
Organophosphorous hydrolase	OPH	39 kDa	94.2 \pm 4.5 %	-
β -lactamase	BL	28.7 kDa	91.1 \pm 7.2 %	-
Firefly luciferase	Fluc	60.0 kDa	98.2 \pm 3.2 %	ATP [‡] + Mg ²⁺

[†]DMAAP: 4-Dimethylaminoantipyrine [‡]ATP: Adenosine-5'-triphosphate

Compared with the conventional immobilization technique on rigid and bulk matrix, the major advantages of our approach include: 1) the encapsulation procedure is conducted under a mild

condition similar to physiological environment, posing minor influence on the fragile 3D structure of proteins; 2) the thin layer of the polymer network does not restrict the diffusion of the substrate and product of the enzyme; 3) the elastic polymer allows the conformational change during catalysis. With these unique characteristics, we are able to give enzyme a membrane without interfering the bioactivity mediated by the core enzyme.

4.4. Nanocapsules define microenvironment around enzyme surface

Beyond the well-retained activity, we discovered that the apparent activity could be enhanced after encapsulation in some enzyme systems. Herein, we use cationic OPH nanocapsule (nOPH) to discuss this distinct property of nanocapsules.

Cationic nOPH is fabricated following the same protocol as we presented in ¹³⁷, with AAm and APm as monomers. After modification with NAS, OPH activity is well-retained. After formation of OPH nanocapsules, however, OPH activity increased to 175% at pH 8.5. To further understand the influence of the polymer shell on enzymatic kinetics, we conducted kinetic studies on native OPH and nOPH. It was found that nOPH exhibits a K_m of 0.077 mM, slightly higher than that of the native OPH (~ 0.046 mM). Note that traditional immobilization techniques (e.g., immobilization enzymes within polymers or silica) often dramatically increase the substrate-transport resistance, leading to significantly increased K_m and reduced overall enzymatic activity ¹³⁹. The smaller K_m observed for the nOPH, in comparison with the traditional immobilized enzymes, is attributed to their thin polymer shells with extraordinary substrate permeability. Interestingly, it was found that nOPH exhibits a higher k_{cat} than that of the native OPH (790 s^{-1} vs. 450 s^{-1}). It is important to point out that the traditional immobilization techniques generally result in dramatic k_{cat} decline. In this study, the observed

increase in k_{cat} is probably attributed to the polymer shells that change the local environment around encapsulated OPH.

To further explore this unique property, activities of native OPH and nOPH at different pH were compared (Figure 13a). Clearly, both OPH and nOPH show increasing activity with increasing pH. Moreover, nOPH generally exhibits superior activity than the native OPH over the tested pH range. While native OPH experiences a steep fall after the pH decreased below its optimum pH (~ 8.5), nOPH retains a comparatively stable activity from pH 7.8 to 9.7.

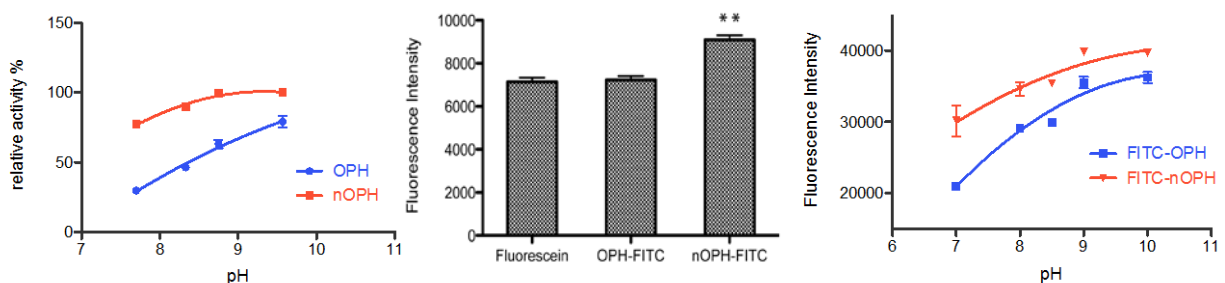


Figure 13 (left) Relative enzyme activity of native OPH and nOPH under various pHs, activities were normalized using their activities at pH 10.5 as 100% standards (mean±SEM, n=3); (middle) Fluorescence intensity of free fluorescein, OPH-FITC, and nOPH-FITC containing the same amount of fluorescein (n = 3, ** p < 0.01); (right) Fluorescence intensity of FITC-OPH and FITC-nOPH as a function of pH values (mean±SEM, n=3)

This observation can be explained by the local basic microenvironment provided by buffering effect of poly[N-(3-aminopropyl) methacrylamide] (pKa ~10)^{140,141}. The difference between local pH in a gel and outside the gel has been reported in bulk gel system¹³⁷. In a nano-scaled polymeric matrix, however, such phenomenon is less explored. To verify this hypothesis, we probe the local pH environment with fluorescein, a pH sensitive fluorescence dye with higher fluorescence emission at higher pH^{142,143}. Compared with free fluorescein in solution (Figure 13b), FITC bound to nOPH emits stronger fluorescence. FITC conjugated to native OPH, as a comparison, does not exhibit significant fluorescence enhancement. To further validate our hypothesis, we measured the fluorescence in a series of buffers with different pH. As shown in

Figure 13c, the fluorescence intensity of FITC bound to native OPH increases with increasing pH, due to the pH responsive characteristic of FITC. In the case of FITC-nOPH, as a comparison, the fluorescence intensity is generally higher than FITC-OPH, validating the local basic environment. Additionally, the fluorescence increases less significantly compared with FITC-OPH, consistent with the buffering effect of polyAPm. Therefore, we can conclude that, by engineering the polymer composition of nOPH, we could readily manipulate the microenvironment around the encapsulated OPH, and thus adjust the enzymatic activity.

4.5. Summary

To summarize, because the process of nano-encapsulation is conducted in neutral aqueous solution at room temperature or 4 °C, the activity of the protein can be preserved. A variety of protein can used in this process with only ~10% loss of activity. In addition, the polymer layer around the protein surface makes significant contribution to the microenvironment of the protein. This allows us to optimize the microenvironment for protein independent of the bulk solution composition.

Chapter 5. Enhanced Stability of Nanocapsules

5.1. Introduction

Despite the amino acid sequence, the 3D conformation of a protein is heavily dependent on pH, temperature, and ion strength. Outside their natural cellular environment, proteins may experience a series of both covalent and noncovalent structural alterations, caused by a number of external factors, leading to deterioration of protein bioactivity, if not complete loss. A variety of factors can damage the protein structure, including³:

- Elevated temperature

- Altered ionic strength
- Unfavorable pH value
- Reactive chemicals, such as oxygen
- Freeze and thaw process
- Protease and macromolecular binding agents
- Hydrophobic interface, including air-water interface

Developing strategies to endow protein the resistance to these inactivating factors paves the road for the wide application of protein as therapeutic, catalytic and analytic agents. Besides, understanding the factors that influence a particular protein's activity (and the precautions that might be introduced to minimize their effects) contributes greatly to the rational design and realization of strategies for protein stability enhancement.

In this chapter, I would like to present an outstanding property of our system-enhanced stability. By encapsulating proteins in polymeric shells, the core protein gains resistance to a wide spectrum of denaturation factors, such as heat, protease, organic solvent, and freeze thaw cycles. In addition, taking glucose oxidase as an example, I explored the underlying reason caused the stability benefit.

5.2. Experimental

OPH Stability assay: Thermal stability test was conducted by incubating both native OPH and nOPH at 60 °C at a concentration of 1mg/ml in 50 mM pH 8.5 HEPES buffer. Aliquots of samples were taken out and placed immediately on ice at different time point. The activity of OPH of the aliquots is then measured and normalized to the original activity.

OPH stability in organic solvents: The solvent stability test was conducted by incubating both native OPH and nOPH in different fraction of DMSO or methanol for 30 min. After that, the residual activity of OPH was assayed and normalized to the original activity.

OPH stability at 4 °C: Long-term storage stability test was conducted by incubating both native OPH and nOPH at 4 °C at a concentration of 1 mg/ml in 50 mM pH 8.5 HEPES buffer. Aliquots of samples were taken out and placed immediately and assayed for OPH activity at different time point. The activity is normalized to the original activity.

OPH stability in freeze-thaw cycle: In each of the freeze-thaw cycle, OPH or OPH nanocapsule is quickly frozen in liquid nitrogen and thaw under room temperature. After each freeze-thaw cycle OPH activity is assayed and normalized to the original OPH activity.

GOx thermal stability: Thermal stability test was conducted by incubating both native GOx and nGOx at 60 °C at a concentration of 1mg/ml in 50 mM pH 8.5 HEPES buffer. Aliquots of samples were taken out and placed immediately on ice at different time point. The activity of OPH of the aliquots is then measured and normalized to the original activity. The aliquots were also subjected to fluorescence spectroscopy scan with an excitation wavelength of 280 nm.

Protease Stability of SOD: 1 mg/mL SOD and nSOD with the same protein content were incubated with 0.1 mg/mL pepsin at 37°C in pH 2.0 Glycin-HCl buffer for different time point. After the incubation, samples were taken out and immediately placed on ice. The activity of SOD were tested and normalized to the original activity.

5.3. Enhanced protein stability after encapsulation

Organophosphorous hydrolase (OPH) is chosen as a model system to demonstrate the enhanced stability after nanoencapsulation. Figure 14a compares the relative stabilities of nOPH and native OPH at 65 °C. Distinct from the fast and continuous inactivation, which the native OPH

experienced (loss of total activity after 90-min incubation), nOPH underwent a slower decrease of catalytic activity in the first 20 min and maintained 60% of its original activity thereafter. The enhanced thermal stability of nOPH is believed to be the result of multiple covalent attachments of the enzyme core to the polymer shell, which effectively hinder the OPH conformation change upon heating. To confirm the stabilizing effect, OPH was attached with increasing numbers of polymerizable groups, allowing the formation of nOPH with increasing numbers of covalent linkages between the OPH core and the polymer shell. Experimentally, this was achieved by reacting OPH with increasing amounts of NAS, followed by subsequent polymerization process. Figure 14b shows the relative activities of native OPH and nOPH prepared with different NAS/OPH molar ratios (from 10/1 to 50/1) after incubation at 65 °C. Consistent with the finding in Figure 14a, nOPHs exhibit significantly higher stabilities than the native OPH. As expected, increasing NAS/OPH ratio results in increased relative stability, confirming that more covalent linkages between OPH and the polymer shells favor OPH stabilization.

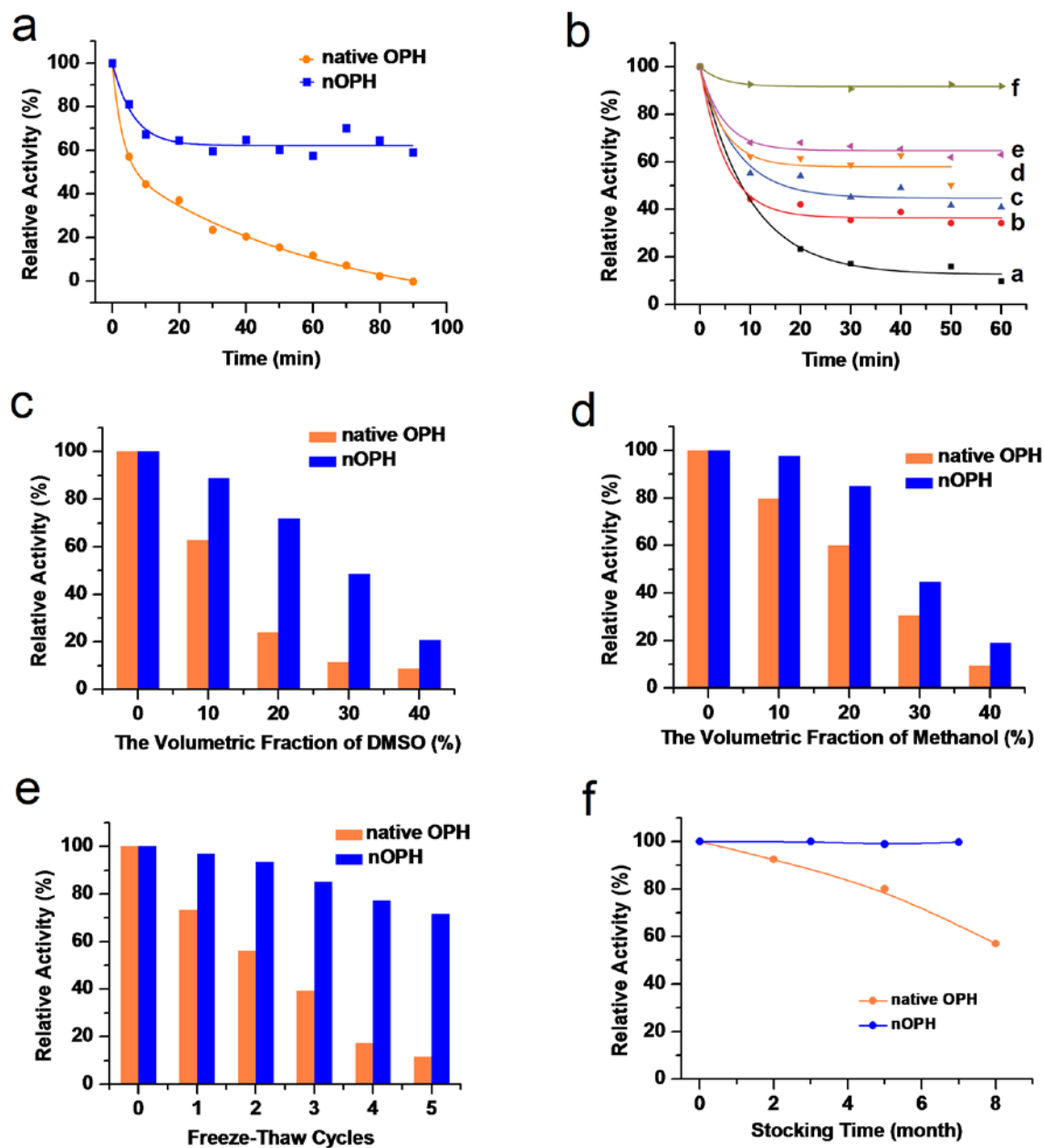


Figure 14 nOPH with Enhanced Enzyme Stability. a) Relative activities of native OPH and nOPH incubated at 65 °C. b) After incubation at 65 °C, relative activities of native OPH (a) and nOPH prepared from OPH treated with increasing NAS/OPH molar ratio of (b) 10:1, (c) 20:1, (d) 30:1, (e) 40:1 and (f) 50:1. Relative activities of native OPH and n(OPH) exposed to 50mM HEPES buffer (pH=8.5) solution containing different diffractions of c) DMSO or d) methanol, e) subject to 5 freeze-thaw cycles, and f) stored at 4 °C in solution.

It has been proposed that the thermal inactivation of OPH involves a two-step process: the denaturation of native dimeric protein to an intermediate and a following inactivation step

from the intermediate to completely unfolded subunits (eq. 1)¹⁴⁴. Consistent with this mechanism, we observed a biphasic exponential decay of OPH activity during the thermal inactivation of the native OPH (Figure 14a&b). As a comparison, the inactivation of nOPHs best fit monophasic exponential decay followed by a plateau (Figure 14a&b). The most direct rationale of this phenomenon is the changing of the mechanism from two-step inactivation to one-step equilibrium (eq. 2). The second step, the breakdown of dimer into subunits, is completely eliminated due to the restriction of the polymeric shell around the dimeric protein. In addition, because the polymer layer is covalently bond to OPH, it affects the kinetics of the inactivation. To further investigate the impact of the multi-covalent bonding on inactivation kinetics, the theoretical activity profile (eq. 3)¹⁴⁵ was derived and used to evaluate the rate constants of the forward (k_1) and reverse reaction (k_2) in eq. 2. As shown in Table 8 and Figure 15, the rate of the forward reaction ($N_2 \rightarrow D_2$) decreases with the increasing covalent bond between the OPH and the polymer shell. On contrary, the rate of the reverse reaction ($N_2 \leftarrow D_2$) increases with the increasing NAS/OPH ratio. These observations clearly demonstrate that the polymer shell stabilizes the native and active form of OPH by inhibiting the denaturation and enhancing the renaturation.



$$activity = \frac{k_2}{k_1 + k_2} + \left(1 - \frac{k_2}{k_1 + k_2}\right) e^{-(k_1 + k_2)t} \quad \text{Equation 3}$$

Table 8 Rate constants of the forward and the reverse reaction of nOPH thermal inactivation

NAS/OPH	10	20	30	40	50
---------	----	----	----	----	----

k_1 (min^{-1})	0.124	0.077	0.090	0.077	0.019
k_2 (min^{-1})	0.070	0.062	0.122	0.140	0.212

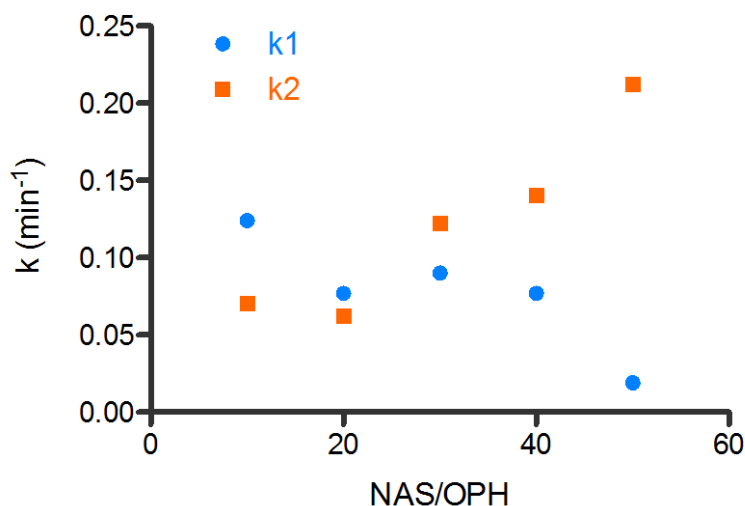


Figure 15 Rate constants of the forward and the reverse reaction of nOPH thermal inactivation

The enhanced enzyme stability in the existence of the organic solvents was demonstrated by exposing native OPH or nOPH to organic solvent-water mix solvents with different volume fractions of dimethylsulfoxide (DMSO) (Figure 14c) or methanol (Figure 14d). Compared with non-polar solvents such as hexane, polar organic solvents are more detrimental to proteins, since they compete with water to form hydrogen bonding with protein backbones, destroying protein conformation. As presented in Figure 14c, nOPH retains higher residual activity in DMSO-water mixture: nearly 3 times more than that of the native OPH in 20% DMSO solution. Similar result was observed from the test with methanol, confirming that nOPH has an improved stability in non-aqueous media (Figure 14d). This improved performance of nOPH can be attributed to the “essential water” kept by its hydrophilic shell, which otherwise would be depleted by polar organic solvent^{146,147}. Maintaining enzyme activity in non-aqueous environment is challenging

but holds great promise for a broad range of industrial and environmental applications. The nanocapsule technique is a meaningful step towards this challenge.

The enhanced freeze-thaw and long-term enzyme stability are demonstrated in Figure 14e and Figure 14f, respectively. After five freeze-thaw cycles, nOPH retains more than 70% activity while the native OPH suffers severe activity drops with less than 10% of its original activity left (Figure 14e). Moreover, a prolonged storage time of nOPH has been proved through an 8-month storage test at 4 °C. Compared with a loss of ~50% original activity of native OPH, nOPH remains unchanged activity throughout the 8 months (Figure 14f). Prolonged shelf life can provide a major advantage in practical applications, since it can dramatically lower the cost to store and replace the enzyme stocks.

How does the polymeric shell stabilize the enzyme against the alteration of physical and chemical environment? To further explore the underlying reason, we explored the structural change during thermal inactivation of glucose oxidase. Similar to OPH, GOx gains boosted thermal stability after nanoencapsulation. As shown in Figure 16, after incubation at 60 °C in pH 7.0 PBS solution, activity of native GOx dramatically dropped to 11.8%, whereas GOx nanocapsules still retain 72.3% of its original activity.

According to Gouda *et. al.*, dissociation of coenzyme FAD from holoenzyme was responsible for the thermal inactivation of GOx (Figure 17a)¹⁴⁸. Dissociation of FAD also resulted in the loss of secondary and tertiary structure, leading to the unfolding and nonspecific aggregation of the enzyme molecule because of hydrophobic interactions of side chains. To explore the stabilizing mechanism of GOx nanocapsules, we studied the process of FAD dissociation. Due to the change of microenvironment, fluorescent intensity of FAD molecules in their free state differs from that bound to GOx. In our research, we measured the fluorescent spectra of GOx and GOx

nanocapsules after incubation at 60 °C for 0, 20, 40, and 80 min. From Figure 17b, we could observe the fluorescent intensity of emission peaks at 323 nm and 350 nm increase significantly with incubation time, which indicate the dissociation of FAD from native GOx during incubation. In the case of GOx nanocapsules (Figure 17c), although the fluorescent intensity did increase with time, the increase was far less significant compared with native enzyme. The above results suggest that polymeric shell could stabilize GOx by preventing the dissociation of FAD.

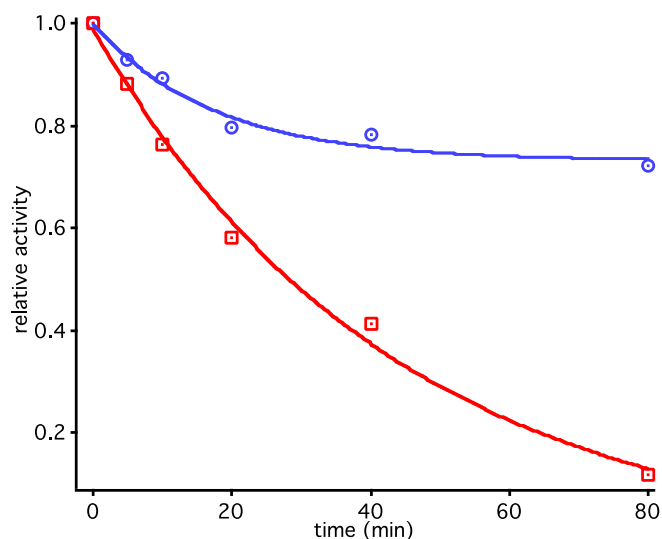


Figure 16 reactivity decrease of GOx and nGOx at 60 °C. red line: native GOx; blue line: GOx nanocapsules

In the field of enzyme immobilization, most enzymes could be stabilized by multipoint immobilization. The multipoint covalent bonds could hold the enzyme, making it less vulnerable to inactivation factors. In our systems, the polymer shell was also linked to the enzyme via multipoint covalent bonds, though the polymer shell is less rigid. Via similar mechanism, glucose oxidase inside polymeric shell could be stabilized by fixing the FAD-associated form. On the other hand, the ability of polymer shell to prevent the aggregation of holoenzyme also contributes to the stabilization effect. Dissociation of FAD is a reversible process, the irreversible nature of thermal inactivation is caused by the conformational change and aggregation. The following irreversible step plays a deleterious role, since it breaks the balance of the free and the bound FAD. Polymer layers around GOx hold and shell the enzyme, preventing the irreversible conformational change and aggregation. By inhibiting the following

irreversible inactivation step, the equilibrium of association and dissociation of FAD is not broken, leading to no significant increase in the release of FAD.

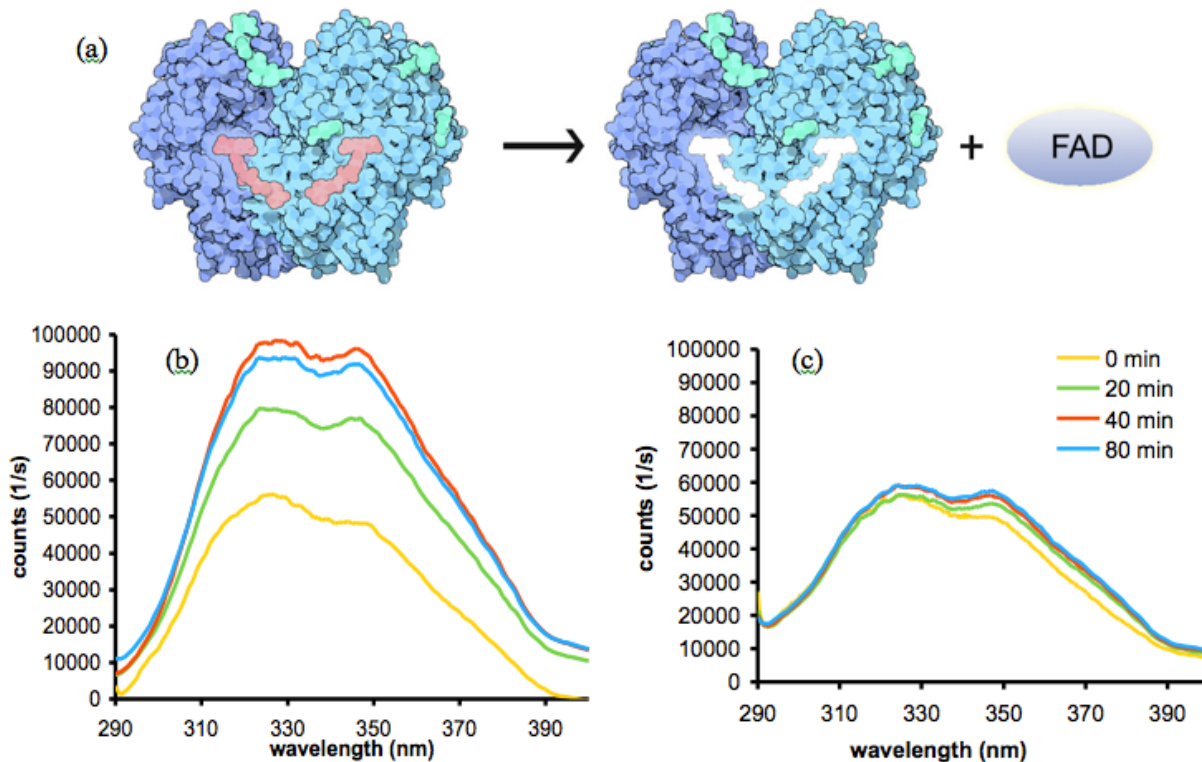


Figure 17 Dissociation of FAD from GOx (a) Schematic illustration of the dissociation of coenzyme FAD, (b) fluorescent emission of GOx solution after incubation for different time, (c) fluorescent emission of GOx nanocapsule solution after incubation for different time

Besides physical destabilization factors such as elevated temperature, freeze-thaw cycles and organic solvents, in biological system, protein faces a class of scavenger- proteases. Protease is an enzyme that cleaves the backbone of other proteins. Proteases widely exist in any organism for numerous metabolic and catabolic processes¹⁴⁹. Pepsin in the stomach and trypsin/chymotrypsin secreted into small intestine mediate the digestion of the protein in food^{150,151}; serum proteases are crucial for blood-clotting¹⁵², lysis of the clots¹⁵³⁻¹⁵⁵, and the immune response¹⁵⁶. Intracellular proteases, mainly localized in the lysosomes, are responsible of breaking down exogenous proteins taken up by cells¹⁵⁷⁻¹⁵⁹. Due to the wide existence of proteases, the therapeutic applications of protein face a critical challenge. Although various approaches based

on protein engineering or protein conjugation have been developed to solve this problem. Successful stabilization strategies must be determined experimentally on a laborious case-by-case basis.

The structure of protein nanocapsule shines a light on this issue. In a protein nanocapsule, the protein is wrapped inside a crosslinked polymer network. The net-like polymer physically separates the protein from the attack of proteases. Therefore, this strategy can be used universally on any protein to resist the digestion of any protease. As an example, I incubated superoxide dismutase (SOD) and SOD nanocapsule (nSOD) with pepsin at 37 °C for different time. As shown in Figure 18, the activity of SOD drops rapidly to 19.2 % of its original activity within 30 min. In the case of nSOD, however, the activity decreases at a much lower rate. After 30 min, the nSOD still retains 81.6 % activity compared with that before digestion.

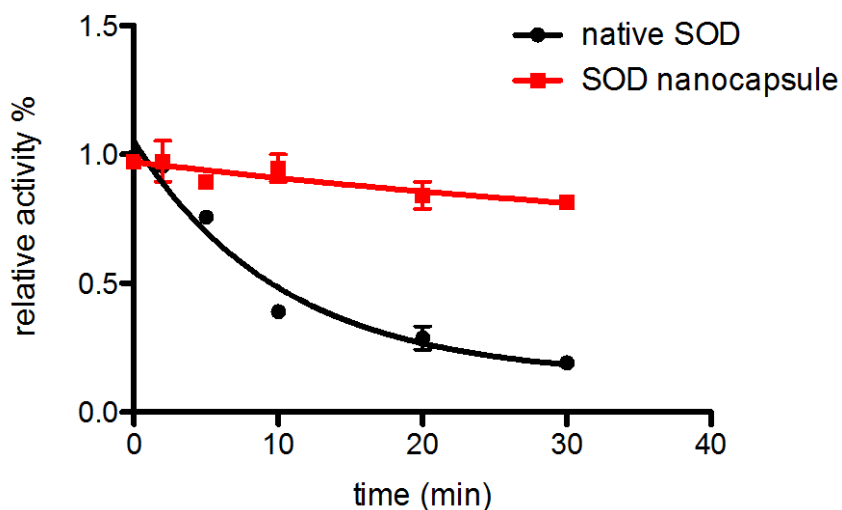


Figure 18 Relative activity of native SOD and SOD nanocapsule after incubation at 37 °C with pepsin for different time

5.4. Summary

To summarize, nanoencapsulation endow protein with enhanced stability. With model proteins such as OPH and GOx, we demonstrate significantly improved stability against various denaturation factors, including elevated temperature, freeze-thaw cycles, long-term storage, organic solvents and proteases, paving the way for the therapeutic and catalytic applications of proteins. With studies on the inactivation kinetics and enzyme structure during inactivation, we discovered that the polymer layer stabilize the 3D conformation of the native form whereas destabilize the denatured form of the core protein. In addition, the polymer layer disables the aggregation or dissociation of proteins, as well as the dissociation of co-factor from the protein. Upon exposure to protease, polymer layer serves as a protecting layer, physically separating the protease from the core protein.

Chapter 6. Cationic Nanocapsules for Intracellular Delivery

6.1. Introduction

An average cell contains thousands of proteins that participate in normal cellular functions and most diseases are somehow related to the malfunction of specific proteins. Protein therapy^{160,161}, which delivers proteins into the cell to replace the dysfunctional one, is considered the most direct and safe approach for treating diseases. However, this method has been limited by low delivery efficiency and poor stability against proteases in the cell that digest the protein. Here we show a novel delivery platform based on nanocapsules consisting of a protein core and a thin permeable polymeric shell that can be engineered to either degrade or remain stable at different pHs. Non-degradable capsules have long term stability while degradable ones break down their shells and maintain their activity once inside the cells. Multiple proteins can be delivered to cells

with high efficiency, activity and low toxicity for potential applications in imaging, therapy and cosmetics.

Intracellular use of therapeutic proteins is of great importance for treatments of cancers and protein-deficient diseases; however, they are still rare in clinical applications partially due to poor stability and low cellular permeability^{88,160}. Although proteins may be translocated into cells by receptor-mediated endocytosis^{162,163}, they may be entrapped within the endosomes and degraded in the lysosome rather than be released to the appropriate cellular compartment. Similarly, liposome-wrapped proteins were shown to be transferred into the cytoplasm but with a low efficiency^{95,164}. Recently, cell-penetrating peptides (CPPs) were used to assist protein delivery with significantly improved efficiency^{88,165-167}; however, stability of proteins^{3,168}, particularly protease digestion¹⁴⁹, still hampers their therapeutic applications.

We herein report a novel intracellular delivery platform based on nanocapsules that consist of a single-protein core and thin polymer shell anchored covalently to the protein core. As illustrated in Figure 19, polymerizable vinyl groups are covalently linked to the protein (I); subsequent polymerization in an aqueous solution containing monomers (1, 2) and crosslinker (3, 4) wraps each protein core with a thin polymer shell. This scheme enables the synthesis of protein nanocapsules with non-degradable (II) or degradable skin (III) by using non-degradable (3) or degradable crosslinker (4), respectively. Hereinafter, the non-degradable and degradable nanocapsules are denoted as nProtein and de-nProtein, respectively. Judicious choice of the monomer, such as the cationic (2) and neutral monomer (1), allows precise control of the surface charge. The protein cores can be chosen from the vast library of proteins, such as enhanced

green fluorescent protein (EGFP), horseradish peroxidase (HRP), bovine serum albumin (BSA), superoxide dismutase (SOD), and caspase-3 (CAS).

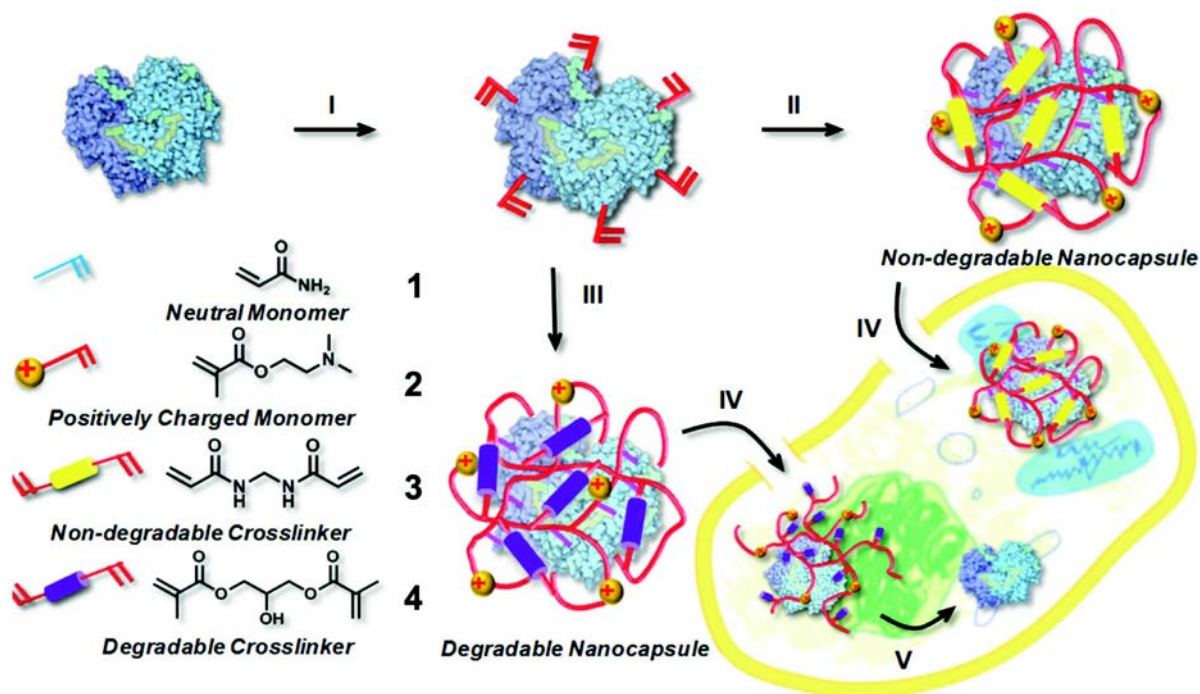


Figure 19 Schematic showing the synthesis and cellular uptake of cationic single-protein nanocapsules with degradable and non-degradable polymeric shells prepared by in situ copolymerization of acrylamide (1), 2-dimethylaminoethyl methacrylate (2) and non-degradable crosslinker methylenebisacrylamide (3) or acid-degradable glycerol dimethacrylate (4): I) formation of polymerizable proteins by conjugating polymerizable acryl groups to the protein surface; II) formation of non-degradable nanocapsules from (1), (2) and (3); III) formation of degradable nanocapsules from (1), (2) and (4); IV) cellular uptake of the degradable or non-degradable nanocapsules via endocytosis; V) Shells of degradable nanocapsules break down after internalization to release the protein cargoes, allowing them to interact with large molecular substrates.

6.2. Experimental

Nanocapsule Synthesis: EGFP and TAT-EGFP fusion proteins were expressed according to previous reports¹⁶⁹. Fusion proteins were expressed in transformed *Escherichia coli* BL21 and purified using Nickel-resin affinity column (Sigma Aldrich). The concentration of EGFP was determined by an extinction coefficient of $53,000 \text{ M}^{-1} \text{ cm}^{-1}$ at 489 nm. Ten milligrams of EGFP

in 3.8 mL of pH 8.5 50 mM carbonate sodium buffer was reacted with 4 mg N-acryloxysuccinimide in 40 μ L of DMSO for 2 h at room temperature. Finally the reaction solution was thoroughly dialyzed against pH 7.0 20 mM phosphate buffer. The degrees of modification were measured using MALDI-TOF mass spectra, which were varied from 5 to 20 vinyl groups per protein (Fig S7, Table S2). To a 5 mL acryloylated EGFP solution at 1 mg/mL, radical polymerization from the surface of the acryloylated protein was initiated by adding 2 mg of ammonium persulfate dissolved in 30 μ L of deoxygenated and deionized water and 4 μ L of N,N,N',N'-tetramethylethylenediamine into the test tube. Then a specific amount of 2-dimethylaminoethyl methacrylate, acrylamide and N,N'-methylene bisacrylamide or glycerol dimethacrylate (molar ratio = 5:5:1) dissolved in 0.5mL deoxygenated and deionized water was added to the test tube over 60 min. The reaction was allowed to proceed for another 60 min in a nitrogen atmosphere. Finally, dialysis was used to remove monomers and initiators. As synthesized EGFP nanocapsules show similar fluorescent spectrum to that of native EGFP (Fig S8). The yield of the protein nanocapsules is higher than 95%; the unmodified EGFP were removed using the size-exclusion chromatography.

The syntheses of Caspase-3, HRP, NIR-667-labeled-BSA, and rhodamine-B-labeled-HRP nanocapsules were similar to that of EGFP nanocapsules. NIR-667-labeled BSA and rhodamine-B-labeled HRP were synthesized by modifying the proteins using a conjugating technique. Caspase-3 was expressed and purified using the method similar to that of EGFP; the plasmid used, pHC332, was a generous gift from Dr. A. Clay Clark, North Carolina State University. Cu, Zn-SOD from bovin erythrocytes and horseradish peroxidase (from Sigma-Aldrich) were used after dialysis against 20mM pH 7.0 phosphate buffer. For the synthesis of HRP nanocapsules, 4-

dimethylaminoantipyrine (1:10 weight ratio to HRP) was added into the reaction mixture as a stabilizer during acryloylation and polymerization steps.

Stability of the nanocapsules in the presence of proteases: EGFP or EGFP nanocapsules were incubated with both of trypsin and α -chymotrypsin at 1 mg/mL at 50 °C in PBS buffer. Fluorescent intensity of the EGFP and EGFP nanocapsules was determined at different time intervals with an excitation wavelength at 489 nm.

***In vitro* cellular internalization:** Cellular internalization studies were assessed via fluorescence microscopic technique and fluorescence-activated cell sorting (FACS). HeLa cells were cultured in Dulbecco's modified Eagle's medium (DMEM) supplemented with 10% bovine growth serum (BGS) and 1% penicillin/streptomycin. Cells (20000 cells/well, 24-well plate) were seeded the day before adding the nanocapsules. Nanocapsules or native proteins with different concentrations were added into the cell medium. After incubation at 37 °C for 2 to 4 hrs, the cells were washed three times with PBS and either visualized with a fluorescent microscope or trypsinized, centrifuged, and re-suspended in PBS and analyzed via FACS. The endosome/lysosome staining was performed according to manufacture's manual. Briefly, after incubation with rhodamine-labeled HRP nanocapsules, cells were briefly washed, fixed with 2% formaldehyde, permeated with PBS/1% Triton, blocked with 5% BSA and treated with rabbit anti-EEA antibody (for early endosome) or rabbit anti-Rab7 antibody (for lysosome) overnight. Cells were stained with Alexa488 goat anti-rabbit IgG and then observed with confocal microscope.

Cell proliferation assay: The toxicity of the nanocapsules was assessed by the MTT assay using native proteins as control. HeLa cells (7000 cells/well) were seeded on a 96-well plate the day before exposure to the nanocapsules. Nanocapsules with different concentrations were

incubated with the cells for 2-4 hrs, removed from the mixture, and incubated with fresh media for different time. The MTT solution (20 μ L) was added to each well and incubated for 3 h. The medium was then removed and 100 μ L DMSO was added onto the cells. The plate was placed on a shaking table, 150 rpm for 5 min to thoroughly mix the solution, and then absorbance readings were measured at 560 nm. Untreated cells were used as the 100% cell proliferation control.

Endocytosis Inhibition HeLa cells (20000 cells/well, 24-well plate) were seeded the day before adding the nanocapsules. Before the experiment, the medium was then replaced with 0.5 ml of fresh medium with 2mM amiloride (inhibitor for macropinocytosis), 20 μ g/mL chloroproamzine (CPZ, inhibitor for clathrin-mediated endocytosis), or 5 mM β -cyclodextrin (β -CD, inhibitor for caveolae-mediated endocytosis). After 30 min, 50 nM EGFP nanocapsules were added into cell medium and incubate at 37°C for 2 h. After washing with PBS, the cells were trypsinized, centrifuged, re-suspended in PBS and analyzed via FACS. HeLa cells incubated in medium without endocytosis inhibitors were used as control.

Apoptosis Assay. Apoptosis was detected in isolated HeLa cells using a commercially available APO-BrdU Terminal Deoxynucleotidyl Transferase dUTP Nick End Labeling (TUNEL) assay kit. Briefly, cells were seeded onto six-well plates at a density of 100,000 cells per well and cultivated in 2 mL of Dulbecco's Modified Eagle's Medium (DMEM) with 10 % bovine growth serum (BGS). The plates were then incubated in 5% CO₂ at 37 °C for 12 h to reach 70-80% confluency before the addition of protein/nanocapsules. After 24 h incubation, cells were first fixed with 1% paraformaldehyde in phosphate-buffered saline, pH 7.4, followed by treatment with 70% ethanol on ice. The cells were then loaded with DNA labeling solution containing terminal deoxynucleotidyl transferase and bromodeoxyuridine (BrdUrd). Cells were then stained

with Alexa Fluor® 488 dye-labeled anti-BrdUrd antibody. The cells were finally stained with propidium iodide (PI) solution containing RNase A and visualized under a fluorescence microscope (Zeiss, Observer Z1) using appropriate filters for Alexa Fluor 488 and PI.

nEGFP subcutaneous delivery: 1 C3H mouse from Jackson labs was used in this experiment. The animal was maintained in a cage with free access to chow and water and subjected to normal night/day cycles. The mouse was anesthetized with 5% isoflurane in an oxygen environment before being injected. In the first study, two injection sites were selected for the mouse, one on the left side of the back, and one on the right side. The injection sites were marked with a permanent marker. The left site was treated with the positively charged nano-encapsulated EGFP, and the right site was treated with the native EGFP. Prior to injection, the activities of the proteins were determined using fluorescence. The activity of the encapsulated protein was found to be 50% that of the native. Hence, in order to keep the total activity injected in each side constant, 30 μ L of the native EGFP was injected into the dermis on the left site, and 60 μ L of the encapsulated EGFP was injected into the right. EGFP signal in the live animal was measured and quantified using the Maestro imaging system. The animal was imaged at 2 min, 15 min, 1 hr, 24 hr, 48 hr and 72 hr post injections. In the second study, the center of the back was selected for injection and was marked with a permanent marker. 60 μ L of the encapsulated EGFP was injected into the dermis of the mouse. EGFP signal in the live animal was measured and quantified using the Maestro imaging system. The animal was imaged at 2 min and every 1-2 days post injection until no fluorescence signal could be detected. Prior to each imaging, the animal was anesthetized using 5% isoflurane. After the images were obtained, they were spectrally unmixed to remove the background fluorescence. Images were quantified using region of interest (ROI) analysis software that is supplied with the Maestro system.

Tissue processing for histology:

injection site was harvested for histology. The samples were preserved in OCT at -80 °C overnight, and sent to the Pathology department at UCLA on dry ice for frozen sectioning. Slides were first washed with PBS to remove residual OCT, then stained with Prolong Gold Antifade (with DAPI) mounting media and imaged using a fluorescence microscope.

Cellular β -Lactamase Activity assay: The CEM cells were seeded at a density of 5×10^5 cells/mL into 96-well plates in a volume of 100 μ L (50,000 cells). The following morning, nLac or nLac-lipid-PEG were incubated with cells for 3 hours with or without 150 nM bafilomycin. After treatment, cells in 96-well microplates were assayed with GeneBLAzer® FRET Cell-based Assay from Invitrogen. Fluorescent measurements were made using a Synergy 4 Hybrid Microplate Reader. All measurements were made from the bottom using a 400/30-excitation filter and both a 460/40 and 528/20 emission filters.

6.3. Intracellular delivery of the non-degradable nanocapsules

Cell transduction efficiency was studied using nEGFP and HeLa cells. The cells with nEGFP show significantly higher fluorescence intensity than those with native EGFP (Figure 20). Compared with the CPP-assisted delivery, our strategy is more advantageous (Figure 21). At the same protein concentration, cells incubated with nanocapsules shows two to three orders higher fluorescence intensities than those with TAT-EGFP fusion proteins (Figure 21a) or antennapedia-EGFP conjugates (Figure 21b), where TAT and antennapedia are CPPs derived from HIV-Tat protein and antennapedia homeodomain, respectively. It was found that the uptake of the nanocapsules increased with time, concentration and zeta potential; however, no significant impact of nanocapsule size was observed (Figure 22).

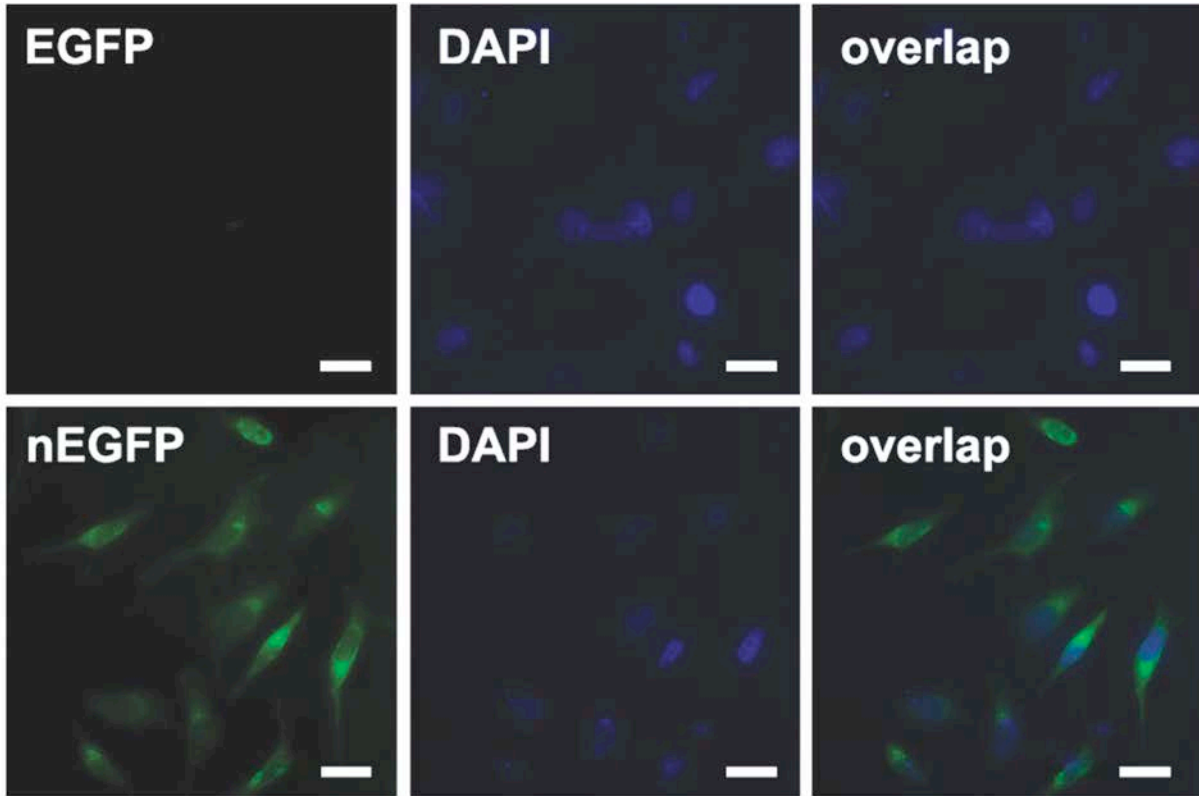
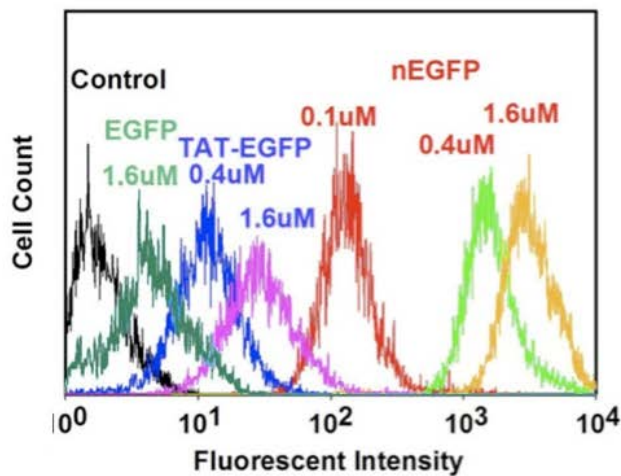


Figure 20 Fluorescent images show uptake of nEGFP but not native EGFP after 3 hr incubation. Cells were counter-stained with DAPI for nuclei.

(a) TAT: **RKKRRQRRR**



(b) Antp: **RQKIWFQNRRMKWKK**

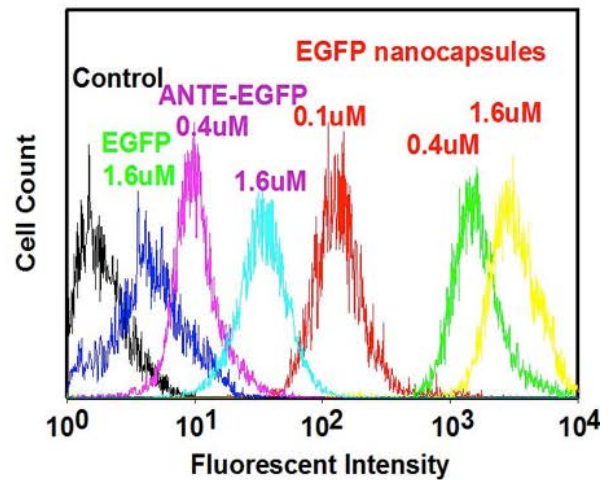


Figure 21 Fluorescence-assisted cell sorting of HeLa cells incubated with different concentrations of nEGFP (11.7nm, zeta potential 10.9 mV), TAT-EGFP fusion proteins, Antp-EGFP fusion protein or native EGFP.

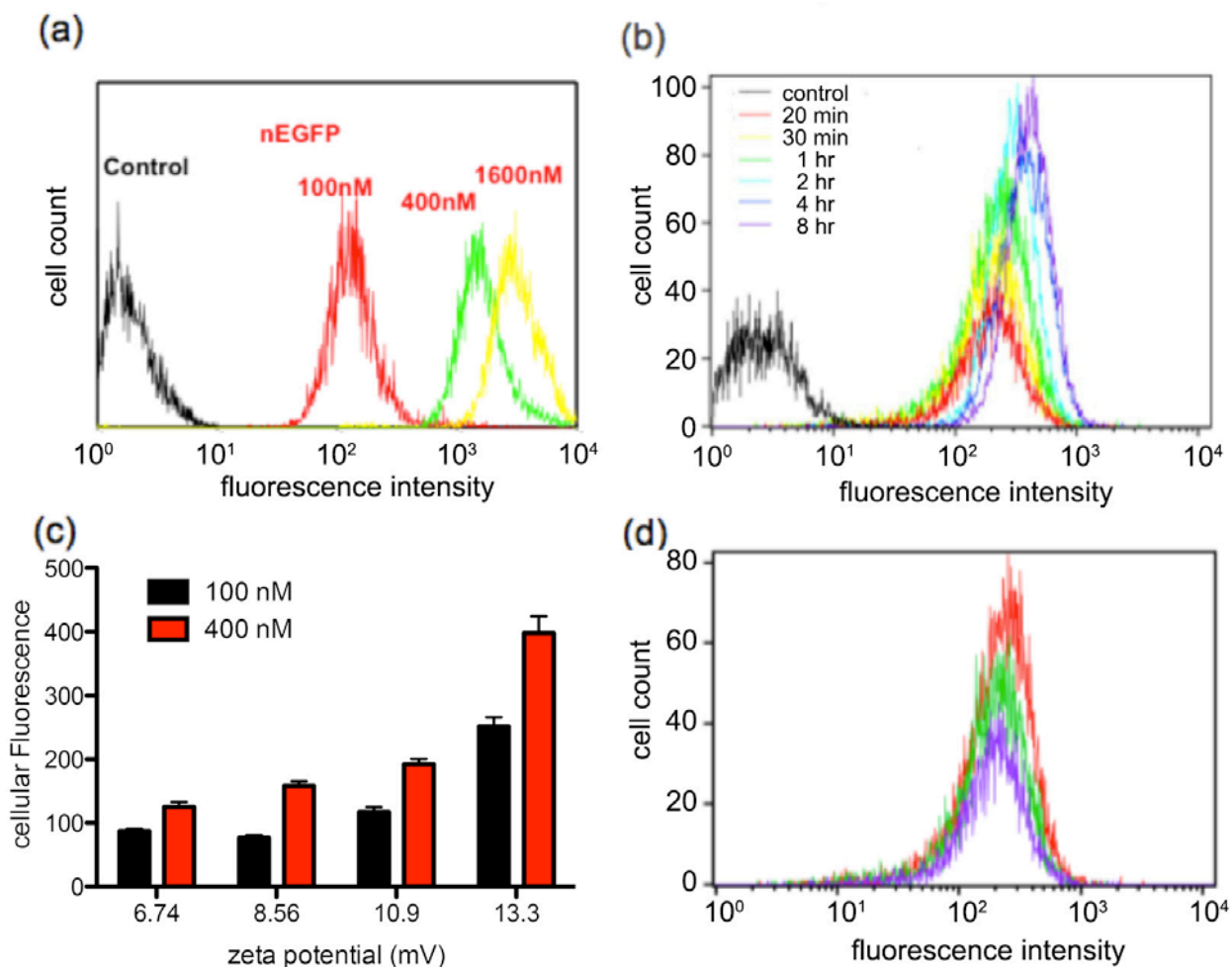


Figure 22 (a) Cellular fluorescence distribution of HeLa cells after incubation with nEGFP; (b) HeLa cell fluorescence intensity after incubation with 400 nM nEGFP for different time; (c) Uptake of nEGFP by HeLa cells increased with zeta potential after 3hr (mean \pm SD, acquired from the FACS histogram); (d) Cellular fluorescent intensity distribution of HeLa cells after incubation with nEGFP with different sizes (red: 7.53 nm, green: 10.6 nm, purple: 15.7 nm)

Incubating HeLa cells with nEGFP at 4 °C showed a much lower cellular uptake than that at 37 °C (Figure 23), which is consistent with those of most cationic CPPs and polymer based nanoparticles^{90,133,170,171}. Among three endocytosis inhibitors, only β -cyclodextrin effectively inhibited the nanocapsule uptake (Figure 23), suggesting a caveolae-mediated endocytosis pathway^{172,173}. Moreover, endosomal and lysosomal staining of the cells incubated with

rhodamine-B-labeled nHRP reveals co-localization of nHRP with the early endosomes and lysosome after 30 min, which were gradually released to the cytosol (Figure 24) possibly by the “proton-sponge” effect^{174,175}.

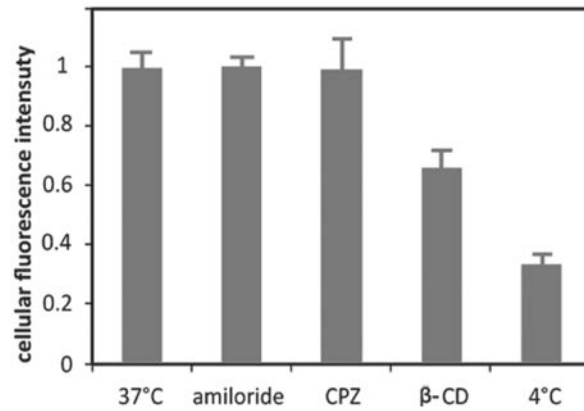
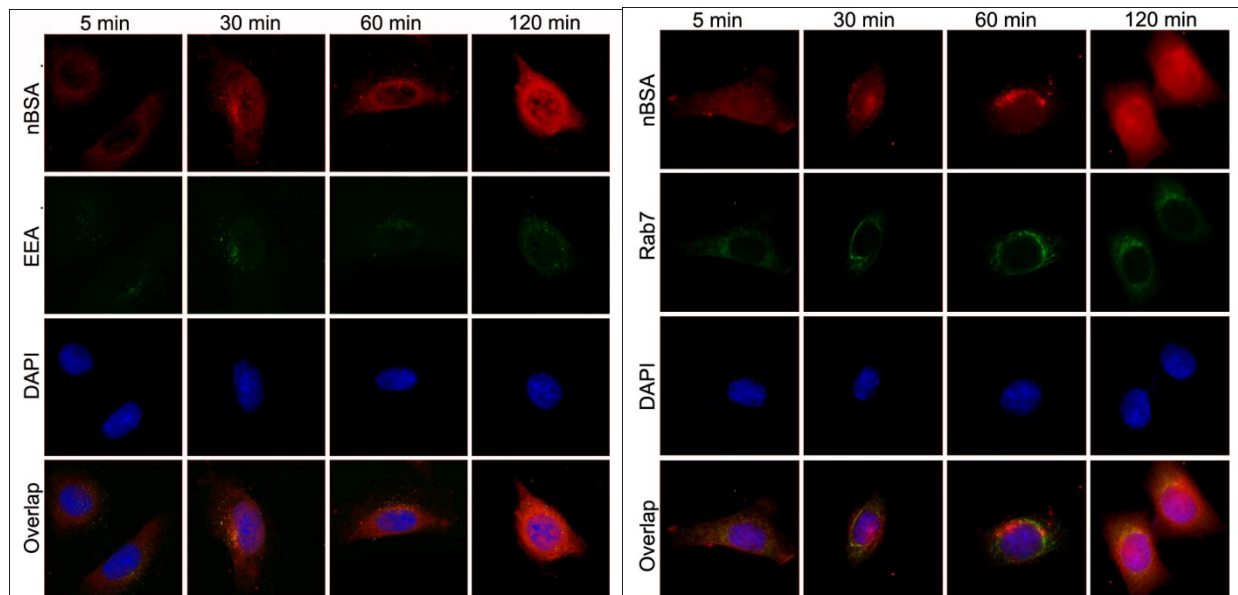


Figure 23 Average cellular fluorescence intensity of HeLa cells at different temperatures and in the presence of endocytosis inhibitors. Fluorescence intensity normalized to cells incubated with nEGFP at 37 °C.



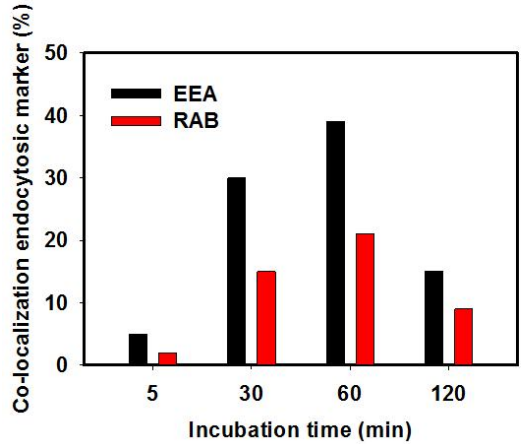


Figure 24 (Up) Trafficking of Rhodamine B-labeled nBSA through endocytosis. Early and late endosomes were stained by EEA1 antibody (Up-left) and Rab7 antibody (Up-right), respectively. HeLa cells were incubated with 400 nM nBSA at 37 °C for various time points of 5, 30, 60 and 120 min. (Bottom) Quantification of nEGFP co-localized with EEA1 (black) or Rab7 (red) endosomes at different incubation times.

Besides the high efficiency, protein nanocapsules have low toxicity. Figure 25 compares the viability of HeLa cells after exposure to different nEGFP and native EGFP, suggesting similar cytotoxicities for both the nEGFP and native EGFP. Even under the exposure to 1 μ M nanocapsules, the cell viability decreased by only 15%.

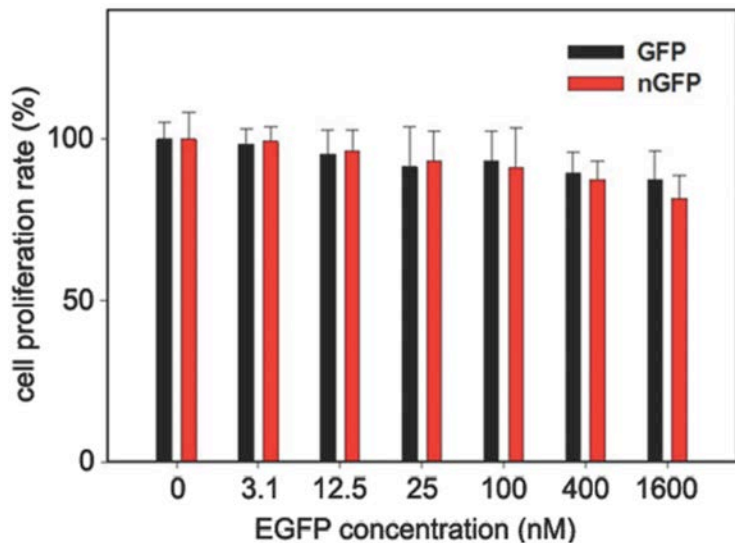


Figure 25 MTT assay showing nEGFP has similar cytotoxicity to native EGFP after 3 hr (mean \pm SD, n = 3)

Note that proteases are commonly present in physiological environment in which proteins are readily degraded. The polymer shell, nevertheless, well protects the protein core from proteolysis. Figure 26a compares fluorescence intensities of native EGFP and nEGFP after exposure to 1 mg/mL proteases (trypsin and α -chymotrypsin) at 50 °C for 3 hrs. The native EGFP only kept 60% of its original fluorescence intensity whereas the nanocapsules retained more than 90%. Intracellular stability was examined by comparing the temporal fluorescence intensities after transduction (Figure 26b). Inevitably, the cellular fluorescence decreased with time as a result of cell propagation; nevertheless, the stability of nEGFP is significantly improved over those of TAT-EGFP.

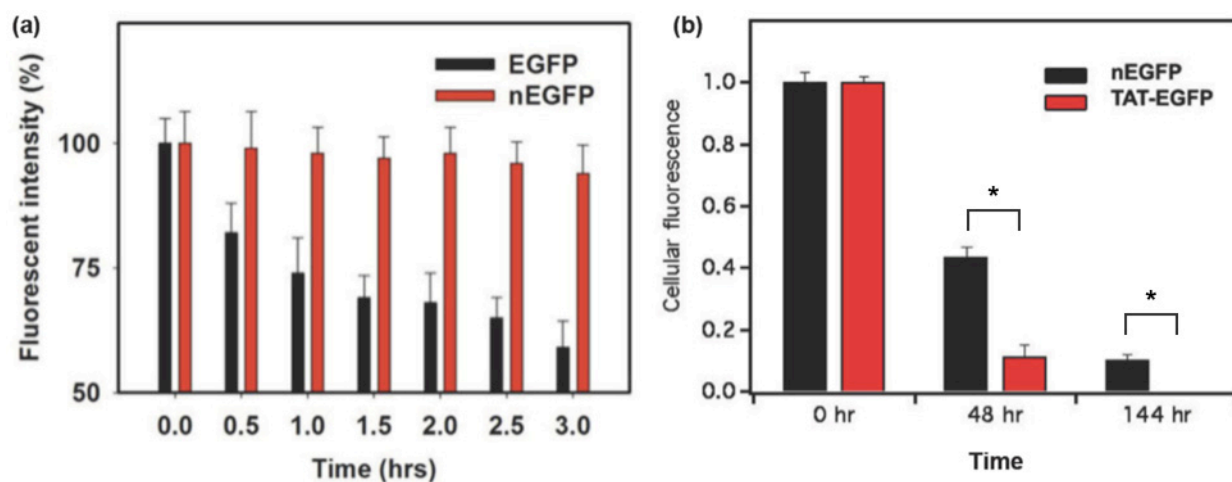


Figure 26 Stability of nanocapsules. (a) Fluorescence intensity of native EGFP and nEGFP after exposure to trypsin and chymotrypsin. Fluorescence intensities normalized to native EGFP before exposure to protease (b) Cellular fluorescence intensity (mean \pm SD) of cells after treatment with nEGFP or TAT-EGFP fusion proteins at different times. * $p < 0.005$

Enhanced green fluorescence protein was selected as a model system to probe the long-term stability of nanocapsules in vivo. Figure 27 shows the overlay of the optical image and fluorescence image of the animal at different times post injections. The fluorescence signal from the native EGFP was not visible at 24 hr post injection while the signal from the positively charged encapsulated EGFP was still visible at 72 hr. The animal was sacrificed at 72 hr and

tissue from the injection sites was harvested in order to determine if the encapsulated EGFP was intracellular. Figure 28 is the graph of the total fluorescence signal at each of the injection sites as measured by the imaging software. The total signal from encapsulated EGFP increased by ~9 fold over the first 24 hr and decreased by ~5 fold after 72 hr. Since the fluorescence intensity of green light reduces with depth, we hypothesize that the increase in signal at 24 hr may be due to the protein diffusing closer to the surface. No fluorescence signal from the native EGFP could be measured 24 hr post injection.

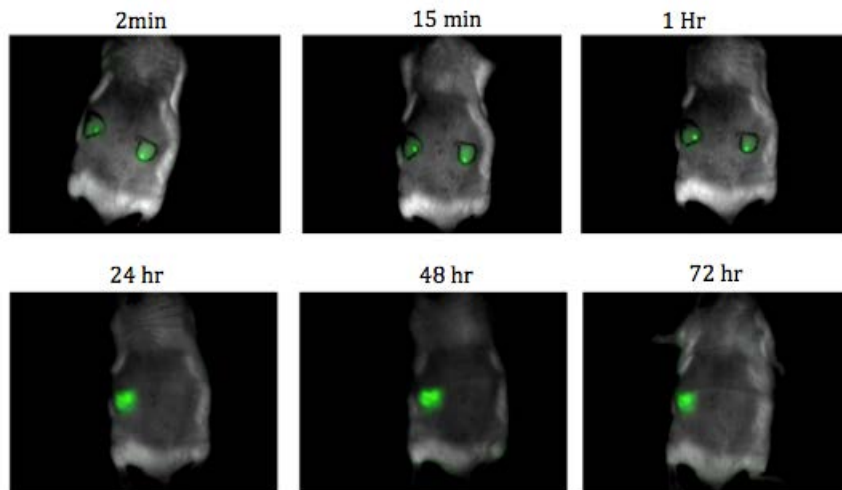


Figure 27 Overlay of the optical image and fluorescence image of mouse subcutaneously injected with nEGFP (left) and native EGFP (right) at different times post injections

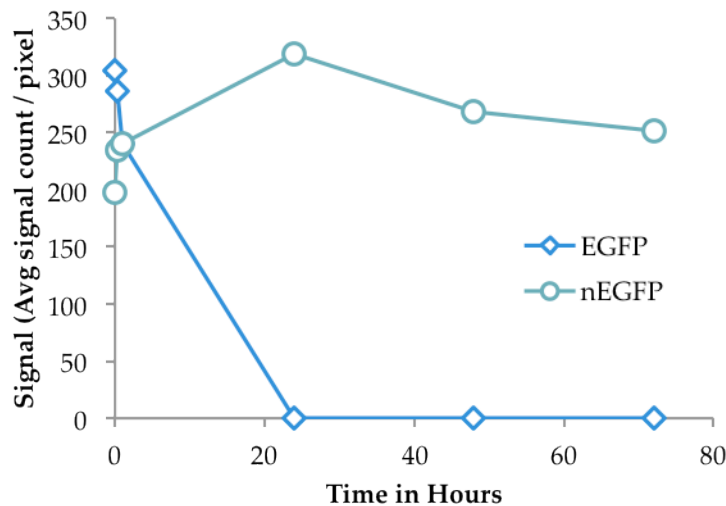


Figure 28 Fluorescence signal of injection site at different times post injection

To further confirm the in-vivo long-term stability, we further conducted an 11-day study. Figure 29 is the overlay of the optical image and fluorescence image of the animal at different times post injections. The fluorescence signal from the positively charged encapsulated EGFP persisted till 9 days post injection. At day 9 the fluorescence signal was faint and at day 11 no signal could be seen even at a higher threshold. Figure 30 is the graph of the total fluorescence signal at the injection site as measured by the imaging software. The total signal from encapsulated EGFP increased by ~ 10 fold over the first 2 days and decreased steadily till no signal was present post Day 9. Since the fluorescence intensity of green light reduces with depth, we hypothesize that the increase in signal at day 2 may be due to the protein diffusing closer to the surface.

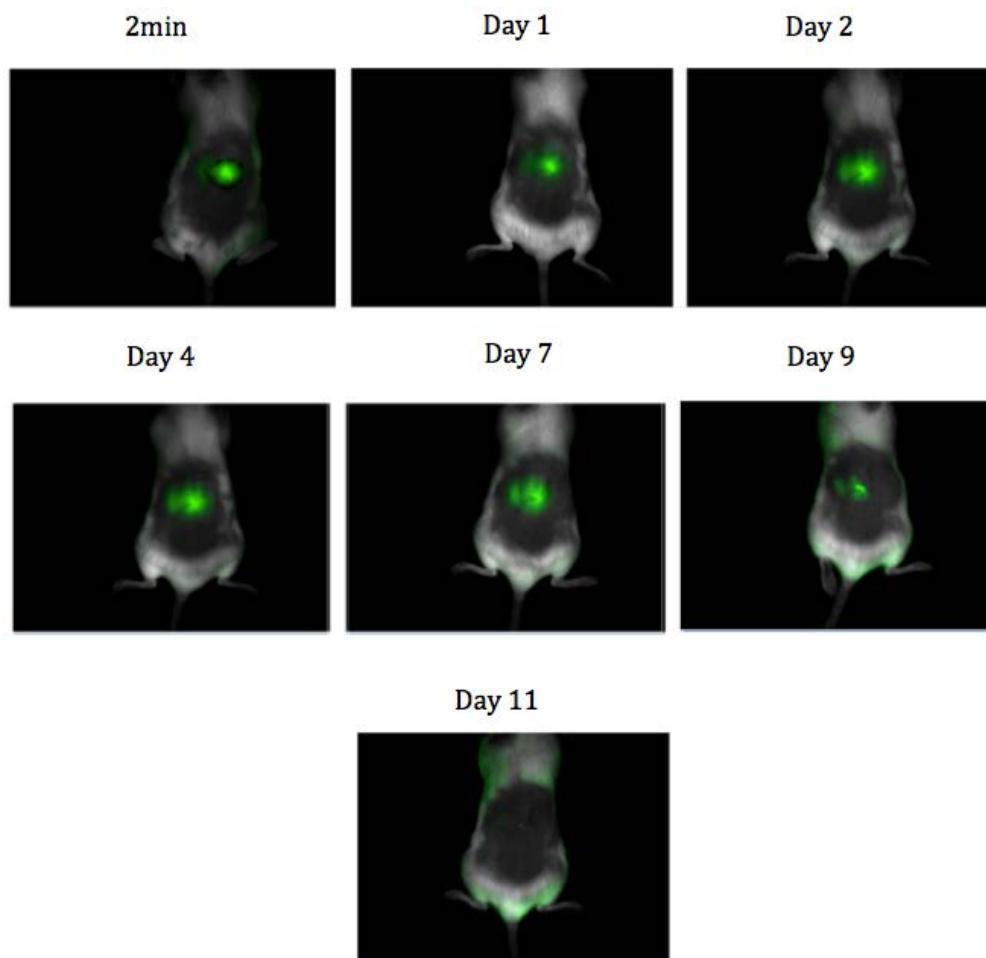


Figure 29 Overlay of the optical image and fluorescence image of mouse subcutaneously injected with nEGFP at different times post injections

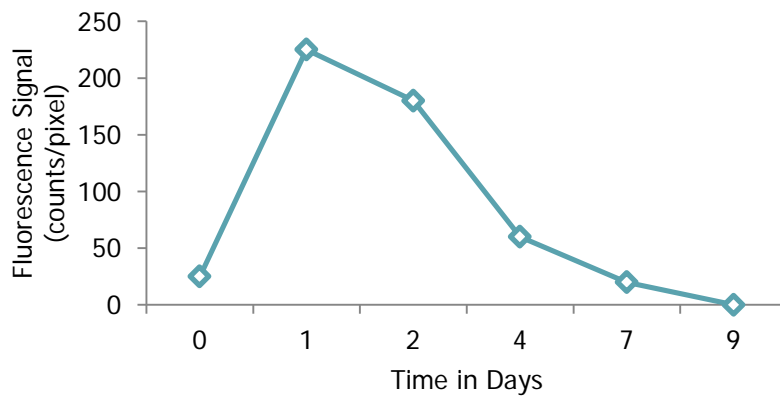


Figure 30 Fluorescence signal of injection site at different times post injection

To visualize the distribution of nEGFP in tissue, mouse skin sections were harvested from the injection sites. Both EGFP and nEGFP were observed in epidermis and dermis tissue at 1 hour after subcutaneous injection. EGFP exhibits a more homogeneous distribution, while nEGFP is localized mainly in the peripheral area round nuclei (Figure 31). Consistent with the observation of in-vivo image, very little native EGFP can be detected in the skin tissue 24 hours after injection, and no observable EGFP is in the epidermis/dermis tissue after 72 hours (Figure 32). On contrary, skin tissue on the injection site of nEGFP retains high fluorescence even after 72 hours, indicating a strong binding with the tissue on the injection site.

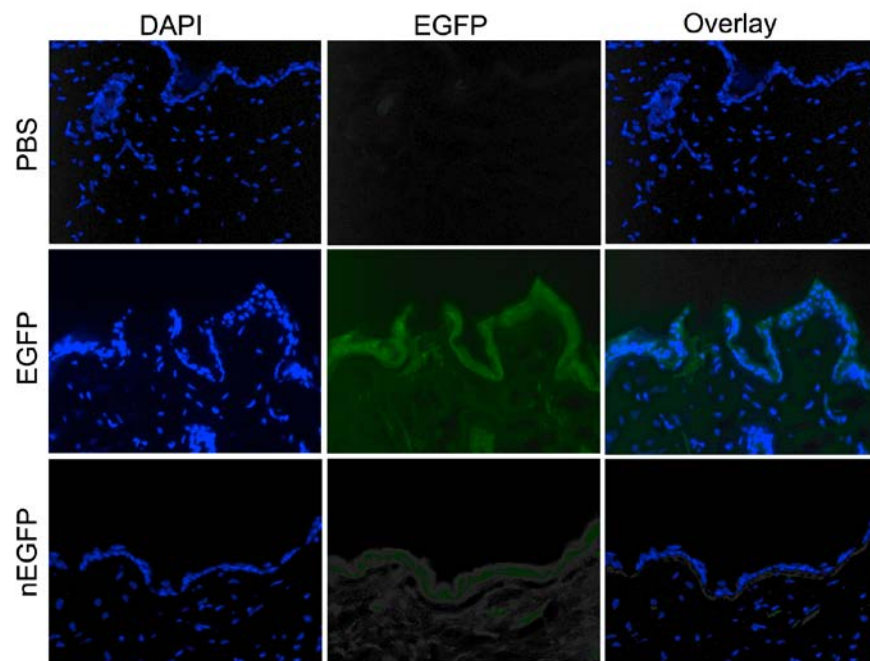


Figure 31 Fluorescence microscope images of mouse epidermis/dermis tissue sections, the slides were counter-stained with DAPI

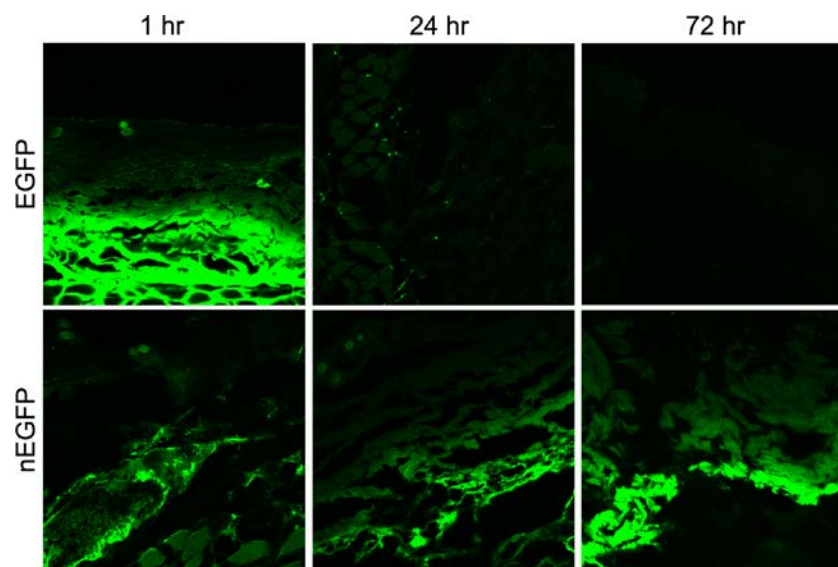


Figure 32 Confocal microscope images of mouse skin tissue

The ability of delivering active nanocapsules with high efficiency, long-term stability, and low toxicity opens a new avenue for protein therapies, imaging, tumor tracking, cosmetic and other applications. For example, the combination of indole-3-acetic acid (IAA) and HRP has recently been proposed as a potential prodrug for cancer therapy^{176,177}. IAA is well tolerated in human, and could be specifically transformed to a free radical intermediate by HRP and induces apoptosis in mammalian cells^{177,178}. nHRPs were firstly incubated with HeLa cells, which were then exposed to a chromogenic substrate. Green color in the cell medium intensified with increasing nanocapsule concentration, indicating a successful delivery of active HRP (Figure 33a). Consistently, the cells incubated with the nanocapsules show rapidly decreasing cell viability with increasing IAA concentration, whereas those with native HRP perform similarly to the untreated cells (Figure 33a), suggesting great potentials of using nanocapsules for cancer therapies.

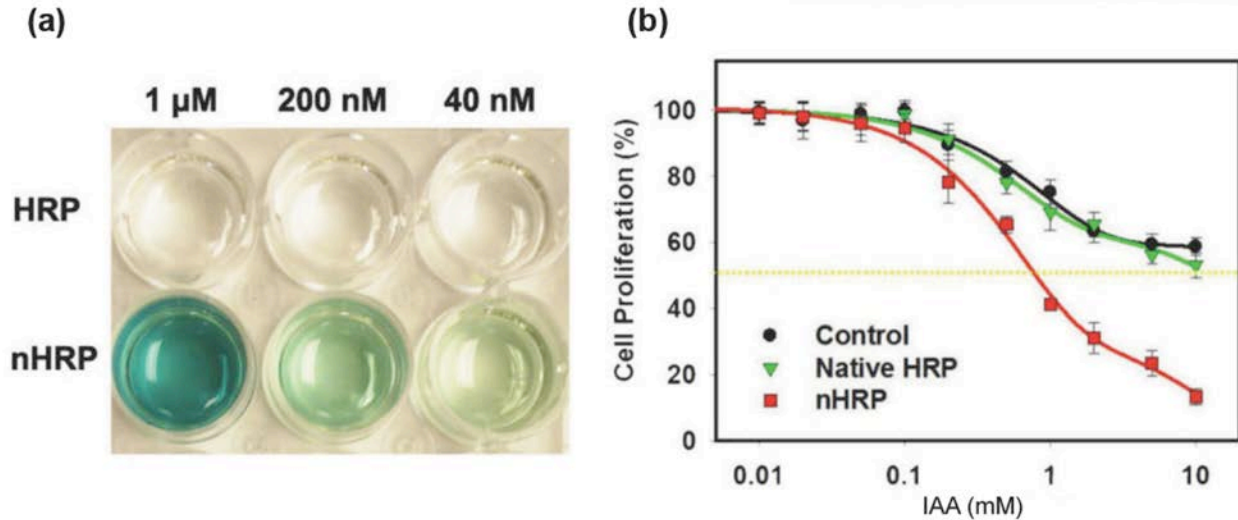


Figure 33 (a) HeLa cells after incubation with HRP or nHRP at different concentrations, followed by PBS washes and incubation with TMB and H₂O₂. (b) MTT assay showing HeLa cell viability after transduction with native HRP or nHRP and incubation with IAA. Cell proliferation rates normalized to untreated cells.

Similarly, with β -lactamase, we can also demonstrate that the enzymes remain active intracellularly. The activity of lactamase was examined with GeneBLAzer® FRET Assay. CCF2-AM substrate in the GeneBLAzer® FRET Assay is the membrane-permeable, esterified form of CCF2, a FRET dye with excitation wavelength of 405 nm and emission wavelength at 535 nm^{179,180}. CCF2 can be readily cleaved by β -lactamase to separate the fluorescence, generating emission at 460 nm with an excitation wavelength of 405 nm. Compared with CCF2, which is not taken up by cells, CCF2-Am is lipophilic and readily enters the cell. Therefore, monitoring the cellular fluorescence emission wavelength reveals the intracellular β -lactamase activities.

Figure 34 shows the cellular fluorescence of HeLa after incubated with nLac and nLac-lipid and treatment of GeneBLAzer® FRET Assay. VSVG-lac and PBS were used as positive and negative controls. Cells cultured with both nLac and VSVG-lac exhibit blue shift in fluorescence

emission wavelength compared with cells only loaded with CCF2-Am, indicating intracellular β -lactamase activity.

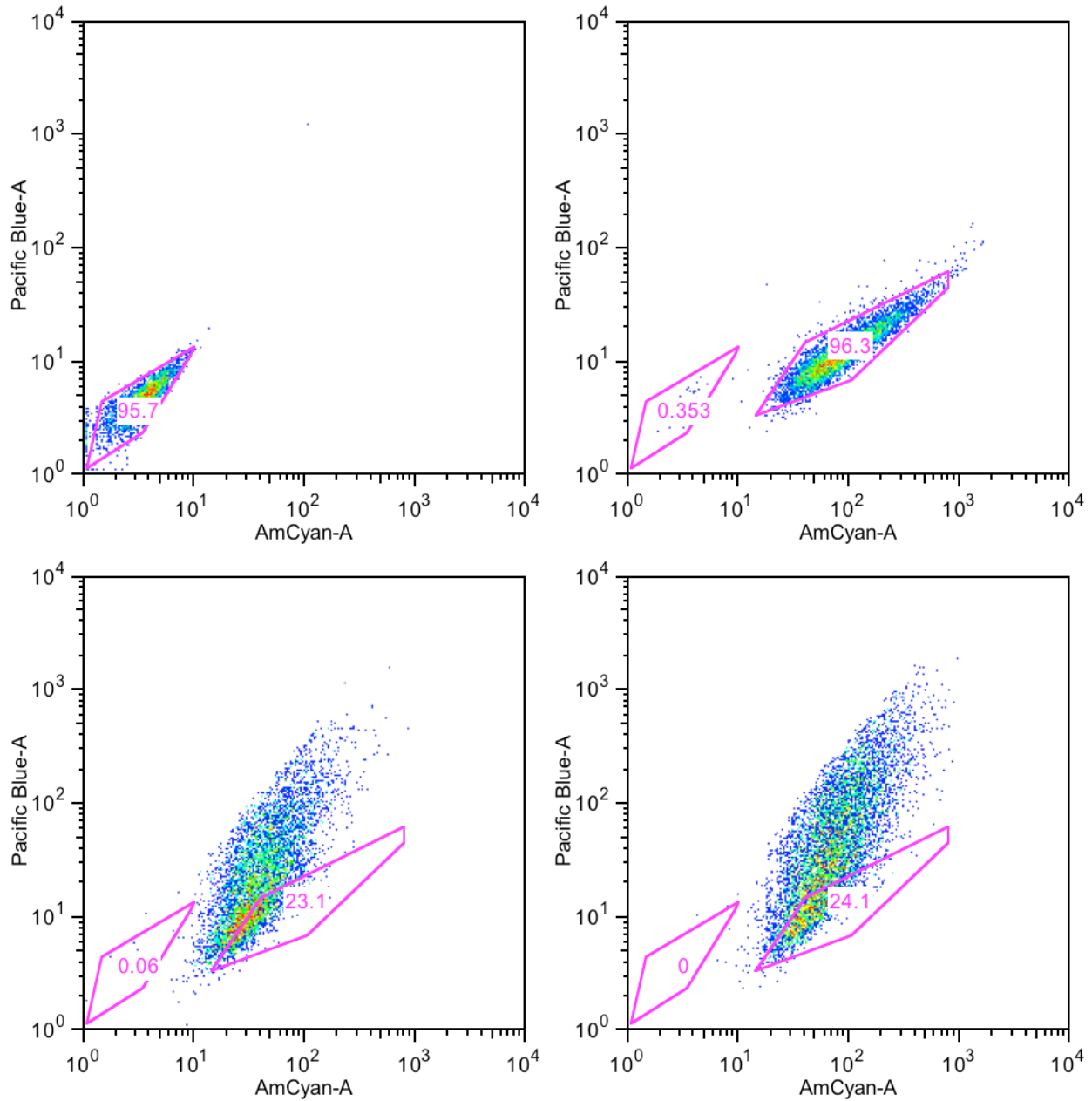


Figure 34 Intracellular lactamase activity CCR5 cells pre-incubated with VSVG-lac, nLac, nLac-lipid. 150 nM Bafilomycin is used to inhibit the acidification of endocytosis.

6.4. Intracellular delivery of the degradable nanocapsules

Using the non-degradable nanocapsule platform, we have demonstrated that proteins for small molecular substrates can be effectively delivered with long-term stability and high activity. For macromolecular substrates, however, the polymer skin may prohibit their access to the core protein. It is well-known that serum and late endosomes shows pH \sim 7.4 and 5.5, respectively. Acid-degradable nanocapsules were therefore developed to overcome this obstacle. Using de-nCAS and nCAS as example, we firstly studied their size evolution at pH 7.4 (Figure 35a) and 5.5 (Figure 35b). nCAS are stable in both pHs while de-nCAS is only stable at pH 7.4. At pH 5.5, the average diameter of de-nCAS rapidly decreases within 3 hours from 20 to 6 nm, a size similar to that of native caspase-3 (\sim 6 nm). Importantly, the degradable nanocapsules are stable against trypsin and chymotrypsin at pH 7.4 (Figure 35c), which allows the degradable nanocapsules to remain stable in the circulation system, to be degraded when inside the endosomes, and to release their protein cargo intracellularly.

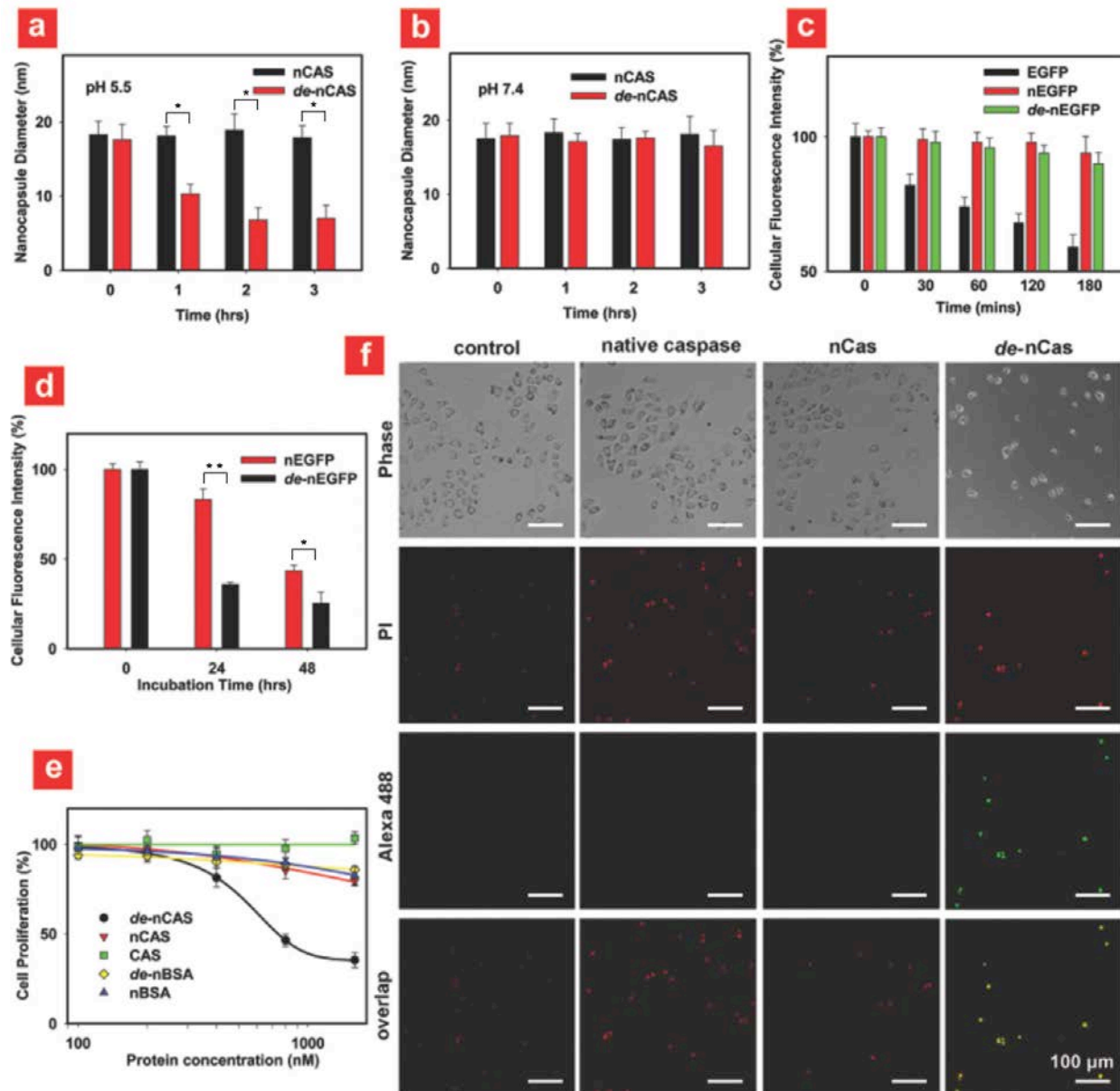


Figure 35 Degradable nanocapsules. Sizes of degradable Caspase-3 nanocapsule (de-nCAS) and non-degradable Caspase-3 nanocapsule (nCAS) at pH 7.4 (a) and pH 5.5 (b). mean \pm SD * $p < 0.005$ c, Fluorescence intensity of native EGFP, non-degradable EGFP (nEGFP) and degradable EGFP nanocapsules (de-nEGFP) after exposure to trypsin and chymotrypsin. Fluorescence intensities normalized to native EGFP before addition of proteases. d, Fluorescence intensity of HeLa cells at different times after incubation with nEGFP or de-nEGFP for 3 hr followed by incubation in fresh media. Fluorescence intensities were normalized to the respective cells that received no further incubation with fresh media. * $p < 0.05$, ** $p < 0.005$ e, MTT assay showing cell proliferation profile after incubation with various concentrations of de-nCAS, nCAS, caspase-3, de-nBSA or nBSA for 48 hrs. Data normalized to untreated cells. f, APO-BrdUTM TUNEL assay showing of

HeLa cells transduced *de*-nCAS, nCAS or caspase-3. PI-stained nuclei (red) and Alexa Fluor 488-stained nick end label (green) in cells incubated with *de*-nCAS show apoptotic DNA fragmentation.

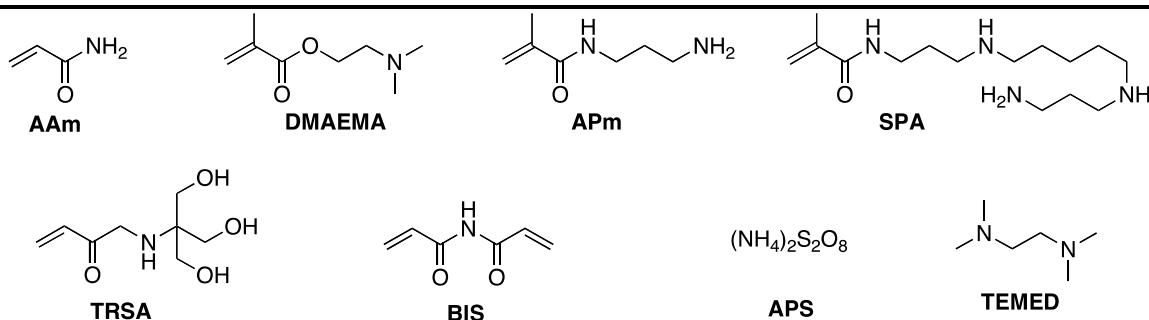
To further quantify the intracellular degradation, de-nEGFP and nEGFP were delivered to HeLa cells. Cellular fluorescence intensities of the cells with de-nEGFP are significantly lower than those with nEGFP after 24 hour (Figure 35d), confirming the degradable nanocapsules can strip off their shells in response to the acidic intercellular environment. Although a de-protection process inevitably exposes the cargo proteins to protease attack, it enables their functions with large substrates. For example, caspase-3, a member of cysteine proteases that play essential roles in apoptosis, necrosis and inflammation, cleaves other protein substrates within the cells to trigger apoptosis¹⁸¹⁻¹⁸³. As shown in Figure 35e, incubation of HeLa cells with native caspase-3, nCAS, de-nBSA or nBSA show similar viabilities that are significantly higher than those with de-nCAS. TUNEL assay (Figure 35f) confirms the apoptosis triggered by de-nCAs. Unambiguously, this work demonstrates the effective delivery of proteins while maintain their function with large substrates, a step closer to practical protein therapies.

6.5. Polymer composition and intracellular delivery

As the polymer composition can be readily adjusted by simply incorporating different monomer in the polymerization step, this method can be used to screen for suitable polymer composition for defined application purposes. In my research, I chose four different polymer compositions and investigated the influence of the polymer shell on cellular uptake of nanocapsules. The constitutions of the four polymers are listed in Table 9. Compared with nHRP1, nHRP2 has different neutral monomer. nHRP3 and nHRP4, however, possess different cationic monomer. The ratio of protein : neutral monomer : cationic monomer : crosslinker (BIS) : initiators (APS/TEMED) remains the same for these four nanocapsules.

Table 9 Mole ratio of monomers, crosslinker and initiators to protein in the synthesis of nHRP nanocapsules

	Protein	AAM	TRSA	DMAEMA	APm	SPA	BIS	APS	TEMED
nHRP1	1	4500	0	1500	0	0	300	300	600
nHRP2	1	0	4500	1500	0	0	300	300	600
nHRP3	1	4500	0	0	1500	0	300	300	600
nHRP4	1	4500	0	0	0	1500	300	300	600



All four nanocapsules show positive surface charge around 6 mV (Figure 36). Agarose gel electrophoresis also confirms the positive charge of the nHRPs, as they all migrate toward the cathode. The rates of migration for the four nHRPs are on the same level, possibly due to their similar size and charge.

	<u>zeta potential (mV)</u>
HRP	-1.33
<u>nHRP1</u>	7.11
<u>nHRP2</u>	7.06
<u>nHRP3</u>	5.08
<u>nHRP4</u>	6.43

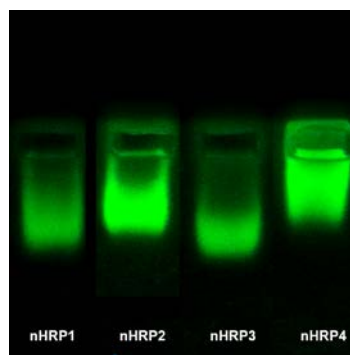


Figure 36 Image of agarose gel electrophoresis of fluorescence-labeled nHRP nanocapsules and zeta potential of nHRP nanocapsules

Although the sizes and surface potentials of the nHRPs are similar, they exhibit significantly different performance when incubated with cells. Figure 37 shows the cell viability after HeLa cells were incubated with nHRPs at different concentrations. Among the four nanocapsules, nHRP2 has the lowest cytotoxicity in the range from 7.2 nM through 720 nM. nHRP3&4 are

more toxic than nHRP1&2. The cells lost total viability after incubation with 720 nM nHRP3&4, whereas those treated with 720 nM nHRP2 retain more than 80% of viability. Interestingly, the cellular fluorescence of cells treated with 7.2 nM nHRP3 and 72 nM nHRP4 is comparable to those treated with 720 nM nHRP1 or nHRP2, indicating a much higher intracellular delivery efficiency of nanocapsules with APm and SPA as monomer. To further investigate the intracellular delivery of these nHRPs, the distribution of nHRP in cells after different incubation time was studied. All of the nanocapsules are internalized by cells with high efficiency. However, the intracellular distributions of nanocapsules are different. nHRP3 and nHRP4 delivered into cells displays punctate distribution, possibly due to endosome entrapment. As a comparison, nHRP1 and nHRP2 shows more cytosolic distributions in addition to vesicular distribution.

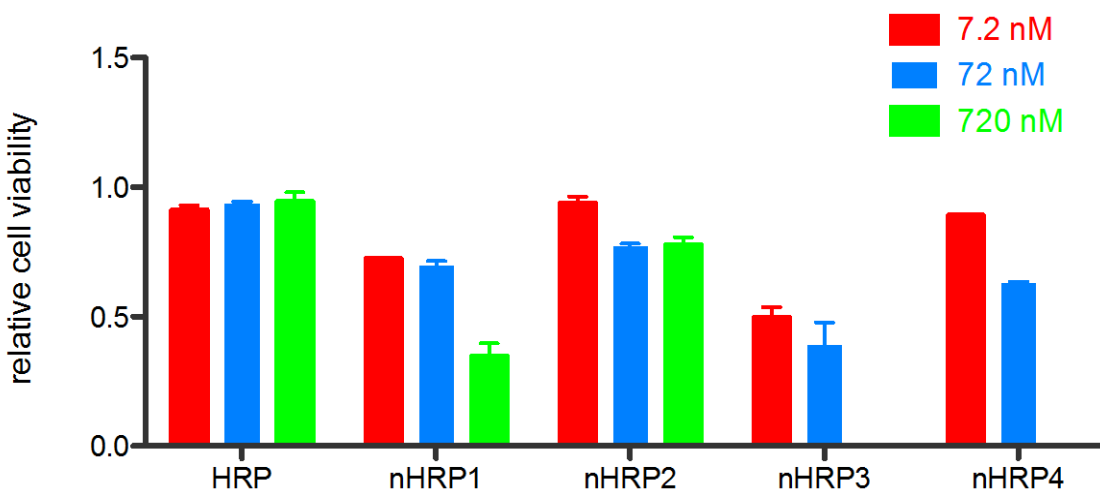


Figure 37 HeLa cell viability (mean \pm SD, n = 3) after incubation with HRP and nHRPs for 48 hours. The cells treated with PBS with equal volume is used as a control whose viability is set to 100%.

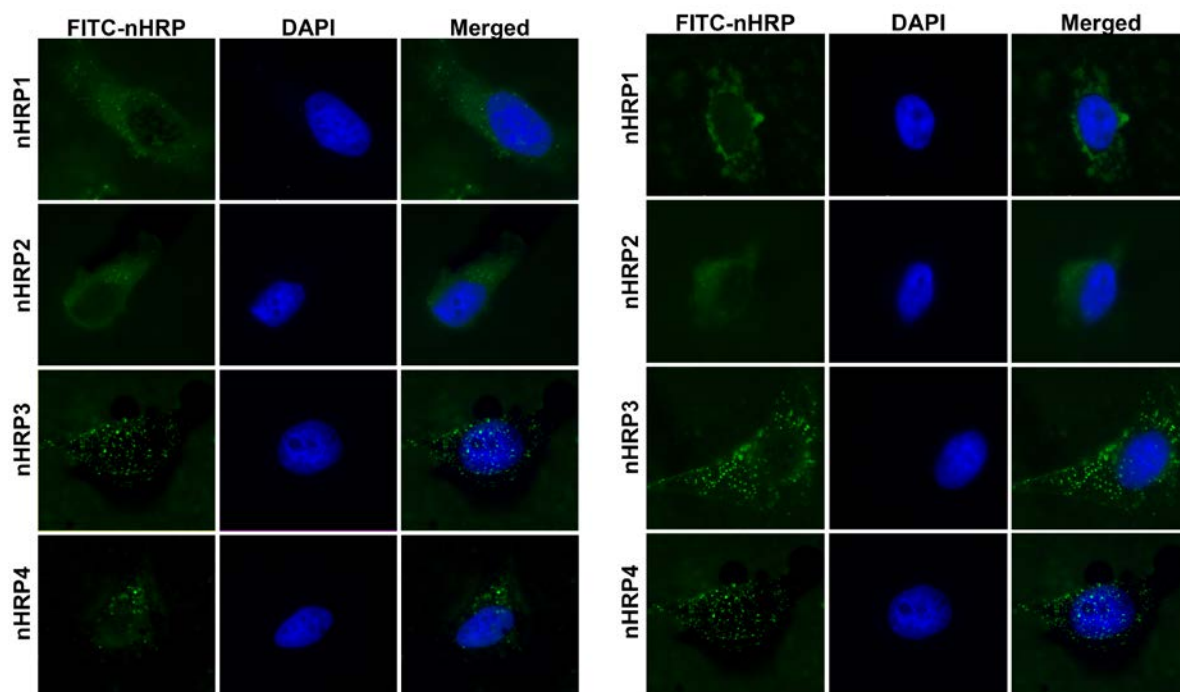


Figure 38 The fluorescence microscope images of HeLa cells after incubation with HRP nanocapsules with different polymer composition for 3 hours (left) or 12 hours (right). Cells were counter-stained with DAPI.

These observations suggest that the interaction of cationic nanoparticles with cells largely depends on the surface functionalities. Cationic monomer poses a major impact on the cellular toxicity, delivery efficiency and endosome entrapment. APm and SPA harbor primary amine group, which is a stronger base than DMAEMA. The strong base is a double-sided sword: it enables stronger interactions with cell surface receptors leading to more efficient cellular uptake. On the other hand, the high pKa (pAPm has a pKa ~ 10)^{140,141} accompanies with less buffering effect during endocytosis, resulting in inefficient endosome escape. Besides the cationic monomer, neutral monomer also has impact on the cell toxicity and intracellular distribution. nHRP2, which has hydroxyl-rich surface, causes lower degree of damages to cells without influence on intracellular delivery efficiency.

6.6. Summary

To conclude, we have demonstrated a general, effective, low-toxic intracellular protein delivery based on cationic single-protein nanocapsules. Cationic nanocapsules can be fabricated via copolymerization of neutral monomer and cationic monomer. The resulted cationic nanocapsules can be delivered into cellular interior with high efficiency and low toxicity. The cellular uptake is through an endocytotic process with partial release of the nanocapsules from the endosome. The nanocapsules delivered intracellularly can exert their biological functions in cells, harboring great potentials for cellular imaging, cancer therapies, anti-aging, cosmetics, and many other applications. Additionally, degradable nanocapsules can be prepared with degradable crosslinkers, which are sensitive to environmental alterations such as change of pH value, redox environment and protease attack. These degradable nanocapsules can release their protein cargo upon endocytosis, enabling the interactions of cargo protein with intracellular macromolecules.

Chapter 7. Nanocapsule as a Platform for Further Functionalization

7.1. Introduction

As the synthetic polymer layer in nanocapsules can be readily engineered, other functionality can be accessed with our design of nanocapsule. In this chapter, I will present bioluminescence nanocapsules based on the conjugation of quantum dot to nanocapsules, with which continuously tunable emission wavelength can be easily achieved.

Bioluminescence¹⁸⁴, the light emission resulted from enzymatic reactions within living organisms, is commonly used for various applications^{185,186}, such as whole-cell biosensors, immunoassays, nucleic-acid hybridization assays and in-vivo imaging. Many of these applications, however, require transfection of bioluminescent reporter genes, accompanied with

many other limitations, such as safety. Moreover, the wavelengths of bioluminescence are still limited to blue/green light, which hinders its use in deep-tissue applications^{187,188}.

Herein, we report a novel class of bioluminescent nanocapsules (BNs) that are robust, cell-permeable, and tunable in wavelength. Figure 39 illustrates our synthesis strategy. Starting with a bioluminescent protein, mild chemical modification attaches the protein with polymerizable vinyl groups; subsequent polymerization in an aqueous solution containing acrylamide (AAm) and N-(3-aminopropyl)methacrylamide (APTAaM) wraps the protein molecule with a thin polymer layer. Finally, linking the polymer-protein conjugate with fluorophores enables the conversion of short-wavelength bioluminescence to long-wavelength emission through bioluminescence resonance energy transfer (BRET)¹⁸⁹.

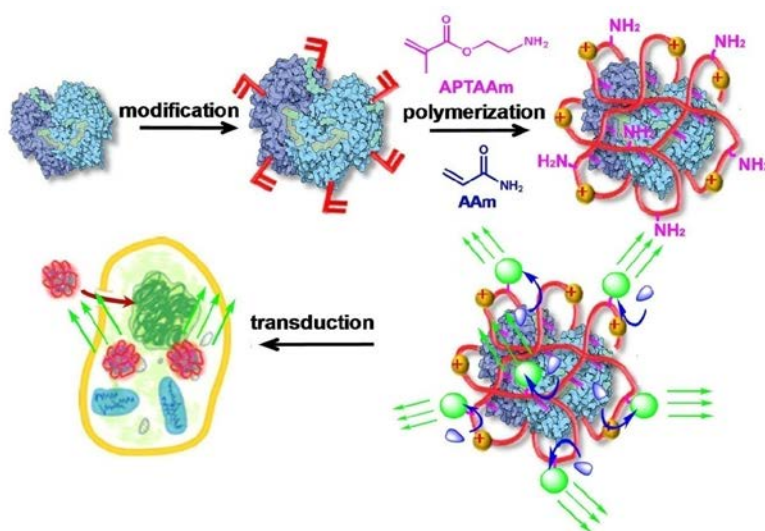


Figure 39 Scheme of forming robust, cell-permeable bioluminescent nanocapsules

This unique architecture endows the BNs with many advantages: 1) the thin polymer layer stabilizes the protein and enables rapid transport of the substrate to the encased protein, ensuring bioactivity and stability of the BNs¹⁹⁰; 2) fluorophores can be attached to the protein conjugates with controlled density, ensuring an efficient BRET. Particularly, quantum dots (QD)^{191,192}, a class of fluorophores with high photo-stability and quantum efficiency, wide-range excitation

and tunable emission, can be readily used as BRET receptors¹⁹³⁻¹⁹⁶; 3) as formed BNs are nano-sized and their surface charge can be readily tuned by controlling the ratio of neutral monomer (AAm) and cationic monomer (APMAAm) used, allowing their effective intracellular delivery; 4) targeting components, such as antibody, may be linked to the BNs for targeting purposes.

7.2. Experimental

Preparation of single HRP nanocapsules: Ten milligrams of HRP was dissolved in 1.8 mL of pH 8.5 50 mM sodium carbonate buffer. Then 4 mg N-acryloxysuccinimide dissolved in 20 μ L of DMSO was slowly added and the reaction was carried out for 2 h at room temperature. Finally the reaction solution was thoroughly dialyzed against pH 7.0 20mM phosphate sodium buffer. A solution containing a specific weight of acryloylated HRP at 4 mg was added to a vial and purged with nitrogen. Radical polymerization from the surface of the acryloylated HRP was initiated by adding 0.2 mg of ammonium persulfate dissolved in 20 μ L of deoxygenated and deionized water and 0.4 μ L of *N,N,N',N'*-tetramethylethylenediamine into the test tube. Then a specific amount of *N*-(3-aminopropyl) methacrylamide (APMAAm), acrylamide and *N,N'*-methylene bisacrylamide (molar ratio = 3:7:1) dissolved in 50 μ L deoxygenated and deionized water was added to the test tube over 60 min. The reaction was allowed to proceed for another 60 min in a nitrogen atmosphere. Finally, gel filtration with Sephadex G-75 was used to remove unreacted proteins, monomers and initiators.

Preparation of CdTe or CdHgTe/CdS Core/Shell QDs: CdTe or CdHgTe/CdS QDs were prepared according to Qian *et al.*'s method¹⁹⁷. CdTe precursor was prepared by adding NaHTe solution to Cd²⁺-MPA solution at pH 8.0-9.0. Briefly, 76 mg of NaBH₄ was transferred to a small flask that was cooled with ice; then, 3 mL of H₂O and 128 mg of Te powder were put into the flask. A small outlet was connected to the flask to release the resulting hydrogen. The black Te

powder disappeared, and white Na_2BO_4 precipitate appeared after 8 h. The resulting clear solution was transferred to 100 mL of degassed water. $\text{CdCl}_2 \cdot 5\text{H}_2\text{O}$ (0.0228 g) and MPA (0.0259 mL) were added to 100 mL of H_2O , and then the pH value of the solution was adjusted to 8.0-9.0. CdTe precursors formed after injection of 5 mL of as-prepared NaHTe solution. The $\text{Cd}^{2+}/\text{NaHTe}/\text{MPA}$ molar ratio was 1:0.5:3 in our experiments.

Hg^{2+} -MPA complex was prepared by dissolving $\text{Hg}(\text{ClO}_4)_2$ (0.5 mmol) and MPA (1.25 mmol) in 100 mL of water and adjusting the pH to 8.0-9.0 with 1 mol/L NaOH. Different amounts of Hg^{2+} -MPA were added to the CdTe precursors under vigorous stirring to prepare CdHgTe precursors. CdHg(5%)Te, CdHg(10%)Te, and CdHg(20%)Te denote the samples prepared when the added Hg^{2+} amount was 5%, 10%, and 20% of the CdTe precursor solution as calculated from the content of added CdCl_2 . In our experiments, the CdHgTe precursors were heated at 90°C for different times to control the size of the CdHgTe QDs.

The Cd^{2+} -MPA-thioacetamide precursor was first prepared by mixing $\text{CdCl}_2 \cdot 5\text{H}_2\text{O}$ (0.114g), MPA (0.129 mL) and thioacetamide (0.0375 g) in 50 mL of ultrapure water, and the pH of this solution was then adjusted to 8.0-9.0. For the preparation of CdTe or CdHgTe/CdS core/shell QDs, we added a solution of the as-prepared Cd^{2+} -MPA-thioacetamide precursors to a given volume of CdTe or CdHgTe QDs (such that the molar ratio of thioacetamide added to initial Te was 1:1), and then the mixture solution was heated at 90°C for 30min to form CdTe or CdHgTe/CdS core/shell nanocrystals.

Conjugation of QDs and nanocapsules: To 100 μL pH 6.0 10^{-4} M MPA-coated CdTe QD solution, 1 mg 1-ethyl-3-(3-dimethylaminopropyl) carbodiimide (EDAC) 1 μL 10% N-hydroxy-succinimide (NHS) were added. After the reaction at room temperature for 1 hour, 1 mg HRP nanocapsules dissolved in 900 μL pH 7.0 20 mM phosphate buffer were added. The reaction was

carried out at room temperature for another 1 hour. Unreacted QDs were removed using an ultra-filtration membrane (Micoron YM-50–50000 NMWL, Millipore, USA) according to the instructions from the manufacture.

Bioluminescence Spectroscopy: During a measurement, to 965 μL pH 9.0 carbonate buffer, 10 μL 50 mM *p*-iodophenol, 10 μL 20 mM luminol and 10 μL 50 mM hydrogenperoxide were added. Vortex the mixture for 15 s, and certain amount of HRP or bioluminescent nanocapsules was added. The emission spectra were immediately measured with QuantaMaster Spectrofluorimeter.

In vitro cellular internalization: HeLa cells were cultured in Dulbecco's modified Eagle's medium (DMEM) supplemented with 10% bovine growth serum (BGS) and 1% penicillin/streptomycin. Cells (25000 cells/well, 24-well plate) were seeded the day before adding the nanocapsules. Nanocapsules or native proteins with different concentrations were added into the cell medium. After incubation at 37 °C for 3 hrs, the cells were washed three times with PBS and either visualized with a fluorescent microscope or trypsinized, centrifuged, re-suspended in PBS and analyzed via Modulus™ Single Tube Multimode Reader (Turner Biosystem). During the measurement of cellular luminescence, 1 μL 50 mM *p*-iodophenol, 1 μL 20 mM luminol and 1 μL 50 mM hydrogenperoxide were added to 200 μL cell suspension and mixed. The luminescence was read immediately.

7.3. Results

To demonstrate this concept, we used horseradish peroxidase (HRP) as a model bioluminescent protein and QDs of CdTe as the model fluorophores. Water-soluble QDs with emission wavelengths of 517, 544, 579, 696, 724 and 754 nm (Figure 40a) were respectively attached to the HRP-polymer conjugates (nHPR), creating a series of BNs with tunable emission (denoted as

BN-wavelength, such as BN-517). Figure 41a shows a representative TEM image of the QDs with an emission wavelength of 544 nm (denoted as QD-544), demonstrating uniform size distribution with an average diameter of 2-3 nm. Figure 41b shows a TEM image of BN-544, suggesting that each BN has an average diameter of 17 nm and contains 3-4 QDs. The zeta potentials of the BNs were typically around 9 mV (Figure 42).

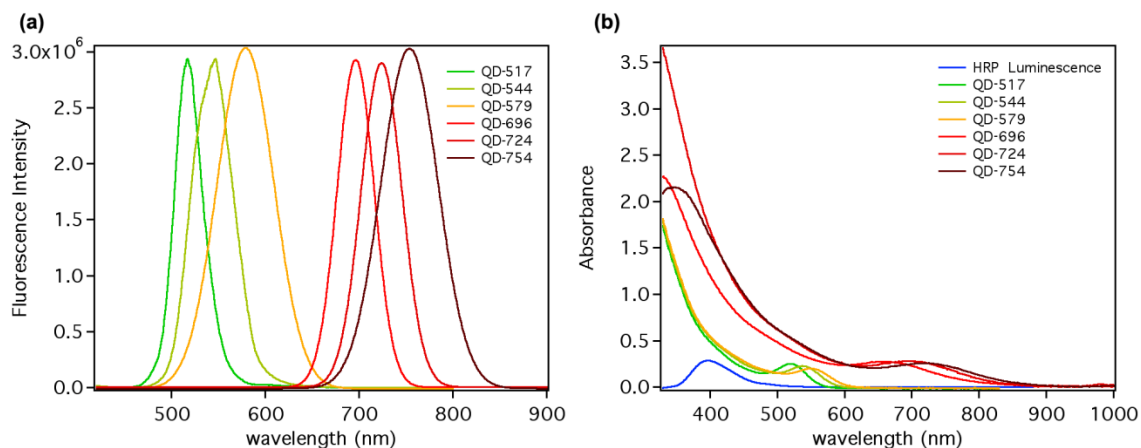


Figure 40 (a) Fluorescence spectra of CdTe QDs (excitation wavelength: 400 nm); (b) Luminescence emission of HRP-catalyzed oxidation of luminol (blue) and UV-Visible absorption of CdTe QDs.

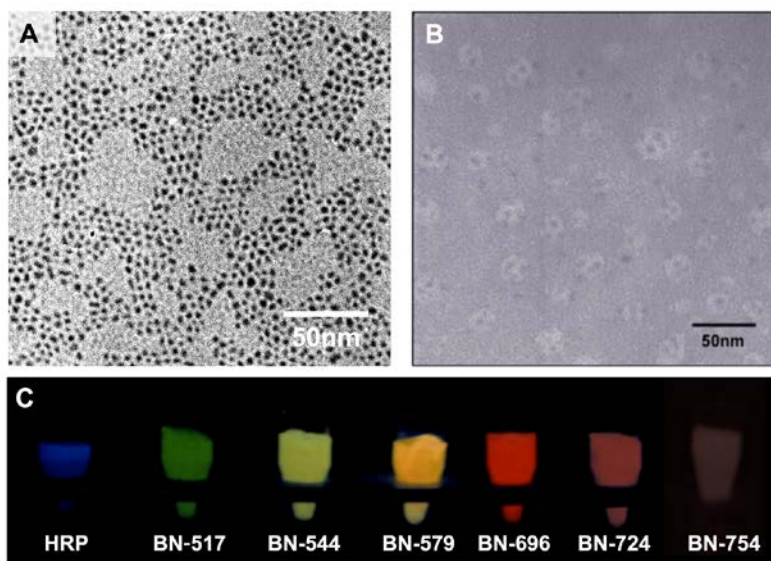


Figure 41 TEM images of (A) QD-544 and (B) BN-544; (C) photographs of HRP and BNs in the presence of H₂O₂, luminol and *p*-iodophenol showing tunable-wavelength bioluminescence

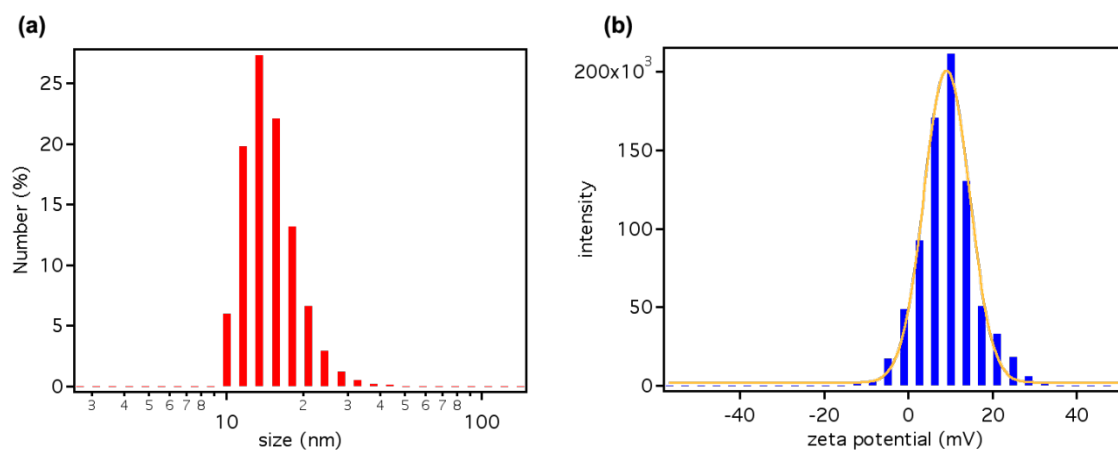


Figure 42 (a) Number distribution of particle size of bioluminescent HRP nanocapsules determined by DLS; (b) Zeta potential distribution of bioluminescent HRP nanocapsules

Note that the absorbance wavelengths of the QDs (Figure 40b) well overlap with that of the bioluminescence generated from HRP-mediated oxidation of luminol (425 nm), which allows their effective energy transfer. Figure 43a shows the fluorescent spectra of BNs with different emission wavelengths. As expected, besides the HRP bioluminescence at 425 nm, these BNs emits additional intense luminescence centered at 517, 544, 579, 696, 724 and 754 nm, respectively, which are in accordance with the fluorescence emissions of their conjugated QDs. Consistently, these BNs show bioluminescence color tunable from blue to red (Figure 41c). BNs with emission wavelength in the range of 700 to 800 nm are, of particular, importance for deep-tissue imaging owing to its deep-tissue penetrating capability^{187,198}.

Besides tunable wavelength, these BNs also show tunable bioluminescent intensity, which was achieved by tuning the number of QDs attached to each BN (denoted as QD/HRP ratio). For example, Figure 43b demonstrates bioluminescence spectra of BN-544 with different QD/HRP ratios. Clearly, the luminescent intensity at 544 nm increases with increasing QD/HRP ratio. The BRET ratios determined are 0.48, 1.39, 5.06 and 8.92 for the QD/HRP ratio of 1.2, 2.3, 4.9

to 9.6, respectively. It has been demonstrated that directly linking luciferase (another bioluminescent protein) to QDs resulted in bioluminescence conjugates containing QD cores and luciferase shells. In this configuration, BRET occurred only between the core QDs and the excitation-state products diffused inwards the conjugates. Consequently, although the conjugates could emit bioluminescence with tunable wavelength, their BRET ratios were significantly lower (i.e., <0.5)¹⁹³. In contrast, the BNs reported herein contain bioluminescent-protein cores and polymer shells containing tunable number of QDs. Such a unique architecture maximizes the harvest of bioluminescence, creating a series of BNs with significantly higher intensity.

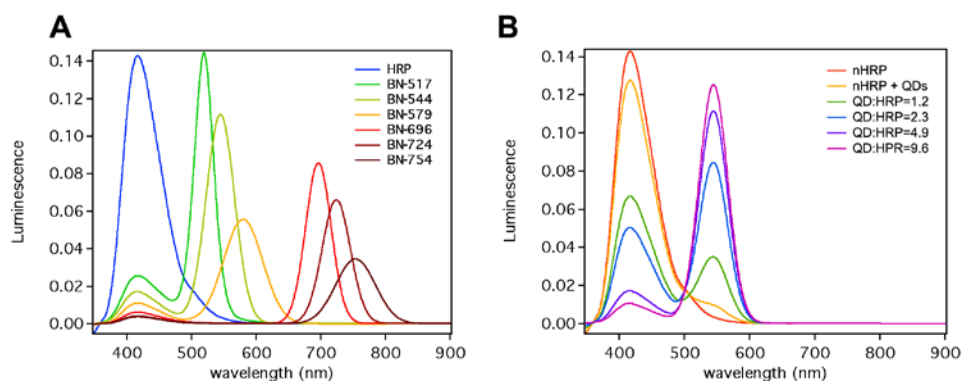


Figure 43 (A) luminescent spectra of (A) native HRP, BN-517, BN-544, BN-579, BN-724 and BN-754, (B) HRP-polymer conjugates (nHRP), mixture of nHRP and QD-544, and BN-544 with various QD/HRP ratios

It is also worth mentioning that BRET occurs only when the distance between donor and acceptor is less than 10 nm¹⁹⁹. To create such a BRET response, the excitation-state products of the enzymatic reaction must be diffused to adjacent QDs before they decay to their stable species. Indeed, mixing the HRP-polymer conjugates with QD-544 resulted in much weaker emission intensity (544 nm), in comparison with BN-544 containing the same HRP to QD ratio (Figure 43b). This observation further confirms BRET is the main mechanism to illuminate the BNs.

Furthermore, such BNs are extremely robust and cell transductable. For example, native HRP lost 52% and 73% of its original luminescence intensity after incubation at 37 °C for 24 hrs and 48 hrs, respectively (Figure 44a). On the contrary, BNs retained 99% and 98% of its luminescence intensity under the same conditions. This result validates our hypothesis that polymer network around HRP could protect the core protein from denaturation. Figure 44b shows a fluorescent image (Inset) of HeLa cells after 3-hour incubation with BN-696, clearly suggesting cellular uptake of the BNs. The bioluminescent intensity increases with increasing BN concentration (Figure 44b), indicating a concentration-dependent cellular uptake and retained intracellular activity. Such robust, cell transductable BNs are of particular interest for *in vivo* imaging and other applications.

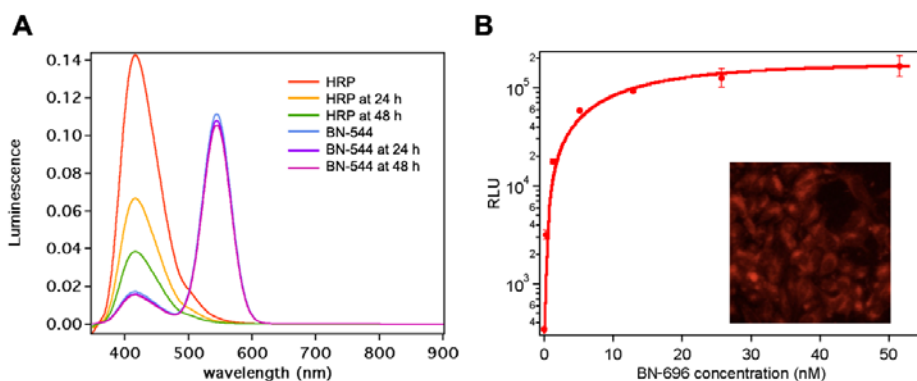


Figure 44 (A) Luminescence spectra of HRP and BN-544 after incubation at 37 °C for 0 hr, 24 hr and 48 hr. HRP and BN-544 were exposed to same amounts of H₂O₂, luminol and p-iodophenol during acquisition of spectra. (B) Relative luminescence unit (RLU) of HeLa cells pretreated with BN-696 with different concentrations. Inset: Fluorescent microscope images of HeLa cells pretreated with BN-696, showing cellular uptake of BNs

7.4. Summary

In summary, we have demonstrated a novel class of robust, cell-transductable bioluminescent nanocapsules with tunable emission wavelengths by conjugating quantum dot to bioluminescent nanocapsules. The bioluminescence emitted by the protein can be effectively transferred to the

adjacent quantum dots (QD) via bioluminescence resonance energy transfer (BRET). The QD-nanocapsule conjugates, therefore, obtained red-shifted wavelength, suitable for in-vivo bioluminescence imaging. The BRET ratio can be readily adjusted by altering the QD/nanocapsule ratio. The capability to transfer the cellular membrane enables the intracellular applications of QD/nanocapsule conjugates. This technique provides us new potentials for bioluminescence imaging, therapeutic and other applications.

Chapter 8. Non-endocytotic Delivery of Nanoparticles

8.1. Introduction

The cell membrane is a natural barrier that prohibits foreign polar molecules from entering the cell interior. Although it is an excellent defense system against harmful substance in the extracellular environment, it also prevents therapeutic agents especially macromolecules to access their intracellular targets. Over the years, numerous researchers have devoted themselves to develop drug delivery approaches to overcome this natural barrier. Various strategies have been invented, including the utilization of liposomes^{95,96,200}, cell-penetrating peptides^{88,165}, virus capsids^{201,202}, and other vehicles. With these vehicles mediate the cellular uptake of therapeutic macromolecules primarily via an endocytotic pathway¹⁷³. This process, however, is commonly associated with limited endosomal release, and efficiency depended on cell type. Although nature presents us excellent delivery strategies to bypass endocytosis, e.g. paramyxovirus²⁰³, the non-endocytotic pathway is rarely explored. Recently, we developed a novel strategy to deliver protein and genes across the plasma membrane via a non-endocytotic pathway. By encapsulating proteins in a cationic polymer shell, we could intracellularly deliver the proteins with high efficiency. The delivered protein is uniformly distributed in cytosol after cellular uptake.

Moreover, similar levels of cellular uptake were achieved even in the presence of inhibitions of low pH-dependent endocytosis. We believe that delivery through non-endocytotic pathways represents a breakthrough novel approach in the drug delivery field.

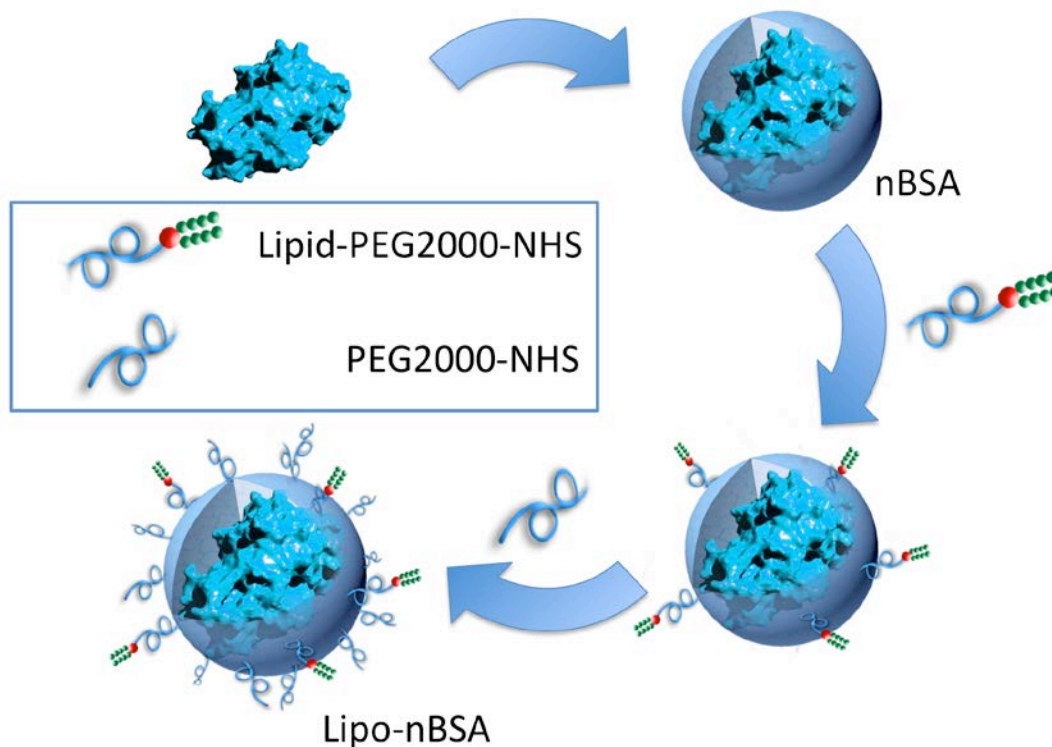


Figure 45 Schematic illustration of the synthetic approach for PEG-lipid conjugated nanocapsules

8.2. Experimental

Acryloylation of bovine serum albumin (BSA): All buffers should be degassed before use. 30 mg of bovine serum albumin at 5 mg/mL concentration in 20 mM sodium phosphate buffer pH 7.0 is reacted with 15 μ L of 10% w/v of N-acryloxysuccinimide in DMSO (20:1 molar ration of NAS to protein) for 2 hr at room temperature. The solution is stirred gently and the vial must be kept covered during the reaction. After 2 hrs the reaction solution should be thoroughly dialyzed against 10 mM phosphate buffer pH 7.0 at 4C with stirring using a 10kDa membrane.

Polymerization: Add the required amounts of 200mM phosphate buffer pH 7.0 and DI water to the vial according to the recipe below. To this solution add the required amount of acryloylated MSA in 20mM phosphate buffer pH 7.0 solution so that the final concentration in the reaction mixture is 1mg/ml Then add specific amounts of monomer (acrylamide, AAm, 20% w/v aqueous solution), co-monomer (APm 20% w/v aqueous solution) and crosslinker (N,N'-methylene bisacrylamide, BIS, 10% w/v DMSO solution) to the protein solution as mentioned in the table below. Add monomer followed by co-monomer and crosslinker sequentially. Free radical polymerization from the surface of the acryloylated protein was initiated by adding N,N,N',N'-tetramethylethylenediamine (TEMED) followed by the addition of ammonium persulfate (APS, 10% w/v aqueous solution). The vial was covered and the mixture was stirred gently. The reaction was allowed to proceed for 2 hours at room temperature. Finally, dialysis at 4 °C using a 10kDa membrane and 10 mM pH 7.0 phosphate buffer was performed to remove monomers and initiators.

The amounts of reagents added into the polymerization reaction are listed in the following table:

Table 10 recipes for encapsulation of BSA

	Protein	AAm	APm	BIS	APS	TEMED
Mol. Weight	67000	71	178.66	154.17	228.2	-
Mol. Ratio	1	2500	500	300	300	-
weight (mg)	1	2.65	1.33	0.69	1.02	2.04
Cstock (mg/mL)	10	200	200	100	100	775
V (μL)	100	13.25	6.67	6.90	10.22	2.64

PEG-Lipid/PEG Conjugtion: To a 1 mL nBSA solution containing 1 mg BSA, 0.86 mg DSPE-PEG(2000) Succinyl (20x mole ratio, 1,2-distearoyl-sn-glycero-3-phosphoethanolamine-N-[succinyl(polyethylene glycol)-2000] (ammonium salt), Mwt = 2890.6 g/mol), 0.28 mg N-(3-Dimethylaminopropyl)-N'-ethylcarbodiimide hydrochloride (100x mole ratio, EDAC, Mwt =

191.7 g/mol) and 3.5 3.4 μ L 5 mg/mL N-Hydroxysuccinimide aqueous solution (10x mole ratio, NHS, Mwt = 115.09 g/mol) were added. The mixture was stirred gently at 4 °C for 1 hour and 0.6 mg O-[(N-Succinimidyl)succinyl-aminoethyl]-O'-methylpolyethylene glycol 2000 (20x mole ratio, PEG2000-NHS) was added. The reaction was carried out for another 1 hour at 4 °C and the conjugated nBSA was then dialyzed thoroughly against 10 mM pH 7.0 phosphate buffer.

Determining Number of PEG-lipid and PEG: The average number of lipid and PEG conjugated on the each type of enzymes was determined by measuring the residual (unreacted) lysine on the protein with a fluorescamine assay. The assay can be described as follow. Fluorescamine was first dissolved in anhydrous DMSO to make a 3 mg/mL stock solution. nBSA, nBSA-lipid and nBSA-lipid-PEG were prepared to contain 0.5 mg/mL BSA with 0.1 M phosphate buffer (pH = 7.0), respectively. The native and acryloylated enzymes were diluted with 0.1 M phosphate buffer (pH = 7) to make a series of concentrations with 0.00781, 0.01563, 0.03125, 0.0625, 0.125, 0.25, and 0.5 mg/mL, pipette 100 μ L of each solution to an opaque 96-well plate, respectively. 30 μ L of fluorescamine solution was then added into each well, incubate the plate for 1 h at room temperature (25°C). After incubation, fluorescence intensity (Ex = 360 nm, Em = 465 nm) was read with a plate reader. Glycine solutions with concentrations of 10 μ M, 5 μ M, 2.5 μ M, 1.25 μ M, 0.625 μ M, 0.312 μ M, and 0.156 μ M were used as standard to quantify the amine amount in each sample. The number of residual lysine can be calculated by comparing the fluorescent intensity of acryloylated and native enzymes.

Cell Viability Assay: Cell viability was determined by resazurin assay. NIH/3T3 cells were seeded at a density of 5000/well in a 96-well plate the day before the experiment. 16 hours later, nBSA-lipid-PEG and nBSA with different concentrations were added into the cell medium and incubated for 24 hours. After the incubation, the medium was exchanged and resazurin was

added to a final concentration of 0.01 mg/mL. The cells were incubated at 37 °C for another 3 hours and the fluorescence with 535 nm excitation and 595 nm emission was read. Untreated cells and medium without cells were used as controls.

Intracellular Delivery: Cellular internalization studies were assessed via fluorescence microscopic technique and fluorescence-activated cell sorting (FACS). HeLa cells were cultured in Dulbecco's modified Eagle's medium (DMEM) supplemented with 10% fetal bovine serum (FBS) and 1% penicillin/streptomycin. Cells (20000 cells/well, 24-well plate) were seeded the day before adding samples. Before the experiment, medium was exchanged to fresh DMEM with 1% P/S and incubate for 30 min. nBSA-lipid-PEG or nBSA with different concentrations were then added into the cell medium. After incubation at 37 °C or 4 °C for 2 to 4 hrs, the cells were washed three times with PBS and either visualized with a fluorescent microscope or trypsinized, centrifuged, and re-suspended in PBS or PBS containing trypan blue and analyzed via FACS.

Calcein Uptake and Endocytosis Blockage Experiments: To study the influence of lipid-PEG-nBSA nanoparticles on the uptake of calcein (Invitrogen), 1.4 mg/mL stock of calcein in PBS buffer (pH 7.4) was used. Nanoparticles at a final concentration of 0.02 mg/mL (protein content) and calcein at a final concentration of 0.1 mg/mL were added to HeLa cells in serum-free DMEM medium. The incubation time was three hours and washing and imaging done similar to other fluorescence microscopy experiments. Calcein was excited at 488 nm, while the dye functionalized nanoparticles were excited at 633 nm.

To observe the nanoparticles entering the cytosol at 37 °C after blockage of endocytosis, the cells were pretreated with final concentrations of 10 mM and 50 mM of sodium azide (EM Science) and 2-deoxyglucose respectively for 20 min at 37 °C. Then, calcein (0.2 mg/mL final

concentration) was added with or without the nanoparticles (0.02 mg/mL final concentration, based on protein content) and incubated with cells for another 20 min. Thereafter, the cells were washed and imaged as described above. Control samples without calcein and nanoparticles, treated under the same conditions were also studied.

β -Lactamase Nanocapsules: nLac-lipid-PEG was synthesized with similar protocol with BSA.

The reagent amounts used in the process are listed in Table 11 and Table 12.

Table 11 Recipe for synthesis of nLac

	Protein	AAM	APm	BIS	PDC	APS	TEMED
Mol. Weight	33000	71	178.66	154.17	748.91	228.2	-
Mol. Ratio	1	2500	500	300	0	300	-
weight (mg)	0.1	0.54	0.27	0.14	0.00	0.21	0.41
Cstock (mg/mL)	10	200	200	100	100	100	775
V (μ L)	10	2.69	1.35	1.40	0.00	2.07	0.54

Table 12 Amounts of reagents added to conjugate nLac to PEG-lipid and PEG-NHS

	protein	PEG-lipid	EDAC	NHS	PEG-NHS
Mol. Weight	33000	2890.6	191.7	115.1	2000
Mol. Ratio	1	20	100	10	20
weight (mg)	0.1	0.175187879	0.058090909	0.003487879	0.121212121

Cellular β -Lactamase Activity assay: The CEM cells were seeded at a density of 5×10^5 cells/mL into 96-well plates in a volume of 100 μ L (50,000 cells). The following morning, nLac or nLac-lipid-PEG were incubated with cells for 3 hours with or without 150 nM bafilomycin. After treatment, cells in 96-well microplates were assayed with GeneBLazer® FRET Cell-based Assay from Invitrogen. Fluorescent measurements were made using a Synergy 4 Hybrid Microplate Reader. All measurements were made from the bottom using a 400/30-excitation filter and both a 460/40 and 528/20 emission filters.

8.3. Results

The synthetic approach for non-endocytotic nanocapsules is illustrated in Figure 45. Following encapsulating proteins in polymer shell functionalized with amine groups, PEG2000-NHS and lipid-PEG200-NHS are reacted with the nanocapsules, yielding lipid-PEG-nanocapsules (denoted as lipid-PEG-nProtein, such as lipid-PEG-nBSA).

As shown in Figure 46 and Table 13, after conjugation with PEG-lipid and PEG-NHS, BSA nanocapsules have an increased average diameter of 19.5 nm compared with a size around 12.3 nm of nBSA. The zeta potential decreases from 4.08 mV to 1.24 mV, indicating successful conjugation of PEG-lipid and PEG-NHS with the amine groups on nBSA surface. Table 14 validates the successful conjugation. By measuring the surface amine groups on nBSA, we estimated that each nBSA contains ~193 accessible amine groups. Out of this 193 amine groups, ~23 amine groups were reacted to lipid-PEG and ~14 amine groups were reacted with PEG-NHS.

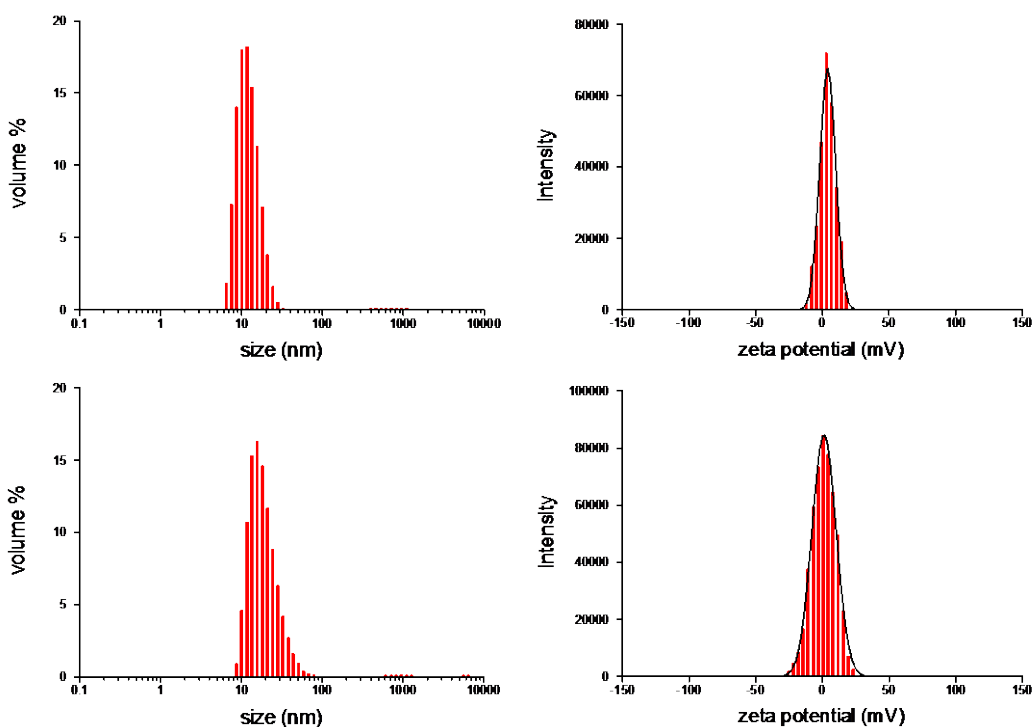


Figure 46 Size and zeta potential distribution of BSA nanocapsules and nBSA-lipid

Table 13 Average size and zeta potential

	Size (nm)	Zeta potential (mV)
nBSA	12.34	4.08
nBSA-lipid	19.46	1.24

Table 14 Number of amine groups on nBSA, nBSA-lipid and nBSA-lipid-PEG

nBSA	nBSA-lipid	nBSA-lipid-PEG
193 ± 16	170 ± 15	156 ± 16

The successful conjugation of PEG-lipid and PEG-NHS to nBSA greatly reduces the cytotoxicity associated with cationic nanocapsules. As shown in Figure 47, increasing nBSA concentration causes decreased cell viability. After incubation with 1.6 μ M nBSA, HeLa cells retain 46% of its original viability. nBSA-lipid-PEG, however, has a much lower cytotoxicity. No significant

cytotoxicity was observed up to a concentration of 1.6 μM . The significantly reduced toxicity can be attributed to decreased surface charge.

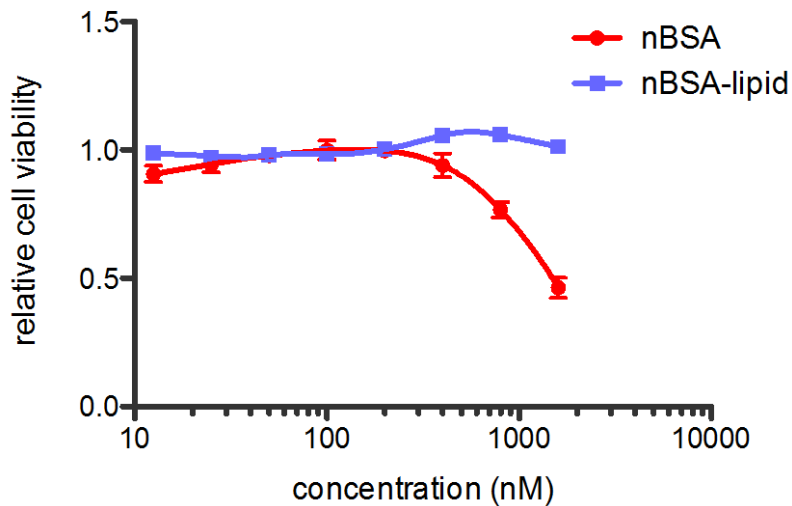


Figure 47 Cytotoxicity of BSA annocapsules and nBSA-lipid in HeLa Cells

Intracellular delivery efficiency was studied with Fluorescein isothiocyanate labeled BSA, nBSA and nBSA-lipid-PEG. Figure 48 is the image of HeLa cells after incubation with BSA, nBSA and nBSA-lipid-PEG for 3 hours. As expected, nBSA can be internalized by cells with a high efficiency. However, nBSA delivered in HeLa cells displays the punctate distribution, possibly due to endosome entrapment. As a comparison, nBSA-lipid-PEG can also be efficiently delivered into HeLa cells. In addition, cytosolic distribution was observed in HeLa cells pre-incubated with nBSA-lipid-PEG.

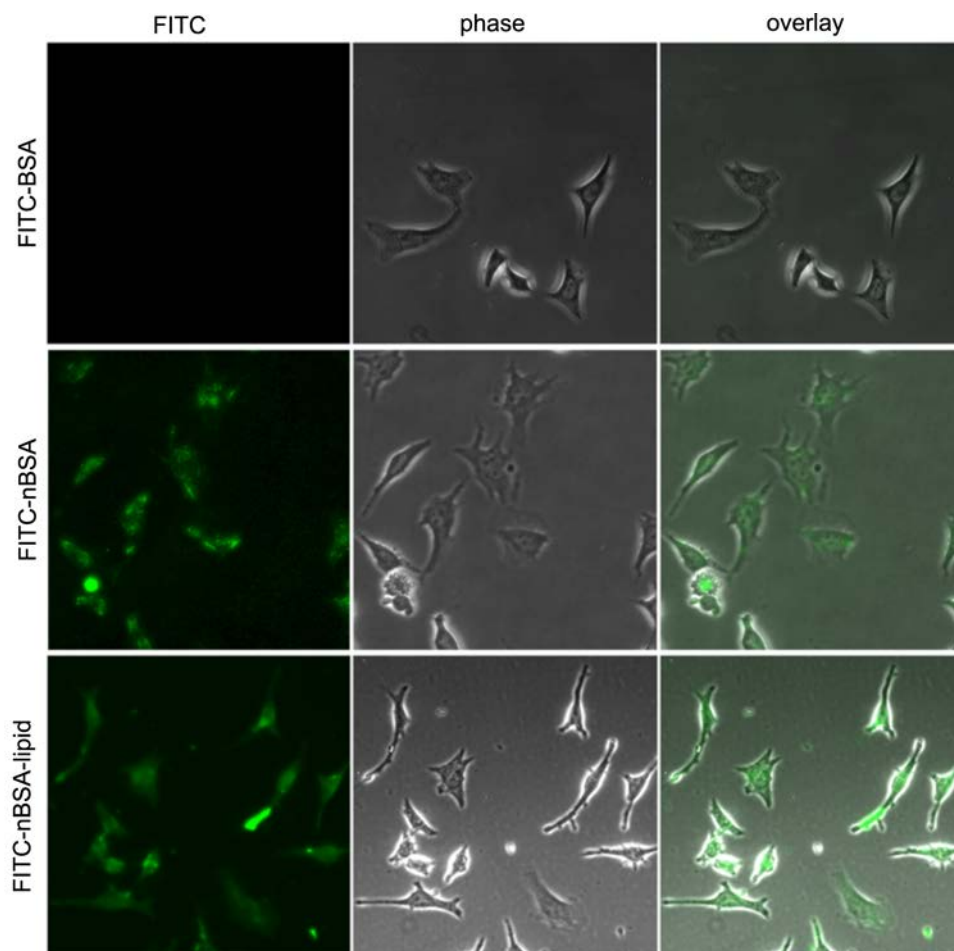


Figure 48 Cellular Uptake of FITC-BSA, nBSA and nBSA-lipid

To confirm the nBSA-lipid-PEG is indeed internalized by HeLa cells rather than absorbing on the cell membrane. We used trypan blue to quench the extracellular fluorescence and the fluorescence bound to the cell membrane. As shown in Figure 49, adding trypan blue to the cell medium prior to Flowcytometry experiment and microscope observation does not significantly affect the cellular fluorescence, confirming the internalization of nBSA-lipid by cells.

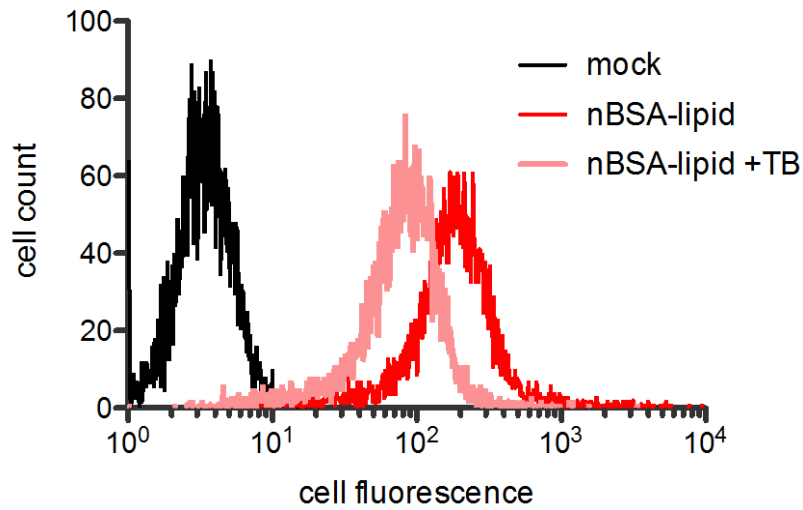


Figure 49 Fluorescence image and cellular fluorescence distribution of HeLa cells after incubation with nBSA-lipid with and without subsequent quenching with trypan blue

To determine whether the uptake pathway is endocytosis, we incubated cells with nBSA and nBSA-lipid at 4 °C. The fluorescence intensity of cells incubated with nBSA decreased significantly at 4 °C (Figure 50), where the cells incubated with nBSA-lipid retains similar cellular fluorescence. This indicates that cellular uptake of nBSA-lipid-PEG is associated with an energy-independent uptake pathway, a non-endocytotic pathway.

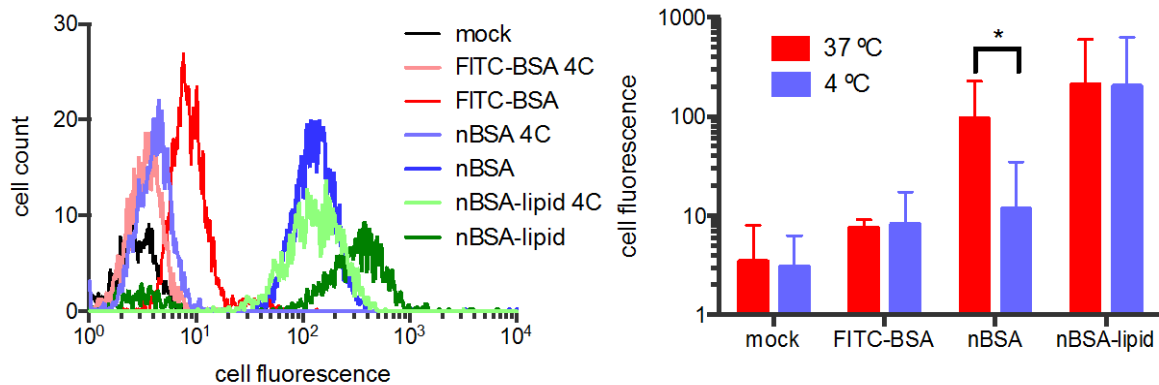


Figure 50 cellular fluorescence distribution of HeLa cells after incubation with FITC-BSA, nBSA and nBSA-lipid * $p < 0.01$

To further explore the uptake pathway, we used NaN_3 and deoxyglucose to inhibit endocytosis²⁰⁴. We used a cell-impermeable dye calcein as an indicator for endocytosis. As shown in Figure 51, NaN_3 /deoxyglucose successfully inhibits the endocytosis of calcein and cationic BSA nanocapsules. However, nBSA-lipid still shows high uptake in HeLa cells with the existence of NaN_3 /deoxyglucose.

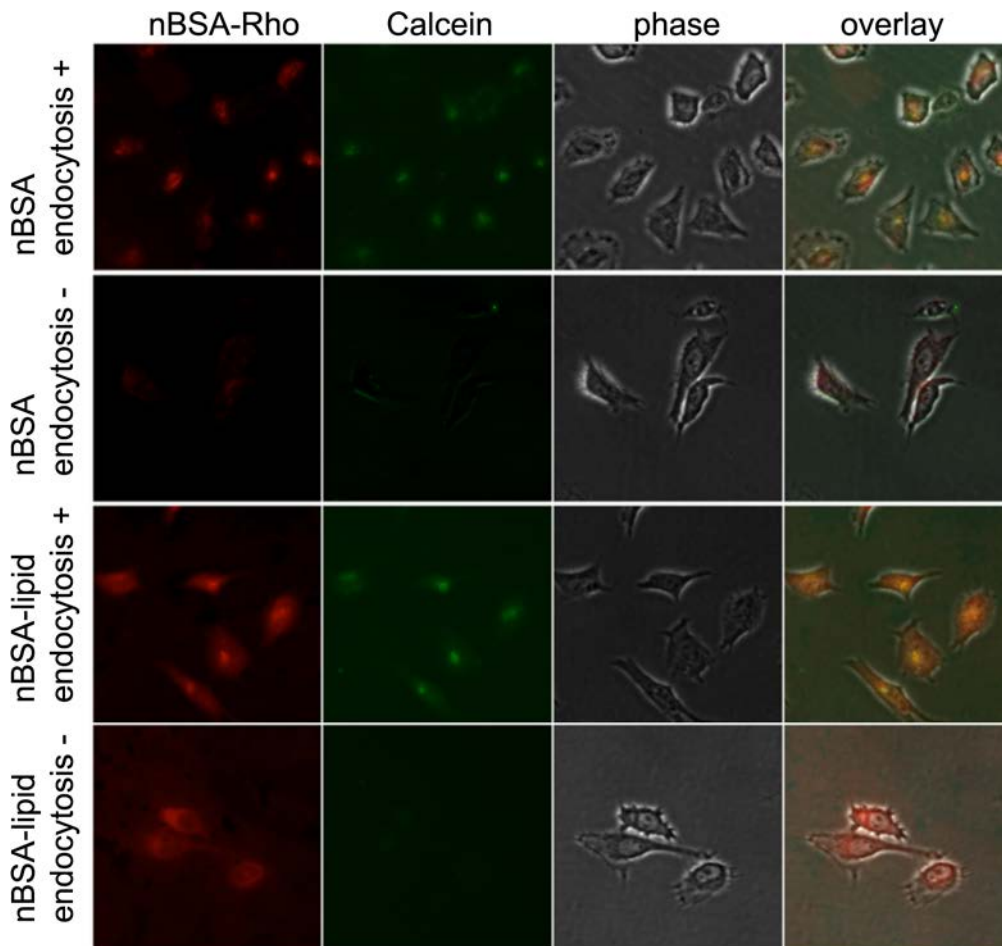


Figure 51 Cellular uptake of nBSA and nBSA-lipid under conditions when endocytosis is inhibited

nBSA-lipid shows a much faster delivery than nBSA in both CEM and HEK-293T-CCR5 cells (Figure 52 & Figure 53), which indicates the driven force is different from endocytosis, through which nBSA is internalized by cells. The incubate time for nBSA-lipid to get the plateau

decreases with the increasing concentration, indicating the concentration gradient plays an important role in particle diffusion as a driven force.

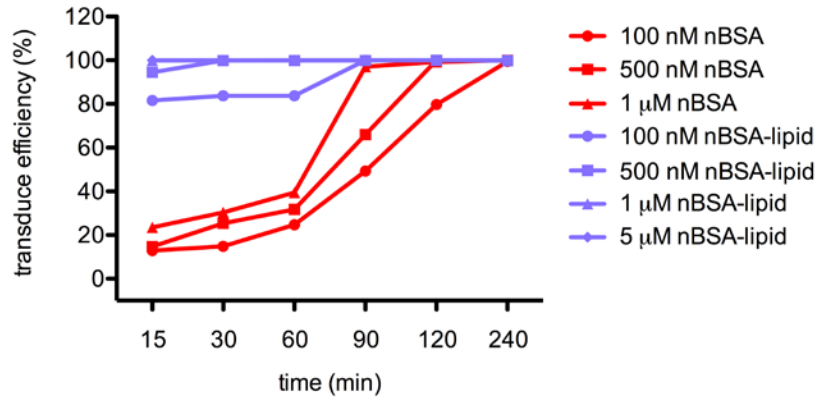


Figure 52 Transduction of FITC labeled nBSA and nBSA-lipid in CEM Cells

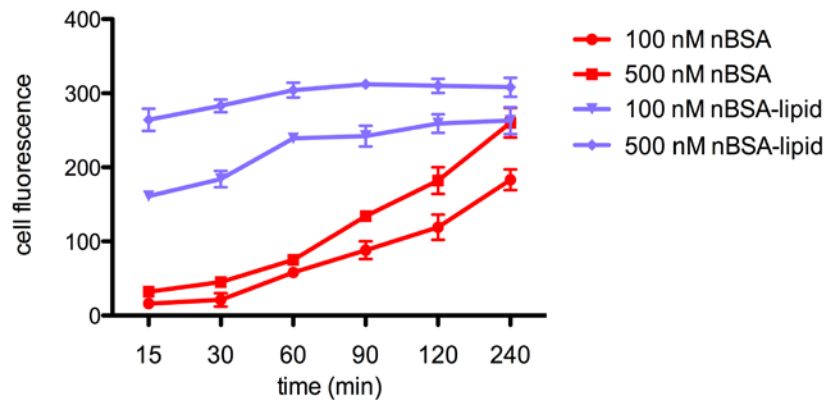


Figure 53 Transduction of FITC labeled nBSA and nBSA-lipid in HEK-293T-CCR5 Cells

We chose lactamase to test the intracellular biofunctionality of nProtein-lipid. Figure 54 shows the activity of lactamase after encapsulation and conjugation. The bioactivity is not significantly affected after encapsulation and conjugation.

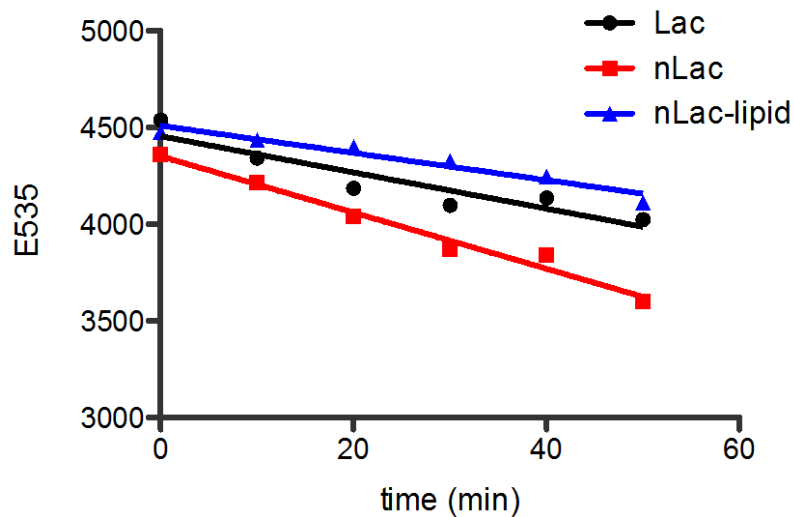


Figure 54 Fluorescence intensity change of GeneBLAzer® FRET Assay after native lactamase, nLac and nLac-lipid-PEG were added to the assay buffer (ex: 405 nm, em: 535 nm)

With lactamase, we demonstrated that the enzymes remain active intracellularly. The activity of lactamase was examined with GeneBLAzer® FRET Assay. CCF2-AM substrate in the GeneBLAzer® FRET Assay is the membrane-permeable, esterified form of CCF2, a FRET dye with excitation wavelength of 405 nm and emission wavelength at 535 nm. CCF2 can be readily cleaved by β -lactamase to separate the fluorescence, generating emission at 460 nm with an excitation wavelength of 405 nm^{179,180}. Compared with CCF2, which is not taken up by cells, CCF2-Am is lipophilic and readily enters the cell. Therefore, monitoring the cellular fluorescence emission wavelength reveals the intracellular β -lactamase activities.

Figure 55 shows the cellular fluorescence of HeLa after incubated with nLac and nLac-lipid and treatment of GeneBLAzer® FRET Assay. VSVG-lac and PBS were used as positive and negative controls. In normal medium without endocytosis inhibitor, cells cultured with both nLac and nLac-lipid exhibited blue shift in fluorescence emission wavelength compared with cells only loaded with CCF2-Am. After endosome acidification inhibitor, bafilomycin^{205,206}, was

added into the medium, however, cells cultured with nLac shows similar fluorescence to that incubated with CCF2-Am only. Similarly, VSVG cannot effectively deliver active β -lactamase under endocytosis inhibiting conditions. On contrary, cells cultured with nLac-lipid still exhibit altered emission wavelength, indicating intracellular β -lactamase activity.

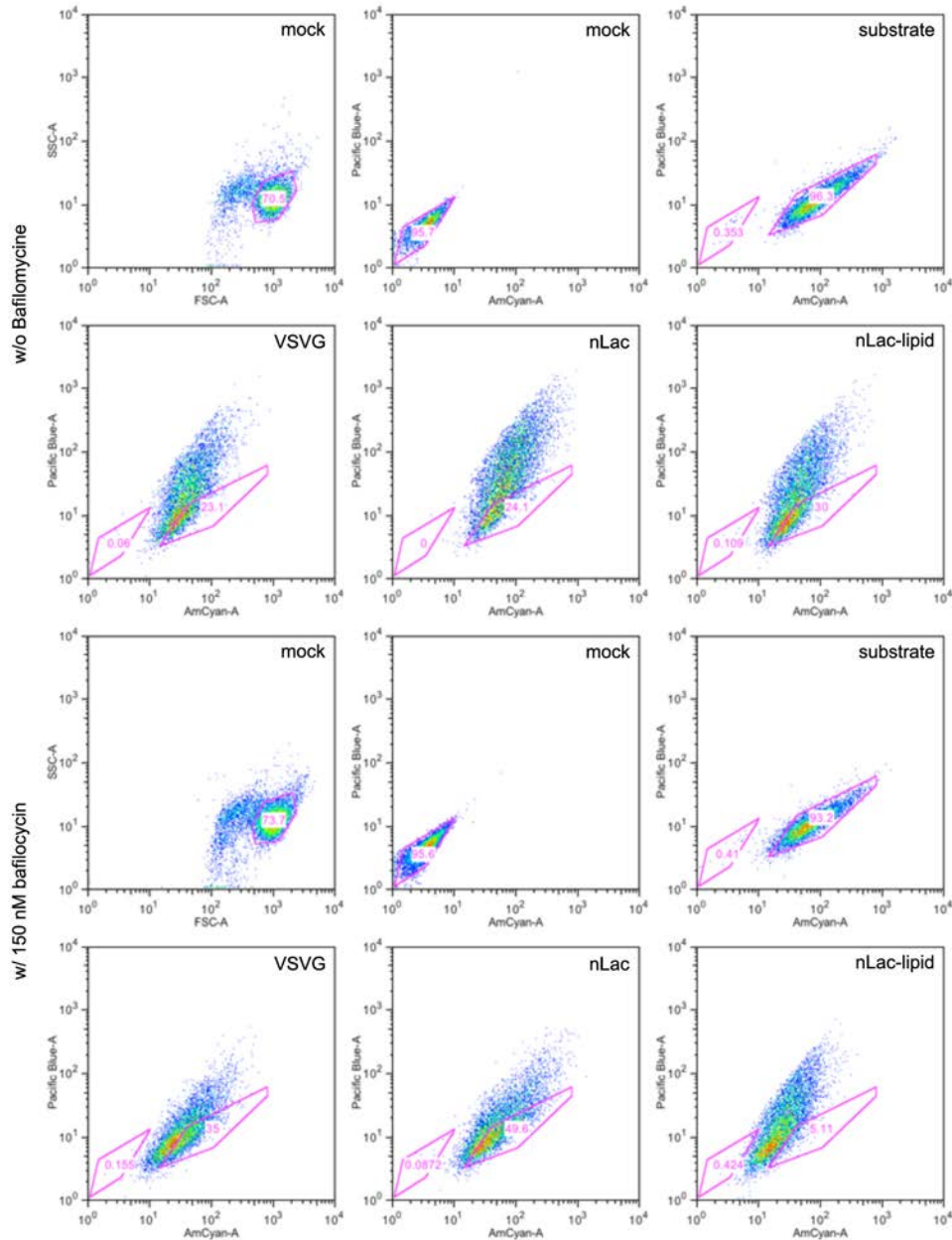


Figure 55 Intracellular lactamase activity CCR5 cells pre-incubated with VSVG-lac, nLac, nLac-lipid. 150 nM Bafilomycin is used to inhibit the acidification of endocytosis.

8.4. Summary

We invented a nanocapsule with alternating hydrophobic-hydrophilic theme that enables the bypass of endocytosis process. By conjugating PEG and PEG-lipid on the nanocapsule surface, we obtained nanocapsule with high intracellular delivery efficiency and decreased cytotoxicity. The delivered protein is uniformly distributed in cytosol after cellular uptake. Moreover, similar levels of cellular uptake were achieved even in the presence of inhibitions of low pH-dependent endocytosis. Active proteins can be delivered into cells to exert their biological functions. We believe that delivery through non-endocytotic pathways represents a breakthrough novel approach in the drug delivery field.

Chapter 9. Conclusions

As a summary, I developed a novel strategy that simultaneously improve protein stability and introduce enzymes with new functionality. This strategy is based on an *in-situ* polymerization on protein surface, conducted in aqueous environment at room temperature, exerting little effects on enzyme activity. This two-step process forms a thin layer of polymer on the enzyme surface, yielding nano-sized enzyme nanocapsules. The first step involves the conjugation of polymerizable groups on protein surface. The increased molecular weight can be detected by MALDI-TOF spectroscopy. By varying the amount of conjugation reagents, protein conjugate with different conjugation degree can be obtained. The second step is an aqueous free radical polymerization, in which a thin layer of polymer network is formed on protein surface. The successful formation of the polymer layer is confirmed with IR spectroscopy, dynamic light scattering, agarose gel electrophoresis, and transmission electron microscopy. The composition of the polymer layer can be readily adjusted by changing the monomer added in the

polymerization. In addition, the surface function can be finely tuned by incorporating copolymerization and varying the ratio between co-monomers.

Because the process of nano-encapsulation is conducted in neutral aqueous solution at room temperature or 4 °C, the activity of the protein can be preserved. A variety of protein can be used in this process with only ~10% loss of activity. In addition, the polymer layer around the protein surface makes significant contribution to the microenvironment of the protein. This allows us to optimize the microenvironment for protein independent of the bulk solution composition. With this strategy, we achieved significantly enhanced activity of OPH nanocapsules compared with native OPH, especially in physiological environment.

Besides the retained bioactivity, nanoencapsulation endows protein with enhanced stability. With model proteins such as OPH and GOx, we demonstrate significantly improved stability against various denaturation factors, including elevated temperature, freeze-thaw cycles, long-term storage, organic solvents and proteases, paving the way for the therapeutic and catalytic applications of proteins. With studies on the inactivation kinetics and enzyme structure during inactivation, we discovered that the polymer layer stabilizes the 3D conformation of the native form whereas destabilizes the denatured form of the core protein. In addition, the polymer layer disables the aggregation or dissociation of proteins, as well as the dissociation of co-factor from the protein. Upon exposure to protease, polymer layer serves as a protecting layer, physically separating the protease from the core protein.

These advantages of enzyme nanocapsules come from their structural characteristics: 1) Multi-covalently attached polymer layer stabilizes the protein 3D structure by “holding” the protein; 2) Hydrophilic polymer layer offers an environment resembling physiological environment, providing proteins the resistance against harsh conditions, such as organic solvents and freeze-

thaw cycles; 3) Net-like polymer allows the free diffusion of substrates and products of enzymes; 4) The nano-scale size is suitable for a wider range of applications compared with bulk immobilized proteins; 5) The polymer layer offers a platform to engineer the surface properties of enzyme without interfering enzyme's intrinsic activity.

The retained activity and enhanced stability provide the pre-conditions for various applications of protein nanocapsules. In addition, the readily engineerable surface presents great chance to introduce new functionalities to proteins. In our research, we have demonstrated a general, effective, low-toxic intracellular protein delivery based on cationic single-protein nanocapsules. Cationic nanocapsules can be fabricated via co-polymerization of neutral monomer and cationic monomer. The resulted cationic nanocapsules can be delivered into cellular interior with high efficiency and low toxicity. The cellular uptake is through an endocytotic process with partial release of the nanocapsules from the endosome. The nanocapsules delivered intracellularly can exert their biological functions in cells, harboring great potentials for cellular imaging, cancer therapies, anti-aging, cosmetics, and many other applications. Additionally, degradable nanocapsules can be prepared with degradable crosslinkers, which are sensitive to environmental alterations such as change of pH value, redox environment and protease attack. These degradable nanocapsules can release their protein cargo upon endocytosis, enabling the interactions of cargo protein with intracellular macromolecules.

By further engineering the surface functions, we invented a nanocapsules with alternating hydrophobic-hydrophilic theme that enables the bypass of endocytosis process. By conjugating PEG and PEG-lipid on the nanocapsule surface, we obtained nanocapsule with high intracellular delivery efficiency and decreased cytotoxicity. The delivered protein is uniformly distributed in cytosol after cellular uptake. Moreover, similar levels of cellular uptake were achieved even in

the presence of inhibitions of low pH-dependent endocytosis. Active proteins can be delivered into cells to exert their biological functions. We believe that delivery through non-endocytotic pathways represents a breakthrough novel approach in the drug delivery field.

The nanocapsules can be further functionalized by conjugating functional modules on the polymer shell. Because the modification sites can be introduced with large quantity to the polymer shell without interference with the core protein, the modification does not pose significant impact on the activity of core protein. In our research, we have demonstrated a novel class of robust, cell-transducible bioluminescent nanocapsules with tunable emission wavelengths by conjugating quantum dot to bioluminescent nanocapsules. The bioluminescence emitted by the protein can be effectively transferred to the adjacent quantum dots (QD) via bioluminescence resonance energy transfer (BRET). The QD-nanocapsule conjugates, therefore, obtained red-shifted wavelength, suitable for in-vivo bioluminescence imaging. The BRET ratio can be readily adjusted by altering the QD/nanocapsule ratio. The capability to transfer the cellular membrane enables the intracellular applications of QD/nanocapsule conjugates. This technique provides us new potentials for bioluminescence imaging, therapeutic and other applications.

Overall, my research establishes a novel strategy to stabilize proteins and create new surface functions of protein. The process involves an in-situ polymerization on protein surface without significant interfering protein bioactivity. The resulted protein nanocapsules gain enhanced stability and various new functionalities. This work opens an avenue for various protein-based applications, such as therapeutics, analysis and biocatalysis.

REFERENCES

1. Chen, R. Bacterial expression systems for recombinant protein production: E. coli and beyond. *Biotechnology Advances* (2012).
2. Huang, C.-J., Lin, H. & Yang, X. Industrial production of recombinant therapeutics in *Escherichia coli* and its recent advancements. *Journal of Industrial Microbiology and Biotechnology* **39**, 383–399 (2012).
3. Fágáin, C. O. Understanding and increasing protein stability. *Biochim. Biophys. Acta* **1252**, 1–14 (1995).
4. Perutz, M. F. Electrostatic effects in proteins. *Science* **201**, 1187–1191 (1978).
5. Torchilin, V. Intracellular delivery of protein and peptide therapeutics. *Drug Discovery Today: Technologies* 1–9 (2009).doi:10.1016/j.ddtec.2009.01.002
6. Johnston, A. P. R., Such, G. K., Ng, S. L. & Caruso, F. Challenges facing colloidal delivery systems: From synthesis to the clinic. *Current Opinion in Colloid & Interface Science* **16**, 171–181 (2011).
7. Bertrand, N. & Leroux, J.-C. The journey of a drug-carrier in the body: An anatomophysiological perspective. *Journal of Controlled Release* **161**, 152–163 (2012).
8. Sheldon, R. A. Enzyme Immobilization: The Quest for Optimum Performance. *Adv. Synth. Catal.* **349**, 1289–1307 (2007).
9. Ó'Fágáin, C. Enzyme stabilization—recent experimental progress. *Enzyme Microb Tech* **33**, 137–149 (2003).
10. Gill, I. & Ballesteros, A. Encapsulation of biologicals within silicate, siloxane, and hybrid sol-gel polymers: An efficient and generic approach. *J. Am. Chem. Soc.* **120**, 8587–8598 (1998).
11. Ispas, C. R., Crivat, G. & Andreescu, S. Review: Recent Developments in Enzyme-Based Biosensors for Biomedical Analysis. *Analytical Letters* **45**, 168–186 (2012).
12. Kim, J. S., Pike, J. D., Coucouvanis, D. & Meyerhoff, M. E. Enzyme electrode with enhanced specificity using outer polymeric membrane doped with substrate selective ditopic carrier. *Electroanalysis* **12**, 1258–1262 (2000).
13. Stempfer, G., HollNeugebauer, B., Kopetzki, E. & Rudolph, R. A fusion protein designed for noncovalent immobilization: Stability, enzymatic activity, and use in an

- enzyme reactor. *Nat. Biotechnol.* **14**, 481–484 (1996).
14. Nouaimi-Bachmann, M., Skilewitsch, O., Senhaji-Dachder, S. & Bisswanger, H. Co-immobilization of different enzyme activities to non-woven polyester surfaces. *Biotechnol. Bioeng.* **96**, 623–630 (2007).
 15. Tiwari, A. K., Gajbhiye, V., Sharma, R. & Jain, N. K. Carrier mediated protein and peptide stabilization. *Drug Deliv* **17**, 605–616 (2010).
 16. Dosoretz, C., Armon, R., Starosvetzky, J. & Rothschild, N. Entrapment of parathion hydrolase from *Pseudomonas* spp. in sol-gel glass. *J Sol-Gel Sci Technol* **7**, 7–11 (1996).
 17. Yu, D. *et al.* Aqueous sol-gel encapsulation of genetically engineered *Moraxella* spp. cells for the detection of organophosphates. *Biosens Bioelectron* **20**, 1433–1437 (2005).
 18. Illanes, A., Wilson, L., Caballero, E., Fernández-Lafuente, R. & Guisán, J. M. Crosslinked penicillin acylase aggregates for synthesis of beta-lactam antibiotics in organic medium. *Appl Biochem Biotech* **133**, 189–202 (2006).
 19. Kim, M. I. *et al.* Crosslinked enzyme aggregates in hierarchically-ordered mesoporous silica: a simple and effective method for enzyme stabilization. *Biotechnol. Bioeng.* **96**, 210–218 (2007).
 20. Abraham, T. E., Joseph, J. R., Bindhu, L. B. V. & Jayakumar, K. K. Crosslinked enzyme crystals of glucoamylase as a potent catalyst for biotransformations. *Carbohydr. Res.* **339**, 1099–1104 (2004).
 21. Blanco, R. M., Calvete, J. J. & Guisan, J. M. Immobilization-stabilization of enzymes; variables that control the intensity of the trypsin (amine)-agarose (aldehyde) multipoint attachment. *Enzyme Microb Tech* (1989).
 22. Ichikawa, S., Takano, K., Kuroiwa, T. & Hiruta, O. Immobilization and stabilization of chitosanase by multipoint attachment to agar gel support. *Journal of bioscience ...* (2002).
 23. Mateo, C., Abian, O., Fernandez-Lafuente, R. & Guisan, J. Increase in conformational stability of enzymes immobilized on epoxy-activated supports by favoring additional multipoint covalent attachment*. *Enzyme Microb Tech* **26**, 509–515 (2000).
 24. Kim, D.-M. *et al.* Enhancement of cellulolytic enzyme activity by clustering cellulose binding domains on nanoscaffolds. *Small* **7**, 656–664 (2011).
 25. Peters, R. J. R. W., Louzao, I. & van Hest, J. C. M. From polymeric nanoreactors to

- artificial organelles. *Chem. Sci.* **3**, 335–342 (2012).
26. Bäumlér, H. & Georgieva, R. Coupled enzyme reactions in multicompartiment microparticles. *Biomacromolecules* **11**, 1480–1487 (2010).
 27. Garcia, J. *et al.* Multilayer enzyme-coupled magnetic nanoparticles as efficient, reusable biocatalysts and biosensors. *Nanoscale* **3**, 3721–3730 (2011).
 28. Schoffelen, S. & van Hest, J. C. M. Multi-enzyme systems: bringing enzymes together in vitro. *Soft Matter* **8**, 1736–1746 (2012).
 29. Shi, J., Zhang, L. & Jiang, Z. Facile construction of multicompartiment multienzyme system through layer-by-layer self-assembly and biomimetic mineralization. *ACS Appl Mater Interfaces* **3**, 881–889 (2011).
 30. Peisajovich, S. G. & Tawfik, D. S. Protein engineers turned evolutionists. *Nat Meth* **4**, 991–994 (2007).
 31. Piatkevich, K. D. & Verkhusha, V. V. Advances in engineering of fluorescent proteins and photoactivatable proteins with red emission. *Current Opinion in Chemical Biology* **14**, 23–29 (2010).
 32. Hibbert, E. G. *et al.* Directed evolution of biocatalytic processes. *Biomol. Eng.* **22**, 11–19 (2005).
 33. Rubin-Pitel, S. B. & Zhao, H. Recent advances in biocatalysis by directed enzyme evolution. *Comb. Chem. High Throughput Screen.* **9**, 247–257 (2006).
 34. Patten, P. A., Howard, R. J. & Stemmer, W. P. Applications of DNA shuffling to pharmaceuticals and vaccines. *Current Opinion in Biotechnology* **8**, 724–733 (1997).
 35. Kolkman, J. A. & Stemmer, W. P. Directed evolution of proteins by exon shuffling. *Nat. Biotechnol.* **19**, 423–428 (2001).
 36. Pantazes, R. J., Grisewood, M. J. & Maranas, C. D. Recent advances in computational protein design. *Current Opinion in Structural Biology* **21**, 467–472 (2011).
 37. Sammond, D. W. *et al.* Computational design of the sequence and structure of a protein-binding peptide. *J. Am. Chem. Soc.* **133**, 4190–4192 (2011).
 38. Jacak, R., Leaver-Fay, A. & Kuhlman, B. Computational protein design with explicit consideration of surface hydrophobic patches. *Proteins* **80**, 825–838 (2012).
 39. Saven, J. G. Computational protein design: engineering molecular diversity, nonnatural enzymes, nonbiological cofactor complexes, and membrane proteins. *Current Opinion in*

- Chemical Biology* **15**, 452–457 (2011).
40. Gupta, N. & Farinas, E. T. Directed evolution of CotA laccase for increased substrate specificity using *Bacillus subtilis* spores. *Protein Eng. Des. Sel.* **23**, 679–682 (2010).
 41. Ruan, B., London, V., Fisher, K. E., Gallagher, D. T. & Bryan, P. N. Engineering substrate preference in subtilisin: structural and kinetic analysis of a specificity mutant. *Biochemistry* **47**, 6628–6636 (2008).
 42. Scheib, H., Pleiss, J., Kovac, A., Paltauf, F. & Schmid, R. D. Stereoselectivity of Mucorales lipases toward triacylglycerols--a simple solution to a complex problem. *Protein Sci.* **8**, 215–221 (1999).
 43. Scheib, H. *et al.* Rational design of *Rhizopus oryzae* lipase with modified stereoselectivity toward triacylglycerols. *Protein Eng.* **11**, 675–682 (1998).
 44. Liu, J. & Tsai, M. D. DNA polymerase beta: pre-steady-state kinetic analyses of dATP alpha S stereoselectivity and alteration of the stereoselectivity by various metal ions and by site-directed mutagenesis. *Biochemistry* **40**, 9014–9022 (2001).
 45. Zheng, H. & Reetz, M. T. Manipulating the stereoselectivity of limonene epoxide hydrolase by directed evolution based on iterative saturation mutagenesis. *J. Am. Chem. Soc.* **132**, 15744–15751 (2010).
 46. Neves-Petersen, M. T. *et al.* Engineering the pH-optimum of a triglyceride lipase: from predictions based on electrostatic computations to experimental results. *Journal of Biotechnology* **87**, 225–254 (2001).
 47. Makde, R. D., Dikshit, K. & Kumar, V. Protein engineering of class-A non-specific acid phosphatase (PhoN) of *Salmonella typhimurium*: modulation of the pH-activity profile. *Biomol. Eng.* **23**, 247–251 (2006).
 48. Tomschy, A. *et al.* Engineering of phytase for improved activity at low pH. *Applied and Environmental Microbiology* **68**, 1907–1913 (2002).
 49. Baker, M. P. & Jones, T. D. Identification and removal of immunogenicity in therapeutic proteins. *Curr Opin Drug Discov Devel* **10**, 219–227 (2007).
 50. Osipovitch, D. C. *et al.* Design and analysis of immune-evading enzymes for ADEPT therapy. *Protein Eng. Des. Sel.* **25**, 613–623 (2012).
 51. Cantor, J. R., Panayiotou, V., Agnello, G., Georgiou, G. & Stone, E. M. Engineering reduced-immunogenicity enzymes for amino acid depletion therapy in cancer. *Meth.*

- Enzymol.* **502**, 291–319 (2012).
52. Kermekchiev, M. B., Kirilova, L. I., Vail, E. E. & Barnes, W. M. Mutants of Taq DNA polymerase resistant to PCR inhibitors allow DNA amplification from whole blood and crude soil samples. *Nucleic Acids Research* **37**, e40–e40 (2009).
 53. Prinarakis, E. E., Miriagou, V., Tzelepi, E., Gazouli, M. & Tzouveleakis, L. S. Emergence of an inhibitor-resistant beta-lactamase (SHV-10) derived from an SHV-5 variant. *Antimicrob. Agents Chemother.* **41**, 838–840 (1997).
 54. Sandberg, W. S. & Terwilliger, T. C. Influence of interior packing and hydrophobicity on the stability of a protein. *Science* **245**, 54–57 (1989).
 55. Perutz, M. F. & Raidt, H. Stereochemical basis of heat stability in bacterial ferredoxins and in haemoglobin A2. *Nature* **255**, 256–259 (1975).
 56. Perry, L. J. & Wetzel, R. Disulfide bond engineered into T4 lysozyme: stabilization of the protein toward thermal inactivation. *Science* **226**, 555–557 (1984).
 57. Clarke, J. & Fersht, A. R. Engineered disulfide bonds as probes of the folding pathway of barnase: increasing the stability of proteins against the rate of denaturation. *Biochemistry* **32**, 4322–4329 (1993).
 58. Kuroki, R. *et al.* Design and creation of a Ca²⁺ binding site in human lysozyme to enhance structural stability. *Proc. Natl. Acad. Sci. U.S.A.* **86**, 6903–6907 (1989).
 59. Schmidt, S. R. Fusion-proteins as biopharmaceuticals--applications and challenges. *Curr Opin Drug Discov Devel* **12**, 284–295 (2009).
 60. Chen, X., Zaro, J. L. & Shen, W.-C. Pharmacokinetics of recombinant bifunctional fusion proteins. *Expert Opin Drug Metab Toxicol* **8**, 581–595 (2012).
 61. Shaner, N. C., Steinbach, P. A. & Tsien, R. Y. A guide to choosing fluorescent proteins. *Nat Meth* **2**, 905–909 (2005).
 62. Quéméneur, E., Moutiez, M., Charbonnier, J. B. & Ménez, A. Engineering cyclophilin into a proline-specific endopeptidase. *Nature* **391**, 301–304 (1998).
 63. Jez, J. M. & Penning, T. M. Engineering steroid 5 β -reductase activity into rat liver 3 α -hydroxysteroid dehydrogenase. *Biochemistry* **37**, 9695–9703 (1998).
 64. Wang, H. & Chong, S. Visualization of coupled protein folding and binding in bacteria and purification of the heterodimeric complex. *Proc. Natl. Acad. Sci. U.S.A.* **100**, 478–483 (2003).

65. Lachmann, R. H. Enzyme replacement therapy for lysosomal storage diseases. *Curr. Opin. Pediatr.* **23**, 588–593 (2011).
66. Altarescu, G. *et al.* Comparative efficacy of dose regimens in enzyme replacement therapy of type I Gaucher disease. *Blood Cells Mol. Dis.* **26**, 285–290 (2000).
67. Pisani, A. *et al.* Enzyme replacement therapy in Fabry disease patients undergoing dialysis: effects on quality of life and organ involvement. *Am. J. Kidney Dis.* **46**, 120–127 (2005).
68. Russell, C. S. & Clarke, L. A. Recombinant proteins for genetic disease. *Clin. Genet.* **55**, 389–394 (1999).
69. Moon, J. J., Huang, B. & Irvine, D. J. Engineering Nano- and Microparticles to Tune Immunity. *Adv. Mater.* **24**, 3724–3746 (2012).
70. Tyagi, R. K., Garg, N. K. & Sahu, T. Vaccination Strategies against Malaria: novel carrier(s) more than a tour de force. *J Control Release* **162**, 242–254 (2012).
71. Lanzavecchia, A. Mechanisms of antigen uptake for presentation. *Curr. Opin. Immunol.* **8**, 348–354 (1996).
72. Barzilay, R., Melamed, E. & Offen, D. Introducing transcription factors to multipotent mesenchymal stem cells: making transdifferentiation possible. *Stem Cells* **27**, 2509–2515 (2009).
73. Sisakhtnezhad, S. & Matin, M. M. Transdifferentiation: a cell and molecular reprogramming process. *Cell Tissue Res.* **348**, 379–396 (2012).
74. Okita, K. & Yamanaka, S. Induced pluripotent stem cells: opportunities and challenges. *Philos. Trans. R. Soc. Lond., B, Biol. Sci.* **366**, 2198–2207 (2011).
75. Madonna, R. Human-induced pluripotent stem cells: in quest of clinical applications. *Mol. Biotechnol.* **52**, 193–203 (2012).
76. Baum, C. Insertional mutagenesis in gene therapy and stem cell biology. *Curr. Opin. Hematol.* **14**, 337–342 (2007).
77. Fehse, B. & Roeder, I. Insertional mutagenesis and clonal dominance: biological and statistical considerations. *Gene Ther* **15**, 143–153 (2008).
78. Baum, C. Chance or necessity? Insertional Mutagenesis in Gene Therapy and Its Consequences. *Molecular Therapy* **9**, 5–13 (2004).
79. Frankel, A. D. & Pabo, C. O. Cellular uptake of the tat protein from human

- immunodeficiency virus. *Cell* **55**, 1189–1193 (1988).
80. Cohen, J. L. *et al.* Enhanced Cell Penetration of Acid-Degradable Particles Functionalized with Cell-Penetrating Peptides. *Bioconjug. Chem.* **19**, 876–881 (2008).
 81. Heitz, F., Morris, M. C. & Divita, G. Twenty years of cell-penetrating peptides: from molecular mechanisms to therapeutics. *Brit J Pharmacol* **157**, 195–206 (2009).
 82. Fawell, S. *et al.* Tat-mediated delivery of heterologous proteins into cells. *Proc. Natl. Acad. Sci. U.S.A.* **91**, 664–668 (1994).
 83. Morris, M. C., Depollier, J., Mery, J., Heitz, F. & Divita, G. A peptide carrier for the delivery of biologically active proteins into mammalian cells. *Nat. Biotechnol.* **19**, 1173–1176 (2001).
 84. Schwarze, S. R. In Vivo Protein Transduction: Delivery of a Biologically Active Protein into the Mouse. *Science* **285**, 1569–1572 (1999).
 85. Dietz, G. P. H. & Bähr, M. Delivery of bioactive molecules into the cell: the Trojan horse approach. *Mol. Cell. Neurosci.* **27**, 85–131 (2004).
 86. Snyder, E. L. & Dowdy, S. F. Recent advances in the use of protein transduction domains for the delivery of peptides, proteins and nucleic acids in vivo. *Expert Opin Drug Deliv* **2**, 43–51 (2005).
 87. Gros, E. *et al.* A non-covalent peptide-based strategy for protein and peptide nucleic acid transduction. *Biochim. Biophys. Acta* **1758**, 384–393 (2006).
 88. Morris, M. C., Deshayes, S., Heitz, F. & Divita, G. Cell-penetrating peptides: from molecular mechanisms to therapeutics. *Biol. Cell* **100**, 201–217 (2008).
 89. Drin, G., Cottin, S., Blanc, E., Rees, A. R. & Temsamani, J. Studies on the internalization mechanism of cationic cell-penetrating peptides. *J. Biol. Chem.* **278**, 31192–31201 (2003).
 90. Poon, G. M. K. & Gariépy, J. Cell-surface proteoglycans as molecular portals for cationic peptide and polymer entry into cells. *Biochem. Soc. Trans.* **35**, 788–793 (2007).
 91. Fittipaldi, A. *et al.* Cell membrane lipid rafts mediate caveolar endocytosis of HIV-1 Tat fusion proteins. *J. Biol. Chem.* **278**, 34141–34149 (2003).
 92. Eguchi, A. *et al.* Protein transduction domain of HIV-1 Tat protein promotes efficient delivery of DNA into mammalian cells. *J. Biol. Chem.* **276**, 26204–26210 (2001).
 93. Wadia, J. S., Stan, R. V. & Dowdy, S. F. Transducible TAT-HA fusogenic peptide

- enhances escape of TAT-fusion proteins after lipid raft macropinocytosis. *Nat. Med.* **10**, 310–315 (2004).
94. Vendeville, A. *et al.* HIV-1 Tat enters T cells using coated pits before translocating from acidified endosomes and eliciting biological responses. *Mol. Biol. Cell* **15**, 2347–2360 (2004).
 95. Gregoriadis, G. Engineering liposomes for drug delivery: progress and problems. *Trends Biotechnol.* **13**, 527–537 (1995).
 96. Martins, S., Sarmiento, B., Ferreira, D. C. & Souto, E. B. Lipid-based colloidal carriers for peptide and protein delivery - liposomes versus lipid nanoparticles. *Int J Nanomed* **2**, 595–607 (2007).
 97. Perugini, P. *et al.* Intracellular delivery of liposome-encapsulated prolidase in cultured fibroblasts from prolidase-deficient patients. *J Control Release* **102**, 181–190 (2005).
 98. HARDING, C., COLLINS, D., SLOT, J., GEUZE, H. & UNANUE, E. Liposome-Encapsulated Antigens Are Processed in Lysosomes, Recycled, and Presented to T-Cells. *Cell* **64**, 393–401 (1991).
 99. Hong, K., YOSHIMURA, T. & PAPAHAADJOPOULOS, D. Interaction of clathrin with liposomes: pH-dependent fusion of phospholipid membranes induced by clathrin. *FEBS Lett.* **191**, 17–23 (1985).
 100. Wenk, M. R. & Seelig, J. Proton induced vesicle fusion and the isothermal L α \rightarrow H II phase transition of lipid bilayers: a 31 P-NMR and titration *Biochimica et Biophysica Acta (BBA)-Biomembranes* (1998).
 101. Gerasimov, O., Boomer, J., Qualls, M. & Thompson, D. Cytosolic drug delivery using pH- and light-sensitive liposomes. *Adv. Drug Deliv. Rev.* **38**, 317–338 (1999).
 102. Andresen, T. L., Jensen, S. S. & Jørgensen, K. Advanced strategies in liposomal cancer therapy: problems and prospects of active and tumor specific drug release. *Prog. Lipid Res.* **44**, 68–97 (2005).
 103. BRISCOE, P. *et al.* Delivery of superoxide dismutase to pulmonary epithelium via pH-sensitive liposomes. *Am. J. Physiol.* **268**, L374–80 (1995).
 104. Suzuki, R., Yamada, Y. & Harashima, H. Efficient cytoplasmic protein delivery by means of a multifunctional envelope-type nano device. *Biol Pharm Bull* **30**, 758–762 (2007).

105. Miller, C., Bondurant, B., McLean, S., McGovern, K. & O'Brien, D. Liposome-cell interactions in vitro: Effect of liposome surface charge on the binding and endocytosis of conventional and sterically stabilized liposomes. *Biochemistry* **37**, 12875–12883 (1998).
106. Zelphati, O. *et al.* Intracellular delivery of proteins with a new lipid-mediated delivery system. *J. Biol. Chem.* **276**, 35103–35110 (2001).
107. Dalkara, D., Zuber, G. & Behr, J.-P. Intracytoplasmic delivery of anionic proteins. *Mol. Ther.* **9**, 964–969 (2004).
108. van der Gun, B. T. F. *et al.* Serum insensitive, intranuclear protein delivery by the multipurpose cationic lipid SAINT-2. *J Control Release* **123**, 228–238 (2007).
109. Iwaoka, S., Nakamura, T., Takano, S., Tsuchiya, S. & Aramaki, Y. Cationic liposomes induce apoptosis through p38 MAP kinase-caspase-8-Bid pathway in macrophage-like RAW264.7 cells. *J. Leukoc. Biol.* **79**, 184–191 (2006).
110. Torchilin, V., Rammohan, R., Weissig, V. & Levchenko, T. TAT peptide on the surface of liposomes affords their efficient intracellular delivery even at low temperature and in the presence of metabolic inhibitors. *P Natl Acad Sci Usa* **98**, 8786–8791 (2001).
111. Furuhashi, M., Kawakami, H., Toma, K., Hattori, Y. & Maitani, Y. Intracellular delivery of proteins in complexes with oligoarginine-modified liposomes and the effect of oligoarginine length. *Bioconjug. Chem.* **17**, 935–942 (2006).
112. Sapra, P. & Allen, T. M. Internalizing antibodies are necessary for improved therapeutic efficacy of antibody-targeted liposomal drugs. *Cancer Res.* **62**, 7190–7194 (2002).
113. Park, J. W., Kirpotin, D. B., Hong, K. & Shalaby, R. Tumor targeting using anti-her2 immunoliposomes. *Journal of controlled ...* (2001).
114. Pirollo, K. F. *et al.* Tumor-targeting nanocomplex delivery of novel tumor suppressor RB94 chemosensitizes bladder carcinoma cells in vitro and in vivo. *Clin Cancer Res* **14**, 2190–2198 (2008).
115. Lee, R. J. & Low, P. S. Delivery of liposomes into cultured KB cells via folate receptor-mediated endocytosis. *J. Biol. Chem.* **269**, 3198–3204 (1994).
116. Visser, C. *et al.* Targeting liposomes with protein drugs to the blood-brain barrier in vitro. *Eur J Pharm Sci* **25**, 299–305 (2005).
117. Sawant, R. M. *et al.* 'SMART' drug delivery systems: double-targeted pH-responsive pharmaceutical nanocarriers. *Bioconjug. Chem.* **17**, 943–949 (2006).

118. Duncan, R. The dawning era of polymer therapeutics. *Nat Rev Drug Discov* **2**, 347–360 (2003).
119. Lee, K. Y. & Yuk, S. H. Polymeric protein delivery systems. *Prog Polym Sci* **32**, 669–697 (2007).
120. Davis, F. F. The origin of peganology. *Adv. Drug Deliv. Rev.* **54**, 457–458 (2002).
121. Hamidi, M., Azadi, A. & Rafiei, P. Hydrogel nanoparticles in drug delivery. *Adv. Drug Deliv. Rev.* **60**, 1638–1649 (2008).
122. Hasadsri, L., Kreuter, J., Hattori, H., Iwasaki, T. & George, J. M. Functional protein delivery into neurons using polymeric nanoparticles. *J. Biol. Chem.* **284**, 6972–6981 (2009).
123. Bayele, H. K. *et al.* Protein transduction by lipidic peptide dendrimers. *J Pharm Sci* **95**, 1227–1237 (2006).
124. Santra, S., Kaittanis, C. & Perez, J. M. Cytochrome C encapsulating theranostic nanoparticles: a novel bifunctional system for targeted delivery of therapeutic membrane-impermeable proteins to tumors and imaging of cancer therapy. *Mol. Pharm.* **7**, 1209–1222 (2010).
125. Hwa Kim, S., Hoon Jeong, J., Joe, C. O. & Gwan Park, T. Folate receptor mediated intracellular protein delivery using PLL-PEG-FOL conjugate. *Journal of Controlled Release* **103**, 625–634 (2005).
126. Lee, Y. *et al.* A protein nanocarrier from charge-conversion polymer in response to endosomal pH. *J. Am. Chem. Soc.* **129**, 5362–5363 (2007).
127. Lee, Y. *et al.* Charge-conversional polyionic complex micelles-efficient nanocarriers for protein delivery into cytoplasm. *Angew. Chem. Int. Ed.* **48**, 5309–5312 (2009).
128. Ayame, H., Morimoto, N. & Akiyoshi, K. Self-assembled cationic nanogels for intracellular protein delivery. *Bioconjug. Chem.* **19**, 882–890 (2008).
129. Murata, H. *et al.* Intracellular delivery of glutathione S-transferase-fused proteins into mammalian cells by polyethylenimine-glutathione conjugates. *J. Biochem.* **144**, 447–455 (2008).
130. Dalkara, D., Chandrashekhar, C. & Zuber, G. Intracellular protein delivery with a dimerizable amphiphile for improved complex stability and prolonged protein release in the cytoplasm of adherent cell lines. *J Control Release* **116**, 353–359 (2006).

131. Mandeville, J. S. & Tajmir-Riahi, H. A. Complexes of dendrimers with bovine serum albumin. *Biomacromolecules* **11**, 465–472 (2010).
132. Heffernan, M. J. & Murthy, N. Disulfide-crosslinked polyion micelles for delivery of protein therapeutics. *Ann Biomed Eng* **37**, 1993–2002 (2009).
133. Futami, J., Kitazoe, M., Maeda, T. & Nukui, E. Intracellular delivery of proteins into mammalian living cells by polyethylenimine-cationization. *Journal of bioscience ...* (2005).
134. Kitazoe, M. *et al.* Protein transduction assisted by polyethylenimine-cationized carrier proteins. *J. Biochem.* **137**, 693–701 (2005).
135. Kitazoe, M., Futami, J., Nishikawa, M., Yamada, H. & Maeda, Y. Polyethylenimine-cationized beta-catenin protein transduction activates the Wnt canonical signaling pathway more effectively than cationic lipid-based transduction. *Biotechnol J* **5**, 385–392 (2010).
136. Murata, H. *et al.* Denatured and reversibly cationized p53 readily enters cells and simultaneously folds to the functional protein in the cells. *Biochemistry* **45**, 6124–6132 (2006).
137. Horta, A., Molina, M. J., Gómez-Antón, M. R. & Piérola, I. F. The pH Inside a Swollen Polyelectrolyte Gel: Poly(N-Vinylimidazole). *J Phys Chem B* **112**, 10123–10129 (2008).
138. Stephanopoulos, N. & Francis, M. B. Choosing an effective protein bioconjugation strategy. *Nat. Chem. Biol.* **7**, 876–884 (2011).
139. Cooney, M. J. Kinetic measurements for enzyme immobilization. *Methods Mol. Biol.* **679**, 207–225 (2011).
140. Lago, M. A., Grinberg, V. Y. & Burova, T. V. Ionic and Polyampholyte N-Isopropylacrylamide-Based Hydrogels Prepared in the Presence of Imprinting Ligands: Stimuli-Responsiveness and Adsorption/Release *Journal of Functional ...* (2011).
141. Vivero, P. A. & Gabriel, E. F. Improving the loading and release of NSAIDs from pHEMA hydrogels by copolymerization with functionalized monomers. *Journal of ...* (2006).
142. Ohkuma, S., Moriyama, Y. & Takano, T. Identification and characterization of a proton pump on lysosomes by fluorescein-isothiocyanate-dextran fluorescence. *Proc. Natl.*

- Acad. Sci. U.S.A.* **79**, 2758–2762 (1982).
143. Wu, M. M. *et al.* Organelle pH studies using targeted avidin and fluorescein-biotin. *Chem. Biol.* **7**, 197–209 (2000).
144. Grimsley, J. K., Scholtz, J. M., Pace, C. N. & Wild, J. R. Organophosphorus hydrolase is a remarkably stable enzyme that unfolds through a homodimeric intermediate. *Biochemistry* **36**, 14366–14374 (1997).
145. Polakovič, M. & Vrabel, P. Analysis of the mechanism and kinetics of thermal inactivation of enzymes: critical assessment of isothermal inactivation experiments. *Process Biochemistry* **31**, 787–800 (1996).
146. Zhu, L. *et al.* Effects of organic solvent and crystal water on γ -chymotrypsin in acetonitrile media: observations from molecular dynamics simulation and DFT calculation. *J Phys Chem B* **116**, 3292–3304 (2012).
147. Peters, G. H., van Aalten, D. M., Edholm, O., Toxvaerd, S. & Bywater, R. Dynamics of proteins in different solvent systems: analysis of essential motion in lipases. *Biophys. J.* **71**, 2245–2255 (1996).
148. Gouda, M. D., Singh, S. A., Rao, A. G. A., Thakur, M. S. & Karanth, N. G. Thermal inactivation of glucose oxidase. Mechanism and stabilization using additives. *J. Biol. Chem.* **278**, 24324–24333 (2003).
149. Doucet, A. & Overall, C. M. Protease proteomics: revealing protease in vivo functions using systems biology approaches. *Mol. Aspects Med.* **29**, 339–358 (2008).
150. Lendeckel, U. & Hooper, N. M. Proteases in gastrointestinal tissues. (2006).
151. Herszényi, L., Plebani, M., Carraro, P. & De Paoli, M. Proteases in gastrointestinal neoplastic diseases. *Clinica chimica acta* (2000).
152. Talens, S., Leebeek, F. W. G., Demmers, J. A. A. & Rijken, D. C. Identification of fibrin clot-bound plasma proteins. *PLoS ONE* **7**, e41966 (2012).
153. Sheehan, J. J. & Tsirka, S. E. Fibrin-modifying serine proteases thrombin, tPA, and plasmin in ischemic stroke: a review. *Glia* **50**, 340–350 (2005).
154. Syrovets, T. & Simmet, T. Novel aspects and new roles for the serine protease plasmin. *Cell. Mol. Life Sci.* **61**, 873–885 (2004).
155. Schaller, J. & Gerber, S. S. The plasmin-antiplasmin system: structural and functional aspects. *Cell. Mol. Life Sci.* **68**, 785–801 (2011).

156. Meyer-Hoffert, U. Neutrophil-derived serine proteases modulate innate immune responses. *Front. Biosci.* **14**, 3409–3418 (2009).
157. Hochstrasser, M. Introduction to intracellular protein degradation. *Chem. Rev.* **109**, 1479–1480 (2009).
158. Knecht, E. *et al.* Intracellular protein degradation in mammalian cells: recent developments. *Cell. Mol. Life Sci.* **66**, 2427–2443 (2009).
159. Hideshima, T., Bradner, J. E., Chauhan, D. & Anderson, K. C. Intracellular protein degradation and its therapeutic implications. *Clin Cancer Res* **11**, 8530–8533 (2005).
160. Leader, B., Baca, Q. J. & Golan, D. E. Protein therapeutics: A summary and pharmacological classification. *Nat Rev Drug Discov* **7**, 21–39 (2008).
161. Krejsa, C., Rogge, M. & Sadee, W. Protein therapeutics: new applications for pharmacogenetics. *Nat Rev Drug Discov* **5**, 507–521 (2006).
162. Vyas, S. P., Singh, A. & Sihorkar, V. Ligand-receptor-mediated drug delivery: an emerging paradigm in cellular drug targeting. *Crit Rev Ther Drug Carrier Syst* **18**, 1–76 (2001).
163. Sato, H., Sugiyama, Y., Tsuji, A. & Horikoshi, I. Importance of receptor-mediated endocytosis in peptide delivery and targeting: kinetic aspects. *Adv. Drug Deliv. Rev.* (1996).
164. Torchilin, V. P. Recent advances with liposomes as pharmaceutical carriers. *Nat Rev Drug Discov* **4**, 145–160 (2005).
165. Stewart, K. M., Horton, K. L. & Kelley, S. O. Cell-penetrating peptides as delivery vehicles for biology and medicine. *Org. Biomol. Chem.* **6**, 2242 (2008).
166. Milletti, F. Cell-penetrating peptides: classes, origin, and current landscape. *Drug Discovery Today* **17**, 694–704 (2012).
167. Patel, L. N., Zaro, J. L. & Shen, W.-C. Cell Penetrating Peptides: Intracellular Pathways and Pharmaceutical Perspectives. *Pharm. Res.* **24**, 1977–1992 (2007).
168. Middaugh, C. R. & Edwards, K. Recent advances in our understanding of protein conformational stability from a pharmaceutical perspective. *Expert Opinion on ...* (1998).
169. Caron, N. J. *et al.* Intracellular delivery of a Tat-eGFP fusion protein into muscle cells. *Mol. Ther.* **3**, 310–318 (2001).

170. Fischer, R., Köhler, K. & Fotin-Mleczek, M. A stepwise dissection of the intracellular fate of cationic cell-penetrating peptides. *Journal of Biological ...* (2004).
171. Brooks, H., Lebleu, B. & Vivès, E. Tat peptide-mediated cellular delivery: back to basics. *Adv. Drug Deliv. Rev.* (2005).
172. Fotin-Mleczek, M., Fischer, R. & Brock, R. Endocytosis and cationic cell-penetrating peptides--a merger of concepts and methods. *Curr. Pharm. Des.* **11**, 3613–3628 (2005).
173. Sahay, G., Alakhova, D. Y. & Kabanov, A. V. Endocytosis of nanomedicines. *J Control Release* **145**, 182–195 (2010).
174. Freeman, E., Weiland, L. M. & Meng, W. S. Computational Study of Inclusion Burst via the Proton Sponge Hypothesis. (2010).
175. Akinc, A., Thomas, M. & Klibanov, A. M. Exploring polyethylenimine- mediated DNA transfection and the proton sponge hypothesis. *The journal of gene ...* (2004).
176. Folkes, L. & Wardman, P. Oxidative activation of indole-3-acetic acids to cytotoxic species - a potential new role for plant auxins in cancer therapy. *Biochem Pharmacol* **61**, 129–136 (2001).
177. Greco, O., Dachs, G. U., Tozer, G. M. & Kanthou, C. Mechanisms of cytotoxicity induced by horseradish peroxidase/indole-3-acetic acid gene therapy. *J. Cell. Biochem.* **87**, 221–232 (2002).
178. de Melo, M. P., de Lima, T. M., Pithon-Curi, T. C. & Curi, R. The mechanism of indole acetic acid cytotoxicity. *Toxicology letters* (2004).
179. Knapp, T., Hare, E., Feng, L. & Zlokarnik, G. Detection of β - lactamase reporter gene expression by flow cytometry. *Cytometry Part ...* (2003).
180. Qureshi, S. A. Beta-lactamase: an ideal reporter system for monitoring gene expression in live eukaryotic cells. *Biotech.* (2007).
181. Oliver, L. & Vallette, F. M. The role of caspases in cell death and differentiation. *Drug resistance updates* (2005).
182. Porter, A. G. & Jänicke, R. U. Emerging roles of caspase-3 in apoptosis. *Cell death and differentiation* (1999).
183. Nicholson, D. W., Ali, A., Thornberry, N. A. & Vaillancourt, J. P. Identification and inhibition of the ICE/CED-3 protease necessary for mammalian apoptosis. (1995).
184. Wilson, T. & Hastings, J. W. Bioluminescence. *Annual Review of Cell and*

- Developmental Biology* **14**, 197–230 (1998).
185. Roda, A., Guardigli, M., Michelini, E. & Mirasoli, M. Bioluminescence in analytical chemistry and in vivo imaging. *Trends in Analytical Chemistry* **28**, 307–322 (2009).
186. Roda, A., Pasini, P., Mirasoli, M., Michelini, E. & Guardigli, M. Biotechnological applications of bioluminescence and chemiluminescence. *Trends Biotechnol.* **22**, 295–303 (2004).
187. Rice, B. W. & Contag, C. H. The importance of being red. *Nat. Biotechnol.* **27**, 624–625 (2009).
188. Badr, C. E. & Tannous, B. A. Bioluminescence imaging: progress and applications. *Trends Biotechnol.* **29**, 624–633 (2011).
189. Xia, Z. Y. & Rao, J. H. Biosensing and imaging based on bioluminescence resonance energy transfer. *Current Opinion in Biotechnology* **20**, 37–44 (2009).
190. Yan, M. *et al.* A novel intracellular protein delivery platform based on single-protein nanocapsules. *Nat Nanotechnol* **5**, 48–53 (2010).
191. Medintz, I. L., Uyeda, H. T., Goldman, E. R. & Mattoussi, H. Quantum dot bioconjugates for imaging, labelling and sensing. *Nat Mater* **4**, 435–446 (2005).
192. Michalet, X. *et al.* Quantum dots for live cells, in vivo imaging, and diagnostics. *Science* **307**, 538–544 (2005).
193. So, M. K., Xu, C. J., Loening, A. M., Gambhir, S. S. & Rao, J. H. Self-illuminating quantum dot conjugates for in vivo imaging. *Nat. Biotechnol.* **24**, 339–343 (2006).
194. Yao, H. Q., Zhang, Y., Xiao, F., Xia, Z. Y. & Rao, J. H. Quantum dot/bioluminescence resonance energy transfer based highly sensitive detection of proteases. *Angew Chem Int Edit* **46**, 4346–4349 (2007).
195. Xia, Z. Y. *et al.* Multiplex Detection of Protease Activity with Quantum Dot Nanosensors Prepared by Intein-Mediated Specific Bioconjugation. *Anal. Chem.* **80**, 8649–8655 (2008).
196. Huang, X. Y., Li, L., Qian, H. F., Dong, C. Q. & Ren, J. C. A resonance energy transfer between chemiluminescent donors and luminescent quantum-dots as acceptors (CRET). *Angew Chem Int Edit* **45**, 5140–5143 (2006).
197. Qian, H. *et al.* High-quality and water-soluble near-infrared photoluminescent CdHgTe/CdS quantum dots prepared by adjusting size and composition. *Journal of*

- Physical Chemistry C* **111**, 16852–16857 (2007).
198. Miyawaki, A. Bringing bioluminescence into the picture. *Nat Meth* **4**, 616–617 (2007).
 199. Pflieger, K. D. G. & Eidne, K. A. Illuminating insights into protein-protein interactions using bioluminescence resonance energy transfer (BRET). *Nat Meth* **3**, 165–174 (2006).
 200. Lian, T. & Ho, R. Trends and developments in liposome drug delivery systems. *J Pharm Sci* **90**, 667–680 (2001).
 201. Verma, I. M. & Weitzman, M. D. Gene therapy: twenty-first century medicine. *Annu Rev Biochem* **74**, 711–738 (2005).
 202. Wu, Z., Asokan, A. & Samulski, R. J. Adeno-associated virus serotypes: vector toolkit for human gene therapy. *Mol. Ther.* **14**, 316–327 (2006).
 203. Lamb, R. A. Paramyxovirus fusion: a hypothesis for changes. *Virology* **197**, 1–11 (1993).
 204. Verma, A. *et al.* Surface-structure-regulated cell-membrane penetration by monolayer-protected nanoparticles. *Nat Mater* **7**, 588–595 (2008).
 205. Bowman, E. J., Siebers, A. & Altendorf, K. Bafilomycins: a class of inhibitors of membrane ATPases from microorganisms, animal cells, and plant cells. *Proc. Natl. Acad. Sci. U.S.A.* **85**, 7972–7976 (1988).
 206. Yoshimori, T., Yamamoto, A., Moriyama, Y., Futai, M. & Tashiro, Y. Bafilomycin A1, a specific inhibitor of vacuolar-type H (+)-ATPase, inhibits acidification and protein degradation in lysosomes of cultured cells. *J. Biol. Chem.* **266**, 17707–17712 (1991).